The Dissertation Committee for Victor Armanda Kusuma certifies that this is the approved version of the following dissertation:

Effect of Network Structure Modifications on the Light Gas Transport Properties of Cross-linked Poly(ethylene oxide) Membranes

Committee:

_____

Benny D. Freeman, Supervisor

_____

Miguel Jose-Yacaman, Co-supervisor

_____

Donald R. Paul

_____

Isaac C. Sanchez

_____

Douglass S. Kalika

Effect of Network Structure Modifications on the Light Gas Transport Properties of Cross-linked Poly(ethylene oxide) Membranes

by

Victor Armanda Kusuma, B.S.ChE.; M.S.E.

Dissertation

Presented to the Faculty of the Graduate School of

The University of Texas at Austin

in Partial Fulfillment

of the Requirements

for the Degree of

Doctor of Philosophy

The University of Texas at Austin

May 2009

To my parents...

for their love, support, prayers, and companionship

in a way that is uniquely theirs.

Thanks.

Really.

This one's for you.

Acknowledgements

It is a relief for me to arrive at this point, after the long course of my graduate work: to finally defeat inertia, overcoming distractions to work and focus, despite all odds, to complete this dissertation. Personally, this dissertation represents a valuable, concrete measure of my overcoming said inertia, marking an important milestone in life. I hope it also signifies my maturity from the idealistic, all-too-young graduate student I was when I first started.

Regardless, I would not have reached this point without the people who made it possible. I am greatly indebted to a number of people over the years who have helped me personally and professionally, and oftentimes both. I would like, first and foremost, to acknowledge my two supervisors, Dr. Benny D. Freeman and Dr. Miguel Jose-Yacaman. Dr. Yacaman has been my supervisor for the first three years of my graduate studies life, and Dr. Freeman continued it to the completion. Both of them have been very encouraging and supportive of my success as a graduate student: I have learned a lot from both, professionally and personally, and enjoyed many good times. I would also

like to acknowledge Dr. Douglass S. Kalika of University of Kentucky, who has been fun to work with – I enjoyed our many fruitful discussions on my work and the close collaboration that produced solid publications, some of which form the basis of this dissertation. My other two committee members: Dr. Donald R. Paul and Dr. Isaac C. Sanchez, for the guidance in many little things, for the support in times of need, and for the general companionship. Finally, to Dr. Charles (Buddy) Mullins, for the friendship and support.

I would like to acknowledge everyone I have worked with over my graduate studies, in both Yacaman and Freeman groups. Every single one of you have made a difference. From Yacaman group, I'd like to acknowledge my former officemates who have moved on to better things: Justin Burt, Jose-Luis Elechiguerra, Alejandra Camacho-Bragado, Ruben Morones, and Domingo Garcia-Gutierrez. Xiaoxia Gao have helped me with a great number of things, especially the Transmission Electron Microscope. Special thanks for our former postdoc, Dr. Claudia Gutierrez, for the discussions and help in various aspects of my work. Also, Michael Dickey, formerly of Willson group, for the collaboration that was fun and educational. From Freeman group, I would first like to acknowledge my former and current officemates: Scott Kelman, Hao Ju, and Dr. Claudio Patricio Ribeiro Jr. for their friendship and good times shared – I'd like to especially thank Claudio for the many discussions we had about the work that really helped at the crucial times. I thank Dr. Clive Bosnyak for his professional advices and personal friendship during my final semester. I would also like to thank the rest of the exceptional Pickle

crew both past and present for their friendship, help and support, especially Kevin Tung, Alyson Sagle, Geoff Geise, Hua (Richard) Li, Bryan McCloskey, Scott Matteucci, James Kyzar, Dr. Ho Bum Park, Brandon Rowe, Wei Xie, Elizabeth van Wagner, Roy Raharjo, Joseph Cook, Keith Ashcraft, Maria Chiara Ferrari, Yuan-Hsuan Wu, and Conor Braman. Dr. Haiqing Lin did not stay long to impart his wisdom, but his solid PhD work and continued help provided a strong foundation for this dissertation, for which I am very grateful. I would like to acknowledge the help of my co-authors from University of Kentucky: Sumod Kalakkunnath, Matt Borns, Michael Danquah, Stephan Smith and Alex Heilman. I also acknowledge the administrative assistance I have had from Ms. Fatima Z. Bridgewater, Ms. Sande Storey, Ms. Kumi Smedley, and Ms. Beatriz Mattos. Ms. Pam Cook and Emily Cartier have worked patiently with me, fixing my abominable English and helping to make that nagging phrase sounds just ever so slightly better, in preparing this manuscript. For procurement assistance, I'd like to acknowledge Ms. Susan Micho and Mr. Steve Orwick. Finally, not to forget the students I have personally worked with in the past: Jose Salazar, Gustavo Espinoza, Josefina Guzman and Anh-Thu Tran.

This particular work is generously sponsored through grants from the U.S. Department of Energy (Grant DE-FG02-02ER15362) and the U.S. National Science Foundation (Grant CBET-0515425). I also acknowledge the grant from the U.S. National Science Foundation (Grant DMR-0423914) that funds the Center for Layered Polymeric Systems (CLiPS) in which I have been involved in some capacity. Activities at the University of Kentucky were supported in part by a grant from the Kentucky Science and Engineering

Foundation as per Grant Agreement KSEF-148-502-05-130 with the Kentucky Science and Technology Corporation. Thank you for making this work possible for me and my co-authors, and this is not being said lightly.

On the personal side, I would first and foremost acknowledge my parents, to which this dissertation is dedicated. It is their wish and pride to have me attain this degree, and their love, support and prayer for this cause has been incredible, even if not appropriate at times. I am especially grateful for their support for the last few years, taking care of the little things in life and enabling me to concentrate on my work. I would like to acknowledge my family, especially my maternal grandmother and my cousins' family, for their various support and prayers (and I could not ask for more). Very special thanks to Cecilia Miké Widyawati, for her encouragement, trust, and help in good and bad, and especially for being patient with me. Finally, thanks to my many friends over the years in the Indonesian Catholic Community of Austin (ICC-Austin), St. Austin Catholic Church Choir, and the Dreu Noctem crew, too numerous to mention here without me forgetting someone I should not, and everyone else I call friends in Austin (you know who you are).

Thanks, y'all!

Effect of Network Structure Modifications on the Light Gas Transport Properties of Cross-linked Poly(ethylene oxide) Membranes

Victor Armanda Kusuma, Ph.D.

The University of Texas at Austin, 2009

Supervisor: Benny Dean Freeman

Co-supervisor: Miguel Jose-Yacaman

Cross-linked poly(ethylene oxide) (XLPEO) based on poly(ethylene glycol) diacrylate (PEGDA) is an amorphous rubbery material with potential applications for carbon dioxide removal from mixtures with light gases such as methane, hydrogen, oxygen and nitrogen. Changing the polymer network structure of XLPEO through copolymerization has previously been shown to influence gas transport properties, which correlated with fractional free volume according to the Cohen-Turnbull model. This project explores strategic modifications of the cross-linked polymer structure and their effect on the chemical, physical and gas transport properties with an aim to develop rational, molecular-based design rules for tailoring separation performance. Experimental results from calorimetric and dynamic thermal analysis studies are presented, along with pure gas permeability and solubility obtained at 35°C.

Incorporation of dangling side chains by copolymerization of PEGDA with methoxy-terminated poly(ethylene glycol) methyl ether acrylate, *n*=8 (PEGMEA) was previously shown to be effective in increasing fractional free volume of XLPEO through the opening of local free volume elements, which in turn increased CO_2 permeability. Through a comparative study of short chain analogs to these co-monomers, incorporation of an ethoxy-terminated co-monomer was shown to be more effective than a comparable methoxy-terminated co-monomer in increasing gas permeability. For instance, copolymerization of PEGDA with 71 wt% ethoxy-terminated diethylene glycol ethyl ether acrylate increased CO_2 permeability from 110 barrer to 320 barrer. Gas permeability increase was not observed when hydroxy or phenoxy-terminated pendants were introduced, which was attributed to reduction in chain mobility due to increased inter-chain chemical interactions or steric restrictions, respectively. Based on these results, incorporation of a co-monomer containing a bulky non-polar terminal group, tris-(trimethylsiloxy)silyl, was examined in order to further increase gas permeability. Addition of 80 wt% TRIS-A co-monomer increased CO_2 permeability of cross-linked PEGDA to 800 barrer. However, the resulting changes in chemical character of the copolymer reduced CO_2/light gas selectivity, even as gas permeability increased. The effect of incorporating a bulky, stiff functional group in the cross-linker chain was studied using cross-linked bisphenol-A ethoxylate diacrylate, which showed 40% increase in permeability compared to cross-linked PEGDA. This study affirmed the importance of polymer chain interaction, in addition to free volume, in determining the gas transport properties of the polymer.

Table of Contents

List of Tables

List of Figures

Chapter 1: Introduction

1.1. Opportunities for Membrane-Based Carbon Dioxide Separations

The use of membranes for light gas separations has been realized industrially only during the past 30 years [1]. However, membrane gas separation processes quickly generated interest as supplements or replacements to major separation processes, such as distillation or absorption, due to their relatively simple and efficient operation with small physical, economic and environmental footprint [4]. In particular, the industrially important separation of carbon dioxide from light gases (especially fuel gases such as methane and hydrogen) has received considerable attention. This was evidenced by the significant interest in topics related to CO_2 removal in the most recent major membrane conference, the International Congress on Membranes and Membrane Processes (ICOM) 2008. Carbon dioxide, as a greenhouse gas and major impurity in energy streams, must be removed to improve the energy value of fuel streams and to meet pipeline specifications [1]. The separation and sequestration of carbon dioxide from flue gas streams (primarily in mixtures with N_2) is also an area of interest, as concern over the potential global warming contribution of carbon dioxide increases [5].

Parts of this chapter have been adapted with permission from an article published in the *Journal of Membrane Science* [2] and from an article published in *Advanced Membrane Technology and Applications* [3], both originally written by the author. © 2008 Elsevier B.V. and 2008 Wiley-VCH, respectively.

Natural gas is an important energy source, long perceived as 'cleaner' than coal and higher hydrocarbons due to its ease of complete combustion. Every year, the world uses close to 100 trillion scf (standard cubic feet) of natural gas [6], and demand keeps growing. Raw natural gas varies in composition: while methane is always the major component (75-90 vol%) with ethane and higher hydrocarbons making up most of the rest, the amount of impurities that must be removed remains significant. Thus, virtually all the gas requires treatment to remove major impurities (water vapor, carbon dioxide, nitrogen and hydrogen sulfide) before it enters the pipeline. Membrane separation has grown rapidly in importance as a treatment option, almost exclusively in removing carbon dioxide [7]. The current U.S. pipeline specification for CO_2 in natural gas is less than 2 vol%, and approximately 10%-20% of all natural gas produced in the U.S. requires significant treatment to meet this specification [6]. The recent surge and fluctuation in natural gas prices, coupled by increased demand, has made membrane separation a very attractive alternative to such conventional processes such as pressure swing absorption (PSA) using amines [4].

Hydrogen gas is a basic constituent in the fertilizer and refinery industries, but it is also quickly gaining importance as an energy storage medium or energy carrier. As a fuel, hydrogen has high energy density, and it can also be converted to energy cleanly and efficiently, with no carbon emission, using fuel cells [8, 9]. Adoption of hydrogen fuel cells as an energy source may reduce humanity's overall carbon footprint, as the task of

carbon capture and sequestration is shifted to hydrogen production sites, where it can be achieved more economically. Most hydrogen production is performed via steam reforming of hydrocarbons, in particular natural gas [8, 10, 11]:

$$C_nH_m + n\ H_2O + \text{heat} \rightleftharpoons n\ CO + (m/2+n)\ H_2$$

followed by a shift reaction to convert CO to CO_2 to obtain additional H_2:

$$CO + H_2O \rightleftharpoons CO_2 + H_2$$

As a result, CO_2 is a major impurity for the finished H_2 product. A major initiative launched in 2004 by the U.S. Department of Energy (*i.e.*, Hydrogen Fuel Initiative) aims to overcome barriers associated with the use of hydrogen as fuel, such as production efficiency, purification, storage and safety. In particular, the success of fuel cell technology is critically dependent on the supply of high purity hydrogen (minimum 99.99%) [11]. One major goal for hydrogen production from natural gas is reducing the cost to $2.50/gge (gasoline gallon equivalent) at the pump by 2010, and an important component of production cost reduction is improved separation of CO_2 from the H_2 product [12]. As such, improvement in membrane separation is an avenue pursued under this initiative.

Another interesting potential application for CO_2 separation membranes is in the area of modified atmospheric packaging (MAP) technology. Food packaging applications rely increasingly upon packaging materials with carefully designed permeation rates to gases such as CO_2 and O_2 to increase produce shelf life [13]. For instance, it is critical to maintain an optimum level of oxygen for fresh fruit and vegetable storage, as these items

continue to respire after harvesting: aerobic respiration at high O_2 concentration breaks down starch, sugars and organic acids into CO_2 and H_2O plus heat and metabolic energy, and this loss of nutrients affects shelf life. On the other hand, anaerobic respiration at low O_2 concentration results in the formation of ethanol, acetaldehyde and organic acids (*i.e.*, fermentation) that can cause not only undesirable odors and flavors, but may also lead to growth of anaerobic pathogens that can cause food poisoning [3, 13]. Various kinds of produce require different optimum levels of CO_2 and O_2, and for these reasons, it is important to control the relative transport rates of CO_2 and O_2 in food packaging. The CO_2/O_2 selectivity of the packaging material is one variable that influences relative transport rates of CO_2 and O_2 [13-15]. For this purpose, polymeric membrane materials with high CO_2/O_2 selectivity can be engineered into packaging to achieve optimum storage conditions.

1.2. Cross-linked Poly(ethylene oxide) for Carbon Dioxide Separations

Cross-linked poly(ethylene oxide) (XLPEO) is a novel membrane material that was developed to improve poly(ethylene oxide) (PEO) [16-18]. Carbon dioxide molecules possess a quadrupole moment that contributes to favorable interactions with polar groups in polymers [19, 20]. A review of interactions between carbon dioxide and various model liquids revealed that among polar groups, ether oxygen moieties – such as those found in PEO – provide good solubility selectivity for carbon dioxide relative to light gases (*e.g.*, hydrogen, nitrogen or methane) [17]. Due to their flexible nature, ether oxygen-containing polymer chains are highly mobile, so polymers containing ethylene

oxide (EO) units often exhibit low glass transition temperatures (T_g) and relatively high gas diffusion coefficients [17]. However, high molecular weight linear PEO has high degree of crystallinity due to the smooth, flexible nature of the PEO chains [16, 21]. The presence of crystalline blocks in polymers markedly diminishes diffusivity, due to the increasing tortuosity factor, and solubility, as the degree of chain packing prohibits the dissolution of even small gas molecules [22]. As a result, gas permeability decreases [23]. For instance, the measured CO_2 infinite dilution permeability in high molar mass, linear PEO (71% crystalline, M_w=10^6) is 12 barrer, while the estimated CO_2 permeability in completely amorphous PEO is 140 barrer [16]. While low molecular weight PEO chains (below ~600 Daltons [21]) are too short to crystallize at ambient conditions, they are also often in a liquid or waxy state, and as such are unsuitable as gas separation membrane materials.

Several methods have been explored to overcome the problem of PEO crystallinity. Low molecular weight PEO has been blended as an additive with other polymers [24]. Another popular tactic is to design phase-separated block copolymers containing ethylene oxide segments that are too short to crystallize [25, 26], the most successful of which is poly(amide-*b*-ethylene oxide) (Pebax®) [27-29]. The two aforementioned methods can be combined to further improve separation performance [30]. The common weakness of these methods, however, is the necessity of incorporating rigid chains, often with lower affinity toward CO_2, into the polymer structure. A more thorough review of these methods is provided in ref. [17].

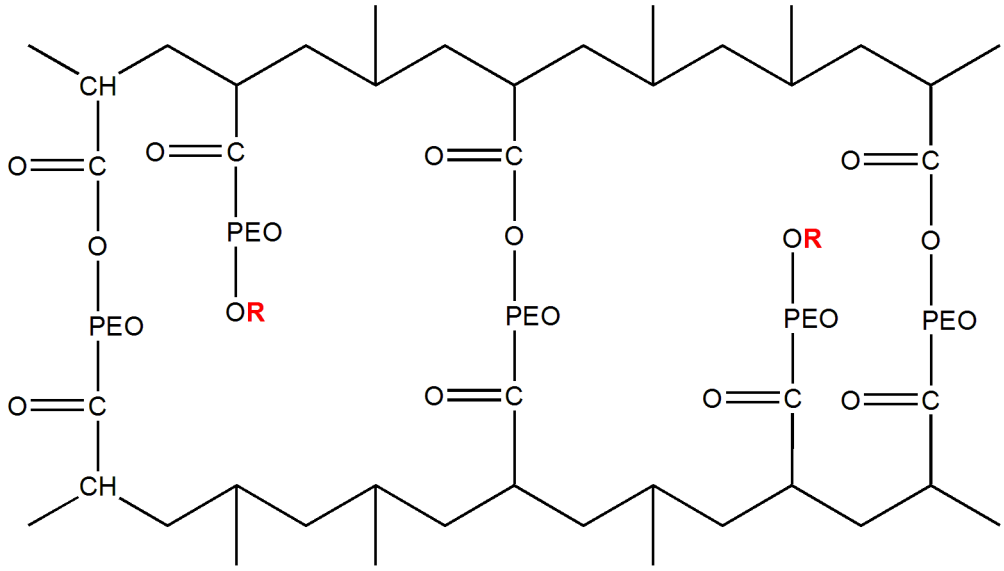

Figure 1.1: Scheme of representative network elements in XLPEO, with **R** representing functional end-group of monoacrylate co-monomer, and PEO representing uninterrupted $-(CH_2-CH_2-O)_n-$ chains.

Cross-linking poly(ethylene oxide) eliminates the crystallinity associated with high molecular weight PEO while keeping overall PEO content high. The polymer can be readily obtained through free-radical polymerization of functionalized linear, low molecular weight PEO, yielding a membrane material that is both solid and completely amorphous. In previous research, the starting materials typically consisted of a cross-linker (difunctionalized PEO) that could be mixed with a co-monomer (mono-functionalized PEO). The functional groups were either methacrylate [5, 31] or acrylate [18, 32], although the acrylate-based polymers tend to have higher permeability due to higher overall chain mobility. Rubbery XLPEO membrane can be quickly and conveniently produced by ultraviolet radiation curing of the pre-polymer solution in the absence of oxygen [18, 33, 34]. Acrylate double bonds often exhibit very high reactivity,

due mainly to large propagation rate constants and relatively low termination rate constants [35], and thus virtually complete conversion can be obtained as long as the polymer network does not vitrify: *i.e.*, the polymer must stay in the rubbery state throughout polymerization to allow diffusion of unreacted monomer. A representative scheme for XLPEO is shown in Figure 1.1.

Conventional gas separation membranes, such as cellulose acetate and aromatic polyimides, are glassy polymers with strong size-sieving ability [36, 37]. Most materials design efforts to date improve separation performance by emphasizing the polymer's size sieving ability to achieve separation, often by changing the polymer's chemical structure. Size discrimination leads to high gas diffusivity selectivity, favoring the diffusivity of smaller penetrants over larger penetrants. However, for separations involving CO_2, the highly condensable CO_2 (and perhaps other impurities such as higher hydrocarbons) are strongly sorbed in the polymer, opening free volume elements and increasing the polymer chain mobility. This effect, known as plasticization, leads to significant reduction in polymer size discrimination ability: although gas permeability increases, it is accompanied by a strong decrease in permselectivity [38-40].

The rubbery nature of XLPEO gives rise to several unique properties. Due to high overall chain mobility, gas diffusivity (and permeability) through rubbery polymers tend to be high [41, 42]. However, this flexibility also means that diffusivity of gases of various sizes through rubbery polymers are more similar to one another than diffusivity

values through glassy, rigid polymers. As a result, rubbery polymers tend to be more weakly size-sieving [3, 43]. To achieve separation, therefore, rubbery membranes often rely mainly on gas solubility differences. In XLPEO, the condensability of CO_2, coupled with its favorable interaction with the polar ether oxygen moieties, leads to much higher CO_2 solubility compared to other light gases. Thus, in contrast to conventional gas separation membranes [18, 32, 44, 45], CO_2 transport is favored even over lighter non-polar gases (such as hydrogen) in light gas separations using XLPEO. Not only does the plasticization effect have no significant impact on gas selectivity, but the increase in permeability and reduced size-discrimination brought about by plasticization may even enhance separation performance of the larger CO_2 molecules over the smaller H_2 molecules, because size discrimination always favors the smaller penetrant [44]. CO_2 separation also tends to be more favorable at lower temperature due to increased CO_2 condensability, which leads to significantly increased CO_2 solubility [44-46]. An interesting feature of CO_2/H_2 separation with XLPEO is the separation of CO_2 as a major component of the low pressure permeate, while most of the H_2 is retained on the high pressure retentate side of the membrane. This strategy reduces the need to recompress H_2 to high pressure for further applications, unlike conventional gas separation, in which the majority of the H_2 product is obtained from the low pressure permeate side [11, 47, 48].

Another advantage of cross-linking acrylate-functionalized PEO is the ability to tune the membrane properties by changing the membrane structure, which is accomplished by varying the monomer composition in the prepolymer solution. Incorporating

monoacrylates containing short runs of ethylene oxide into a prepolymer solution which contains a diacrylate cross-linker may lead to formation of highly mobile branches in the XLPEO network, signified by an overall decrease in glass transition temperature and permeability increase [32]. The resulting transport properties are highly dependent on the chemical character of the branches, dictated by the functional group at the end of the ethylene oxide chain. For instance, permeability was enhanced in networks containing methoxy-terminated branches, but not in hydroxy-terminated branches, due to the ability of the -OH functional group to form hydrogen bonds with the polar network, thus limiting the branch chain mobility [32]. A large number of additional modification possibilities, which may lead to further separation performance improvement, are afforded by the acrylate chemistry. Due to the large scale of the potential applications, even slight improvement in membrane performance would yield significant cost savings.

For commercial applications, XLPEO can be utilized to prepare thin film composite membranes [49]: for example, Polaris™ gas separation membranes from Membrane Technology Research, Inc. (Menlo Park, CA) are believed to be based on materials similar to XLPEO [50].

1.3. Goals and Organization of the Dissertation

This project takes on the challenge of identifying various chemical modification strategies to improve the separation performance of XLPEO. The approach involves exploration of various comparable materials that may not yield immediate improvement

in transport properties, but are instrumental in advancing the understanding of the polymer structure-property relationship. The ultimate aim of this project, therefore, is the development of fundamental, molecular-based design rules that will form the basis of future material modification strategies. This goal is achieved through physical characterization of various XLPEO copolymers, accompanied by pure gas transport measurements at a standard temperature (35°C). Prior to this project, studies were limited to using poly(ethylene glycol) diacrylate, n=14 (PEGDA) as the cross-linker, with possible copolymerization with either poly(ethylene glycol) methyl ether acrylate, n=8 (PEGMEA) or poly(ethylene glycol) acrylate, n=7 (PEGA). This project introduces one more cross-linker series and seven additional co-monomers with five different terminal functional groups.

The dissertation comprises nine chapters, including this introduction. Chapter 2 presents the theory of gas transport in dense, polymeric membranes. Chapter 3 describes materials chosen for this project and measurement/characterization methods for physical and transport properties. A review of XLPEO transport properties, introduced briefly in the previous section, is presented in Chapter 4. This chapter also discusses the modified free volume model developed by Lin et al. to predict the transport properties of XLPEO networks studied previously. Based on these discussions, the rationale for the modification strategies pursued in this project is presented in more detail.

The most promising strategy for improving membrane transport properties, according to earlier work, is choosing monoacrylate co-monomer branches with specific chemical properties. In particular, two short co-monomers with lower ethylene oxide content, one terminating in a methoxy group and the other in a hydroxy group, exhibited striking contrasts in transport properties. This comparison is further extended with an analogous co-monomer terminated with an ethoxy functional group, permitting a direct comparison with another potential functional group that may improve separation properties. This study is described in Chapter 5. Chapter 6 explores the effects of introducing phenoxy-terminated co-monomers into XLPEO networks, noting the deviations from the expected gas transport properties of the networks based on their fractional free volume trends, which suggests a stronger influence of network chain flexibility on transport properties. In Chapter 7, a co-monomer with a bulky, hydrophobic end-group based on a contact lens precursor is introduced, providing an interesting comparison to the other copolymer systems, which have been hitherto composed of inherently co-compatible materials.

Chapter 8 presents the transport properties of copolymers based on a different cross-linker series, bisphenol-A ethoxylate diacrylate (BPAEDA). In this chapter, the effect of the bisphenol-A group in between linear runs of PEO moieties is discussed in terms of physical and transport properties. In addition, this chapter introduces BPAEDA with three different chain lengths and their copolymers with some previously studied co-monomers, and explores the effect of BPAEDA chain length on copolymer properties.

Finally, Chapter 9 presents the conclusions of this study, related to molecular design rules for improving XLPEO transport properties and the need to improve the predictive model by considering the effects of chain flexibility on gas transport properties. Based on the findings of this study, recommendations for future work are offered.

Chapter 2: Theory

2.1. Permeability and Selectivity

Membrane separation processes operate on a simple principle: to achieve separation by allowing one component of a particular mixture to be more permeable than any of the other components [1]. One of the earlier records of polymeric membranes being used for this purpose was in 1866, when Graham enriched air from 21% to 40% O_2 [51]. The key property of the membrane is its ability to control the permeation rate of chemical species through the membrane. This property is determined by the molecular and chemical structure of the membrane, regardless of the nature of the membrane (polymeric or inorganic, dense or porous, homogeneous or heterogeneous). In this chapter, the general theory of gas transport in dense, homogeneous polymeric membranes is described. The effect of polymer structure on gas transport is further discussed in Chapter 4.

Gas transport through a dense polymeric film is often described by the solution-diffusion mechanism [51, 52]. Feed gas at high fugacity in the upstream (retentate) side of the membrane dissolves into the membrane surface, diffuses through the membrane due to a

Parts of this chapter has been adapted with permission from an article published in the *Journal of Membrane Science* [2] and from an article published in *Advanced Membrane Technology and Applications* [3], both originally written by the author.

concentration gradient, and desorbs from the downstream surface on the opposite (permeate) side, which is at lower fugacity. Fick's Law describes the one dimensional flux of gas A (*i.e.*, N_A) through the film in the *x* direction [53, 54]:

$$N_A = -\frac{D_{loc}}{1-w_A}\frac{dC_A}{dx} \qquad (2.1)$$

where D_{loc} is the local gas diffusion coefficient in the film, C_A is the local concentration of dissolved gas, and w_A is the weight fraction of gas A in the film. The steady state gas permeability, P_A, is defined (and experimentally determined) by the expression [55]:

$$P_A \equiv \frac{N_A l}{f_2 - f_1} \qquad (2.2)$$

where l is film thickness, and f_2 and f_1 are the upstream and downstream fugacities of gas A, respectively. Fugacity is used instead of pressure to account for non-ideal behavior in the gas phase, which can be significant for compressible penetrants (such as CO_2) at low temperature and high pressure, particularly in mixtures with other gases [56]. Fugacity can be calculated from the virial equation of state, with parameters available in the literature [57, 58]. Permeability coefficients are expressed in barrer [where 1 barrer = 10^{-10} cm^3(STP).cm/(cm^2.s.cmHg) = 7.5×10^{-18} m^3(STP).m/(m^2.s.Pa)]. By combining Equations 2.1 and 2.2 and integrating from $x = 0$ to $x = l$, permeability can be expressed as:

$$P_A = \frac{1}{f_2 - f_1}\int_{C_1}^{C_2}\frac{D_{loc}}{(1-w_A)}dC_A = D_A\frac{C_2 - C_1}{f_2 - f_1} \qquad (2.3)$$

where D_A is the concentration-averaged effective diffusion coefficient, defined as follows:

$$D_A = \frac{1}{C_2 - C_1} \int_{C_1}^{C_2} \frac{D_{loc}}{1 - w_2} dC = \frac{1}{C_2 - C_1} \int_{C_1}^{C_2} D_{eff}\, dC \qquad (2.4)$$

where D_{eff} is the local effective diffusion coefficient.

When the downstream fugacity is much smaller than upstream fugacity (*i.e.*, $f_2 >> f_1$ and $C_2 >> C_1$) [59], the values of D_{eff} can be obtained by taking the derivative of Equations 2.3 and 2.4 above with respect to f_2. D_{eff} is then expressed as [60, 61]:

$$D_{eff}(C_2) = \left[P_A + f \frac{dP_A}{df} \right]_{f_2} \left(\frac{df}{dC_2} \right)_{f_2} \qquad (2.5)$$

Likewise, Equation 2.3 can be simplified to give the familiar expression for solution-diffusion model [52]:

$$P_A = D_A \times S_A \qquad (2.6)$$

where S_A, the apparent solubility coefficient of penetrant A in the polymer, is defined as the equilibrium concentration of A in the polymer when the gas phase fugacity of A is f_2:

$$S_A = \frac{C_2}{f_2} \qquad (2.7)$$

The ideal selectivity of a membrane is an intrinsic property that defines the relative ease with which two penetrants permeate through the membrane. For gas A over gas B, this is defined as the ratio of their pure gas permeabilities [62]:

$$\alpha_{A/B} = \frac{P_A}{P_B} = \left[\frac{D_A}{D_B} \right] \left[\frac{S_A}{S_B} \right] \qquad (2.8)$$

where D_A/D_B is the diffusivity selectivity, and S_A/S_B is the solubility selectivity. Diffusivity selectivity is strongly influenced by the size difference between the penetrant molecules and the size-sieving ability of the polymer matrix, while solubility selectivity is controlled by the relative condensability of the penetrants and the relative affinity of the penetrants for the polymer matrix [62]. Enhanced gas selectivity, therefore, can be achieved by modifying either diffusivity or solubility selectivity, or both [54].

For permanent gases (*e.g.*, H_2, N_2, and O_2), permeability coefficients are essentially independent of pressure, whereas the permeability coefficients of CO_2 and higher hydrocarbons often increase with increasing feed pressure in rubbery polymers [59]. Therefore, to compare permeability values between gases, they may be extrapolated to infinite dilution from several permeability measurements performed at various pressures. Permeability is often empirically related to fugacity to obtain infinite dilution permeability ($P_{A,o}$) as follows [63]:

$$P_A = P_{A,o}\exp(m_{P,E}\Delta f) = P_{A,o}\exp(m_{P,E} f_2) \qquad (2.9)$$

Here, $m_{P,E}$ is an adjustable constant at a given temperature, and Δf is the difference between the upstream and downstream fugacity, $\Delta f = f_2 - f_1$. Therefore, from Equation 2.9, $P_{A,o}$ is the permeability coefficient when $\Delta f = 0$ (this state is often achieved by allowing both f_1 and f_2 to go to zero, hence the name 'infinite dilution permeability'). Δf can be replaced by f_2 in Equation 2.9 above since the downstream fugacity, f_1, is much smaller than f_2. For permanent gases, the permeability typically changes little with

fugacity and $m_{P,E}f_2$ is very small. In this case, Equation 2.9 can be approximated using Taylor expansion at $f_2 = 0$ into a linear form [16, 59]:

$$P_A = P_{A,o}(1 + m_{P,E} f_2) \qquad (2.10)$$

Infinite dilution solubility and diffusivity can be calculated using similar empirical relationships [59].

2.2. Solubility and Diffusivity

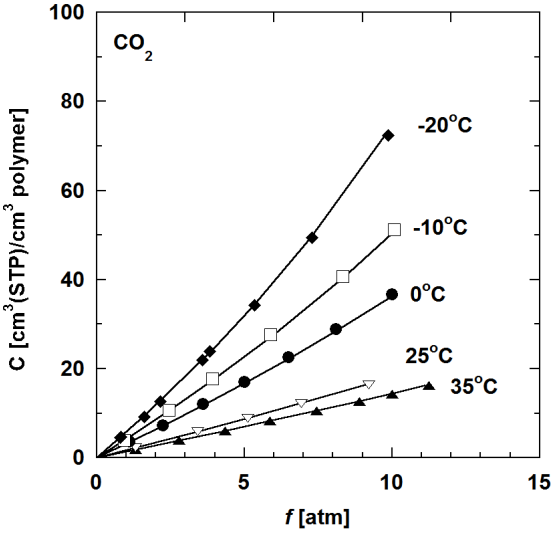

Figure 2.1: Effect of temperature on CO_2 sorption isotherms in XLPEGDA polymerized in the presence of 20 wt% water. The lines and curves through the data are based on the Flory-Huggins model, showing little deviation from Henry's law model (Eqn. 2.11) at 35°C. This figure is reproduced from ref. [56].

Gas solubility in rubbery polymers depends on gas condensability, interaction of the gas with the polymer matrix, and weakly on the free volume of the polymer [62]. Sorption behavior of gases at low activity coefficients usually follows Henry's law [41]:

$$C = k_D f \qquad (2.11)$$

where k_D is the solubility coefficient or Henry's law constant. In the cases of highly sorbing penetrants (such as carbon dioxide) at higher fugacity, deviations from Henry's law may be observed: it may then be necessary to use the Flory-Huggins equation to describe the penetrant concentration in the polymer [46, 64]. However, experiments in this project were performed at 35°C, where the activity of CO_2 at low fugacity is low enough that solubility in XLPEO can be essentially represented by Equation 2.11 [46, 56]. Figure 2.1 shows that the sorption isotherm of CO_2 in pure polymerized poly(ethylene glycol) diacrylate, n=14 (PEGDA) at various temperatures essentially follows Henry's law [56].

Diffusion of small molecules in a polymer was quantitatively related to fractional free volume by Fujita, based on a model proposed by Cohen and Turnbull, as follows [65, 66]:

$$D_A = A_D \exp\left(-\frac{B}{FFV}\right) \qquad (2.12)$$

where A_D is a pre-exponential factor, B is a constant proportional to penetrant size, and FFV is the fractional free volume in the polymer. The diffusion coefficient appearing in Equation 2.12 is, strictly speaking, the gas self-diffusion coefficient and not the binary mutual diffusion, D_{loc}. However, for the cases of interest here, no significant error occurs when D_A replaces the self-diffusion coefficient [43]. Gas diffusivity is also determined by polymer chain flexibility, often characterized by polymer glass transition temperature, T_g [62]. However, the chain flexibility contribution is not reflected in the Fujita-modified

Cohen-Turnbull model. According to this model, diffusivity increases primarily with increasing *FFV*.

Combining Equations 2.6 and 2.12 yields an expression for permeability:

$$P_A = A_P \exp\left(-\frac{B}{FFV}\right) \qquad (2.13)$$

where A_P is a pre-exponential factor that is equal to A_D multiplied by the solubility of penetrant A in the polymer, S_A. A_P is assumed constant only if S_A does not vary significantly among the family of materials being considered; this is mostly true in this study, with one exception (*cf*. Chapter 7). Table 2.1 gives the values of A_D, A_P and B for the five penetrants of interest in this study, as found in previous studies (see note).

Table 2.1: Free volume model parameters for gas transport through cross-linked PEGDA.

Penetrant	A_P **[10^3 barrer]**	B	A_D **[10^{-3} cm^2/s]**
CO_2	360 ± 70	0.95 ± 0.02	1.8 ± 0.4
CH_4	27 ± 5	0.99 ± 0.01	1.5 ± 0.3
H_2	6.0 ± 0.6	0.72 ± 0.01	---
O_2	9.0 ± 0.9	0.89 ± 0.02	---
N_2	7.3 ± 0.7	0.97 ± 0.02	---

Note: These values are used in Equations 2.12 and 2.13 and taken from previous studies [18, 43], based on an XLPEO membrane cast from a prepolymer mixture containing 80 wt% PEGDA and 20 wt% water (*cf*. Figure 4.9b).

To predict the gas diffusivity and solubility selectivity in a polymer, two properties have been utilized previously: critical temperature (a measure of gas condensability, and thus solubility) [56] and kinetic diameter (a measure of gas molecule size, and thus diffusivity) [43]. Kinetic diameter values were determined by the minimum zeolite molecular sieve pore size that allowed gas diffusion of the relevant species [67]. The gas critical temperature values are taken from ref. [68]. For the five light gases studied in this project, the relevant parameters are given in Table 2.2.

Table 2.2: Critical temperature and kinetic diameter of relevant light gases.

Penetrant	Critical Temperature [K]	Kinetic Diameter [Å]
CO_2	304	3.3
CH_4	191	3.8
O_2	155	3.46
N_2	126	3.64
H_2	33	2.89

2.3. Free Volume

Fractional free volume, *FFV,* is commonly used to characterize the efficiency of chain packing and the amount of free space available for gas permeation in the polymer [69, 70]. It can be estimated experimentally by [69]:

$$FFV = \frac{v - v_o}{v} \qquad (2.14)$$

where v is the overall specific volume of the amorphous polymer at the temperature of interest (which is M/ρ_P, the molecular weight of polymer repeat unit divided by density), and v_o is the specific occupied volume at 0 K. Physically, v_o refers to the total volume occupied by only the polymer chains. Van Krevelen recommends estimation of v_o using a group contribution method [71]. Based on the work of Bondi, a good approximation for v_o is given by [72]:

$$v_o = 1.3 \times v_w \tag{2.15}$$

where v_w is the specific van der Waals volume of a representative repeating unit of the polymer molecule, given in cm^3/mol. Combining Equation 2.15 with 2.14:

$$FFV = 1 - \frac{1.3 \times \rho_P \times v_w}{M} \tag{2.16}$$

To obtain a good estimate of v_w, each molecule (or repeat unit, in the case of polymers) is broken down into the fewest possible structural groups, whose individual v_w values have been determined while taking into account the influence of the atomic surroundings. An example for PEGDA appears in Table 5.2. v_w for the molecule is then approximated as the sum of the van der Waals volumes of these constituent structural groups, $v_{w,i}$, the values of which have been compiled by van Krevelen primarily from the work of Bondi [71]. For a binary copolymer consisting of cross-linker A and co-monomer B, FFV is given as:

$$FFV = 1 - 1.3\,\rho_p \left(\frac{w_A \times \sum v_{w,i,A}}{M_A} + \frac{w_B \times \sum v_{w,i,B}}{M_B} \right) \tag{2.17}$$

where w_A and w_B refer to the weight fractions of components A and B, respectively.

The validity of the group contribution method depends on the absence of strong inter-chain interactions, *e.g.*, hydrogen bonding [72], which may change the chemical environment experienced by the functional groups [73]. These interactions may distort individual bonds, changing the van der Waals volume estimate and altering the measured free volume of the network relative to the predictions described above.

2.4. Dynamic Relaxation Characteristics of Polymer Networks

The dynamic relaxation characteristics of the cross-linked polymer networks provide useful insights into the influence of cross-links on the relaxation of polymer chains, as related to the network composition, structure, and local free volumes [74, 75]. Previous studies have utilized dynamic thermal analysis techniques, such as dynamic mechanical analysis (DMA) and broadband dielectric relaxation spectroscopy (BDS), to characterize sub-glass and glass-rubber relaxation characteristics of polymer networks across a wide range of temperatures and timescales, and to relate the time-temperature characteristics to the motional processes due to cross-link density variations [76-80]. Those studies showed that the presence of covalent cross-links typically reduces segmental mobility near the cross-link junctions, manifested by an increase in glass transition temperature T_g. Dielectric response obtained using BDS is particularly useful for studying molecular motions associated with the glass transition, as well as transport and polarization of mobile charged species within the material. A BDS study by Schroeder and Roland revealed an increase over 50°C in T_g for cross-linked poly(dimethylsiloxane) (PDMS) as

distance between cross-links approached 6-7 monomer units [77]. This increase is often accompanied by inhomogeneous broadening of the glass transition, due to the range of relaxation conditions experienced by the chain segments and their relative proximity to chain junctions.

Measurement of the rubbery plateau modulus (E_R) by DMA provides a direct means to assess cross-link density and, potentially, the overall mechanical integrity in polymer networks. Classical rubber elasticity theory [81-83] relates E_R to effective cross-link density (υ_e) as shown below [81]:

$$\upsilon_e = \frac{E_R}{3RT} \qquad (2.18)$$

where R is the gas constant, and T is absolute temperature. DMA measurements also yield time-temperature master curves across a temperature range at different timescales [74]. These curves, constructed by time-temperature superposition methods [84], show the storage modulus as a function of ωa_T, where ω is the applied test frequency ($\omega=2\pi f$, with f expressed in Hz) and a_T is the dimensionless shift factor. The glass-rubber relaxation is satisfactorily described using the Kohlrausch-Williams-Watts (KWW) stretched exponential relaxation time distribution function [85]:

$$\phi(t) = \exp[-(t/\tau_o)^{\beta_{KWW}}] \qquad (2.19)$$

where τ_o is the central relaxation time and β_{KWW} is the relaxation time distribution parameter, which is used to characterize the breadth of the relaxation. β_{KWW} ranges from 0 to 1, with lower values indicating increased intermolecular coupling and broadening of

the relaxation owing to the influence of the cross-links. These plots provide an objective basis for examining the intermolecular cooperativity characteristics of the networks and the apparent activation energy associated with segmental motion [74].

Chapter 3: Materials and Experimental Methods

3.1. Materials and Nomenclature

The principal cross-linker of cross-linked poly(ethylene oxide) (XLPEO) used in this project is poly(ethylene glycol) diacrylate, n=14 (PEGDA; nominal M_w=700), obtained from Sigma-Aldrich Chemical Company (Milwaukee, WI). This material was studied extensively in previous projects, by itself or in conjunction with other co-monomers [18, 32, 43-46, 56, 74, 75, 86-88]. Chapter 8 examines the use of bisphenol-A ethoxylate diacrylate (BPAEDA) as a cross-linker. It was obtained in three molecular weights corresponding to ethylene oxide repeat lengths of n = 2, 4, and 15 [89]. BPAEDA monomers with nominal molecular weights equal to 512 g/mol (n=2) and 688 g/mol (n=4) were obtained from Aldrich. The BPAEDA monomer with molecular weight equal to 1656 (n=15) was obtained from Sartomer Company (Exton, PA). The cross-linker structures are given in Table 3.1.

The selection of co-monomers in this project is based on earlier studies with poly(ethylene glycol) methyl ether acrylate, n=8 (PEGMEA; nominal M_w=454) and poly(ethylene glycol) acrylate, n=7 (PEGA; nominal M_w=375) [32, 44, 45, 74, 88]. In Chapter 5, the co-monomers are 2-hydroxyethyl acrylate (2-HEA; M_w=116, purity 96%),

ethylene glycol methyl ether acrylate (EGMEA; M_w=130, purity 98%), and 2-ethoxyethyl acrylate (2-EEA; M_w=144, purity 98%) [2]. Di(ethylene glycol) ethyl ether acrylate (DEGEEA; M_w=118, technical grade), di(ethylene glycol) phenyl ether acrylate (DEGPEA, listed in the Aldrich catalog as poly(ethylene glycol) phenyl ether acrylate (n=2); M_w ~ 236) and poly(ethylene glycol) phenyl ether acrylate (n=4) (PEGPEA; M_w ~ 324) are studied in Chapter 6 [90]. All co-monomers described previously were obtained from Aldrich. Finally, in Chapter 7, 3-[tris-(trimethylsiloxy)silyl] propyl acrylate (TRIS-A) was obtained from Gelest, Inc. (Morrisville, PA) as SIA0210.0, (3-acryloxypropyl)-tris(trimethylsiloxy) silane (purity 95%) [91]. The structures are given in Table 3.2.

The UV photoinitiator used in this work is 1-hydroxyl-cyclohexyl phenyl ketone (HCPK; purity 99%), obtained from Aldrich. Toluene (extra dry with molecular sieves, 99.85%) for use in combining PEGDA and TRIS-A was obtained from Acros Organics (Geel, Belgium). All reagents and monomers were used as received.

Table 3.1: Chemical structures of PEGDA and BPAEDA

Name	Structure
PEGDA	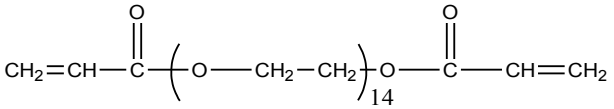
BPAEDA (n = 2, 4, 15)	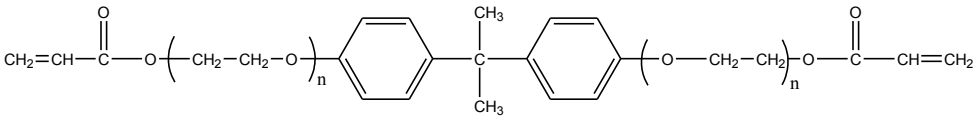

Table 3.2: Chemical structures of various co-monomers

End-group	Name	Structure
-OH	2-HEA	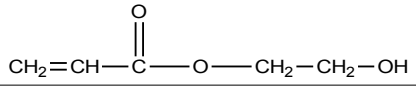
	PEGA	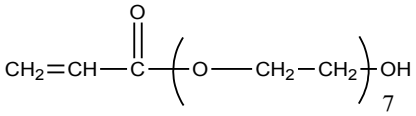
$-OCH_3$	EGMEA	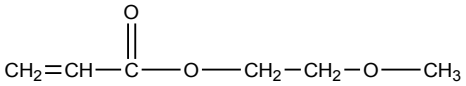
	PEGMEA	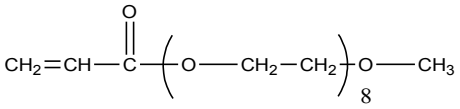
$-OC_2H_5$	2-EEA	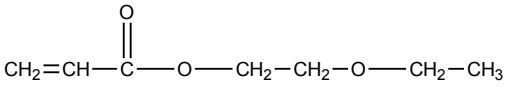
	DEGEEA	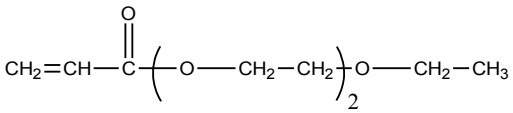
$-OC_6H_5$	DEGPEA	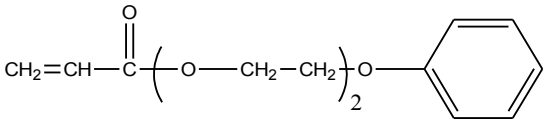
	PEGPEA	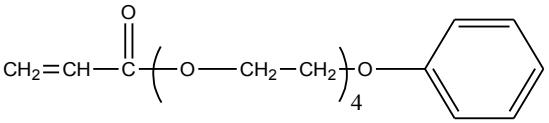
-tris(TMS)	TRIS-A	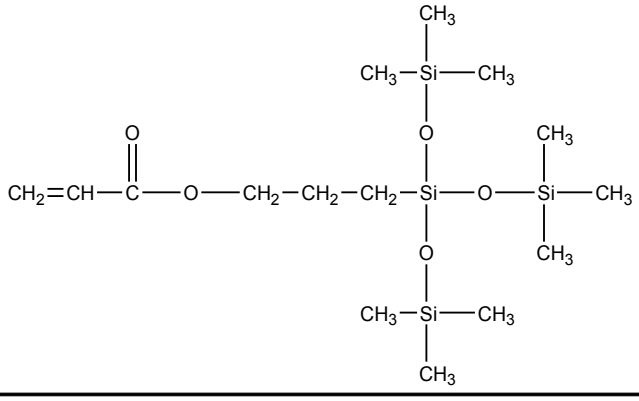

All gases (CO_2, CH_4, O_2, N_2 and H_2) were obtained from Airgas Southwest Inc. (Corpus Christi, TX), with purity of at least 99.9% (except for methane: 99.0%), and they were used as received.

3.2. Cross-linker and Monomer Characterization

The molecular weight and polydispersity of PEGDA were characterized previously [18] using proton nuclear magnetic resonance (^{1}H NMR) and fast atom bombardment mass spectrometry (FAB-MS). This PEGDA has a number-average molecular weight of 743 Daltons (by NMR), consistent with a monomeric repeat value of n~14. Likewise, ^{1}H NMR was used to confirm the molecular weights of the as-received BPAEDA cross-linkers [89]. Samples were prepared by dissolving dry BPAEDA monomers in deuterated chloroform, $CDCl_3$ (99.6 D%) obtained from Aldrich, at concentrations between 5 and 10 wt%. ^{1}H NMR spectra were recorded on a VARIAN INOVA-500 spectrometer operating at 600 MHz, and the data are reported here in ppm relative to the $CDCl_3$ solvent peak at δ 7.24 [92]. The spectrometer was adjusted routinely as follows: spin rate, 20 rpm; pulse width, 2.0 μs; sweep width, 9615 Hz; line broadening (with exponential multiplication), 0.1 Hz with 128 K data points. The relaxation delay was 24s (*i.e.,* $5T_1$). The ^{1}H-NMR peaks with $CDCl_3$ as solvent are assigned as follows: δ 7.06 and δ 6.75 (4 H each, *m* and *o* hydrogen atoms in phenyl rings of bisphenol-A relative to ethylene oxide chain), δ 6.38, δ 6.11 and δ 5.79 (2 H each, *cis*, *gem* and *trans* hydrogen atoms relative to –C(=O)–O– in CH_2=CHR within acrylate end-group), δ 4.27 and δ 3.70 (4 H each, α and β hydrogen atoms in closest CH_2-CH_2-O relative to acrylate group), δ

4.05 and δ 3.79 (4 H each, α and β hydrogen atoms in closest CH_2-CH_2-O relative to bisphenol-A group), δ 3.60 (8×(*n*-2) H in CH_2-CH_2-O not immediately adjacent to acrylate or bisphenol-A groups), and δ 1.58 (6 H, β hydrogen atoms flanked by the two phenyl rings).

The molecular weight of BPAEDA can be confirmed by taking the ratio of the δ 3.60 peak integral (originating from the hydrogen atoms in the middle of the EO chain) to that of any of the other peaks; this approach has been used previously to confirm the molecular weight of PEGDA [18]. For the BPAEDA (*n*=2) crosslinker, the δ 3.60 peak is expected to be absent, according to the peak assignments presented above. Analysis of the experimental spectra verified that the molecular weights of the BPAEDA monomers are consistent with the suppliers' specifications.

Other co-monomers were also analyzed using ^{1}H-NMR to confirm their molecular weights. The spectra and analyses are omitted for brevity.

3.3. Film Preparation

Films were prepared via UV photopolymerization using a procedure similar to that described for PEGDA/PEGMEA and PEGDA/PEGA copolymers [32]. Liquid prepolymerization mixtures were prepared with the desired proportions of PEGDA cross-linker and an acrylate co-monomer, as well as 0.1 wt% HCPK photoinitiator (relative to total amount). This mixture was sandwiched between parallel quartz plates, separated by

spacers, to obtain film thicknesses of 80 to 500 μm (based on expected permeability). The assembly of quartz plates with the prepolymer solution between them was then exposed to 312 nm light for 90 seconds at 3 mW/cm^2 in a UV cross-linking chamber (Spectrolinker XL-1000, Spectronics Corporation, Westbury, NY). Before further use, the resulting freestanding films were extracted for five days using ultrapure water (Milli-Q water purification system, Millipore Corporation, Bedford, MA), with water changed daily. Films so treated consisted of three-dimensional networks (gel) and a negligible amount of low molecular-weight polymer (sol) that was not bound to the network [18]. Afterwards, the films were air-dried at ambient conditions prior to gas transport studies.

Because PEGDA and TRIS-A are not miscible, toluene was added to achieve a homogeneous solution. 2 ml of toluene was added to 3 g of PEGDA/TRIS-A prepolymer mixture, corresponding to 37 wt% toluene. In addition, to analyze the effect of toluene dilution, PEGDA/toluene solutions were made with varying amount of toluene (from 0 wt% to 40 wt% toluene). The prepolymer solutions were mixed in closed screw cap bottles for a maximum of one hour. The UV exposure time for these mixtures, 300 s, is longer than that for other PEGDA-based copolymer systems (as described above) to compensate for the significant UV absorption of TRIS-A at this wavelength, especially at higher concentrations. Significant UV absorption at 312 nm was confirmed by UV/vis spectra of TRIS-A dissolved in methanol (99%, spectrophotometric grade, Aldrich), taken using a Shimadzu BioSpec-mini DNA/RNA/Protein analyzer (Shimadzu Corp., Kyoto, Japan). PEGDA/toluene mixtures for dynamic mechanical studies were cross-

linked using a 90 s UV exposure, which was sufficient to ensure complete reaction [18]. After UV irradiation, these samples were slowly dried at ambient temperature and pressure for at least 24 hours to remove toluene, and then immersed in ethanol (200 proof, ACS/USP grade: Pharmco-Aaper, Shelbyville, KY) for 5 days to extract any unbound low molecular weight polymer (*i.e.*, sol); the ethanol was changed daily. Some weight loss was encountered in films with higher TRIS-A concentrations, but it was typically less than 5 wt%, so the film composition was assumed to be the same as the prepolymer composition. Visual observation revealed transparent films.

The exact thickness of the film was determined within ±1 μm using a digital micrometer (ABSOLUTE Digimatic series 547, Mitutoyo Corp., Japan). The film must be covered with a uniform thin glass plate (*e.g.*, a cover for an optical microscope slide) as the measurement tip can press into flexible films and affect the readings. At least 15 measurements were taken at different points on the film surface; the average value of these (with typical standard deviation ±5 μm) was taken to be the film's average thickness. This method gives a fairly accurate measure of the true film thickness, as confirmed by direct measurement with a low force digital micrometer (Litematic VL-50A series 318, Mitutoyo Corp., Japan) obtained after the commencement of the project. Film thicknesses for the PEGDA/TRIS-A films were determined exclusively using the Litematic VL-50A.

3.4. Film Density

The density of the dry polymer films was determined by hydrostatic weighing using a Mettler Toledo balance model AG204 (Switzerland) and a density determination kit at ambient conditions. The density was determined by comparing the polymer mass in air with its mass in an auxiliary liquid; heptane was chosen for most XLPEO systems in this project because poly(ethylene oxide) has little affinity for alkanes of this length [93, 94] (PEGDA/TRIS-A system is an exception: see below). The sample preparation was slightly different from that of previous studies [16, 18, 95]. Taking into account the affinity of poly(ethylene oxide) to water vapor in the atmosphere, polymer samples were first degassed overnight in a vacuum oven at ambient temperature, then purged and transferred under dry nitrogen into the balance prior to density determination. The time taken for density measurements was much less than the timescale of vapor re-sorption into the polymer, as determined from sorption experiments, and thus the density measurements were performed at ambient conditions without nitrogen blanketing.

Because the PEGDA/TRIS-A copolymers were amphiphilic, a perflourinated alkane was chosen as the auxiliary liquid: following the success of Car et al. with similarly amphiphilic poly(amide-*b*-ethylene oxide) (Pebax®), 3M Fluorinert™ FC-77 (obtained from Acros Organics) was utilized [30]. Using a 100 ml pycnometer, the density (1.765 ± 0.001 g/cm^3 at 23°C) of FC-77 obtained from this source was found to be inconsistent with the manufacturer's specifications (1.781 g/cm^3 at 23°C). The new value for FC-77

was verified by comparing the density of polymerized, undiluted PEGDA measured in FC-77 with the value obtained in *n*-heptane. The density measurements of PEGDA samples prepared with various levels of toluene dilution were conducted in *n*-heptane.

3.5. Fourier Transform Infrared Spectroscopy

Attenuated total reflection Fourier transform infrared spectroscopy (FTIR-ATR) analysis was performed using a Thermo-Nicolet (Madison, WI) Nexus 470 spectrometer, with each average spectrum obtained from 128 scans at a resolution of 1 cm^{-1}. The conversion of acrylate double bonds due to polymerization led to a decrease in sharp peaks at 810 cm^{-1} (ascribed to the twisting vibration of the acrylic CH_2=CH bond), at 1410 cm^{-1} (deformation of the CH_2=CH bond) and at 1190 cm^{-1} (acrylic C=O bond) [32, 96, 97]. The carbonyl (C=O) band at 1725 cm^{-1} was used as a reference to facilitate comparison of the spectra.

3.6. Thermal Analysis

Thermal transitions were determined using a TA Instruments (New Castle, DE) Q100 differential scanning calorimeter (DSC). TA Instruments indicates that the accuracy in the temperature reported by this instrument is ±0.1°C. Samples (~10 mg) were initially quenched to -90°C and scanned twice at a heating rate of 10°C/min up to 150°C under a 50 ml/min dry N_2 purge flow. The glass transition temperature (T_g) was taken as the midpoint of the heat capacity step change that appeared in the second heating scan. No crystallization peaks were observed for any of the new networks examined in this project.

Dynamic mechanical analysis (DMA) was performed using a Polymer Laboratories Dynamic Thermal Mechanical Analyzer (Amherst, MA) operating in single cantilever bending geometry at the University of Kentucky. The films (thickness between 850 to 1000 μm) were held under vacuum at room temperature for at least 24 hours prior to measurement. The sample mounting procedures minimized exposure to ambient moisture. Storage modulus (E') and loss tangent (tan δ) were measured at a heating rate of 1 °C/min with test frequencies of 0.1, 1, and 10 Hz. All experiments were carried out under an inert (N_2) atmosphere. The dynamic mechanical glass transition temperature, T_α, is analogous to the glass transition temperature obtained by DSC, T_g. T_α is obtained from the peak maximum exhibited by the loss tangent (tan δ) curve against temperature (test frequency of 1 Hz), corresponding to the inversion point temperature during the glass-rubber transition exhibited in the storage modulus plot.

Dielectric spectroscopy measurements were made using the Novocontrol "Concept 40" broadband dielectric spectrometer (Hundsangen, Germany) at the University of Kentucky. Dielectric constant (ε') and loss (ε'') were recorded in the frequency domain (0.1 Hz to 1 MHz) at 4°C isothermal intervals from -150°C to 100°C. In order to optimize electrical contact during measurement, concentric silver electrodes were deposited on each polymer sample using a VEECO (Plainview, NY) thermal evaporation system. Samples were subsequently mounted between gold platens and positioned in the Novocontrol Quatro Cryosystem. Each sample was dried under vacuum at room temperature prior to measurement. Dispersion spectra were analyzed using the

Novocontrol WINFIT software to establish relaxation time (τ_{MAX}) as a function of temperature for both the sub-glass and glass rubber relaxation processes.

3.7. Pure Gas Permeation Measurement

Pure gas permeability values for polymers in this project were determined using a constant volume/variable pressure apparatus [28, 98] constructed by the author, with parts supplied by the Swagelok Company (through Arthur Fluid System Technologies, Austin, TX). The schematic of this apparatus is given in Figure 3.1. The permeation cell is a high pressure stainless steel filter holder (47 mm, catalog number XX45 047 00 from Millipore). The upstream transducer is a SuperTJE® transducer (0.05% full scale uncertainty with 1000 psig full scale, from Honeywell Sensotec, Columbus, OH) which is connected to an analog-to-digital converter (USB-6008, National Instruments, Austin, TX) and the downstream transducer is a Baratron® 626A with 10 torr full scale (MKS Instruments, Andover, MA), connected to a PDR-2000 readout (MKS Instruments). Upstream and downstream pressures were recorded using a Microsoft Windows XP PC with National Instruments LabVIEW® 8.0 software. As in previous work, impermeable aluminum tape (Nashua 324A from Covalence Adhesives, Franklin, MA) was used in the upstream and downstream sides of the membrane films to define the permeation area with greater accuracy and to prevent the O-ring inside the permeation cell from directly contacting the fragile membrane [98, 99]. However, due to tape delamination issues encountered with some membrane materials, it was necessary to lightly coat the upstream side of the membrane that would be in contact with the aluminum tape using a thin layer

of low-outgassing epoxy (Devcon 5 Minute® epoxy, Danvers, MA) just prior to aluminum tape application [100]. Care was taken to spread the epoxy thoroughly without affecting the exposed membrane area. After masking, the available surface area for permeation was 1.98 cm^2. The film was mounted with paper backing support.

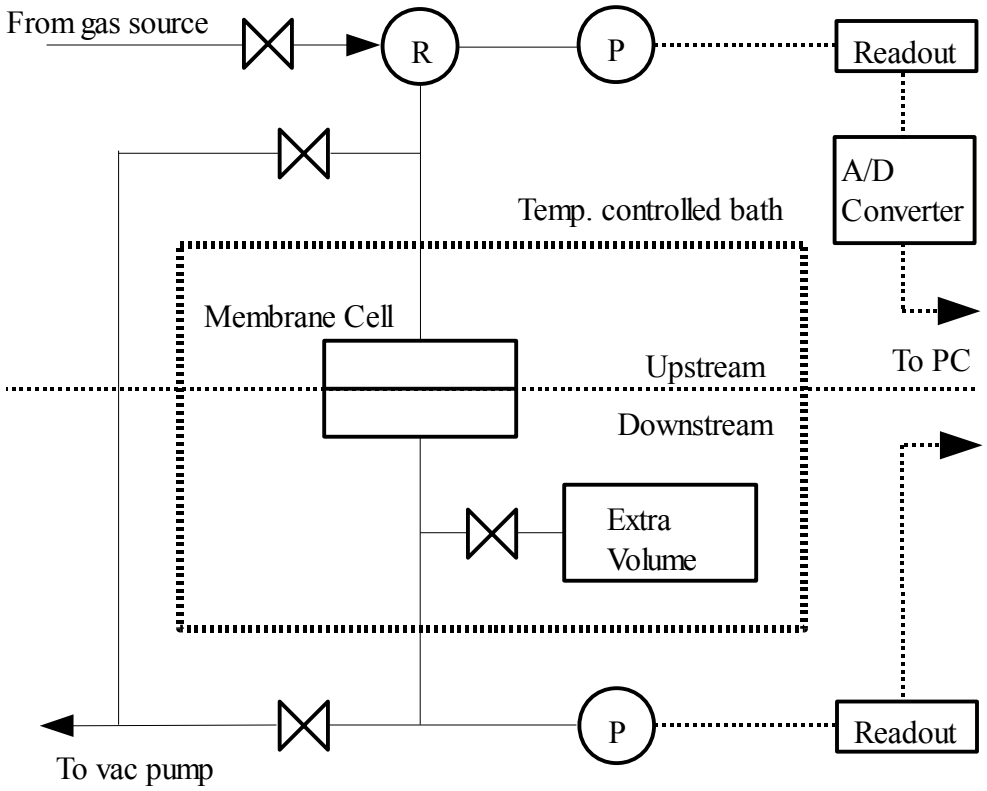

Figure 3.1: Schematic of pure gas permeation apparatus used in this project.

After film mounting, the cell and downstream elements were placed in a temperature-controlled acrylic bath with mounted heating circulator (Lauda E100, LAUDA GmbH, Lauda-Königshofen, Germany) filled with water maintained at (35.0±0.1)°C. The system was placed overnight under vacuum to degas the film from both upstream and

downstream sides. The system leak rate was measured before starting the permeation experiments by isolating both sides while under vacuum. As the pure gas was introduced at high pressure on the upstream side, the pressure increase in the downstream was recorded. Gas permeability was calculated from the steady state rate of pressure increase in a fixed, predetermined downstream volume (*cf*. Equation 2.2 and ref. [98]):

$$P_A = \frac{V_d l}{f_2 A_m RT}\left[\left(\frac{dp_1}{dt}\right)_{ss} - \left(\frac{dp_1}{dt}\right)_{leak}\right] \qquad (3.1)$$

where V_d is the downstream volume (cm^3), l is the film thickness (cm), f_2 is the upstream absolute pressure with applied compressibility factor (cmHg), A_m is the film area available for gas transport (cm^2), R is the gas constant (0.278 cmHg $cm^3/(cm^3$(STP) K), T is the absolute temperature (308 K), and the two end terms refer to steady state rates of pressure rise (cmHg/s) in the downstream volume at a fixed upstream pressure and under vacuum, respectively. The leak rate was usually less than 10% of the steady state rate under pressure. The downstream pressure was always measured below 1.05 cmHg (the downstream transducer upper detection limit), which satisfied the requirement of having the upstream fugacity (from 4 atm up to 15 atm) much higher than the downstream fugacity (*cf*. Equation 2.6).

3.8. Pure Gas Solubility Measurement

Pure gas solubility of polymers in this project was determined using a dual-volume, dual-transducer apparatus, also constructed by the author based on the barometric, pressure-decay method [27, 98]. The schematic of this apparatus is given in Figure 3.2. The

polymer to be measured was placed in a sample cell of known volume, which was connected to a charge cell and a gas cylinder source. Both sample and charge cells were placed in a (35.0±0.1)°C water bath with a heating circulator for temperature control. Prior to experiments, the polymer was degassed by placing both charge and sample cells under vacuum overnight. In the first step, the charge cell of known volume was charged with a target gas at a known pressure. Then, the valve between the charge and sample cells was opened briefly to introduce gas into the sample cell; after valve closure, the sample cell pressure started to decay as the polymer sorbed the gas, and this decay was monitored by the transducers (SuperTJE® with 500 psig full scale range, Honeywell-Sensotec, connected to a National Instruments data acquisition system similar to that described in the previous section). When the sample cell pressure reached equilibrium, maximum sorption at this pressure had been achieved. The amount of gas sorbed into the polymer is thus the difference in the number of moles of gas initially admitted to the sample cell and of gas remaining in the sample cell at equilibrium. In the second step, more gas was introduced into the charge cell, and the aforementioned procedure was repeated. At step m, the number of moles of gas sorbed by the polymer, $n_{p,m}$, is [98]:

$$n_{p,m} = n_{p,m-1} + \left[\frac{p_{c,m-1} V_c}{RT Z_{c,m-1}} + \frac{p_{s,m-1}(V_s - V_p)}{RT Z_{s,m-1}} \right] - \left[\frac{p_{c,m} V_c}{RT Z_{c,m}} + \frac{p_{s,m}(V_s - V_p)}{RT Z_{s,m}} \right] \qquad (3.2)$$

where V_c, V_s and V_p are the volumes of the charge cell, sample cell, and polymer sample, respectively. The subscripts m and m-1 represent the properties at the step m and (m-1), respectively. Z refers to the compressibility factor of the gas at pressure p and can be calculated using the virial coefficients available from sources such as Dymond et al. [57]

for many gases at various temperatures. From these sequential measurements, the gas sorption isotherm (*i.e.*, as concentration *vs*. fugacity plot) in the polymer can be obtained, and the solubility can be calculated based on Equation 2.7.

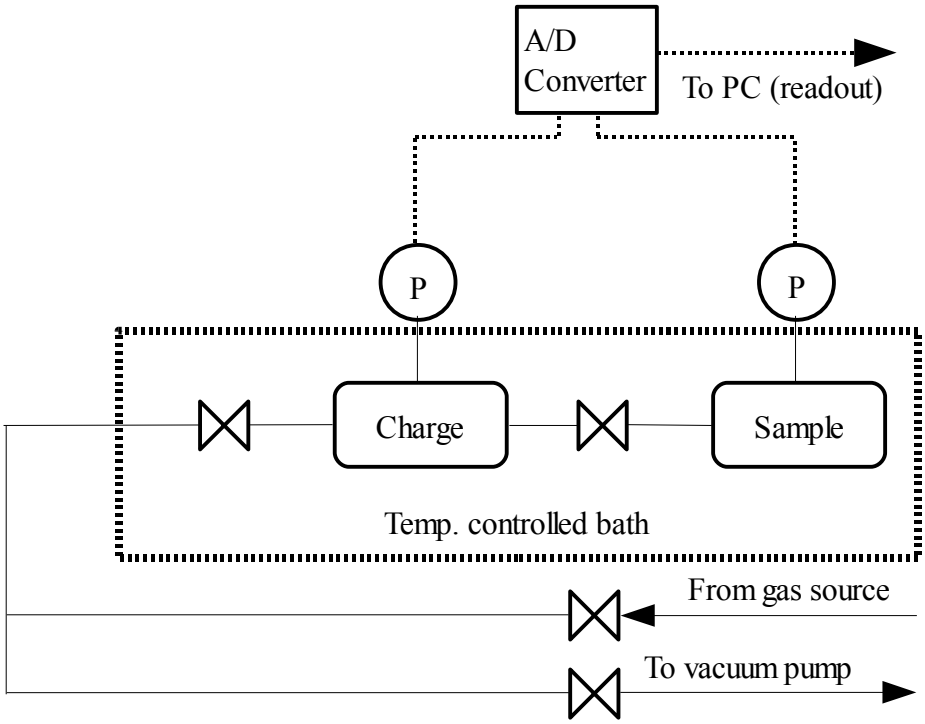

Figure 3.2: Schematic of pure gas sorption pressure-decay apparatus used in this project.

Accurate measurement of XLPEO gas solubility requires an understanding of the polymer's characteristics. In these polar materials, solubilities of non-polar gases are generally low [41]. As the value of $n_{p,m}$ is a result of subtraction of two much larger numbers (the amount of gas in the gas phase is much greater than in the polymer), steps were taken to minimize the measurement uncertainty. The SuperTJE® transducers, selected due to their high precision, were used to carefully calibrate the charge and sample cell volumes using the Burnett expansion method and steel balls with known

volume to modify the sample cell volume [101]. The uncertainty in cell volumes were estimated based on standard deviation of multiple pressure expansion measurements. Accurate measurements of the polymer volume and mass were needed as well, because XLPEO is hygroscopic [49] and can sorb a significant amount of water vapor from the atmosphere (typically up to 3 wt% at ambient conditions). Polymer mass measurements were thus typically performed at the same time as density measurements (*cf.* Section 3.4), yielding both mass and density (and thus volume) values for the degassed polymer films. The increased measurement rigor may result in different solubility values than previously reported for gases with lower solubility, such as methane. For instance, the infinite dilution solubility of methane in polymerized 100% PEGDA reported in this project, 0.075±0.03 cm^3(STP)/(cm^3 atm), is lower than the value reported by Lin et al., 0.11±0.02 cm^3(STP)/(cm^3 atm) [18]. The author has confirmed the recovery of sorption value reported by Lin et al. by performing the experiment on 100% PEGDA without the necessary mass and density corrections using this apparatus.

3.9. Uncertainty Analysis

All measurement uncertainties reported in this project were estimated using a standard propagation of errors analysis, where uncertainties of individual measured parameters propagate and contribute to the uncertainties of the parameters of interest [102], unless specified otherwise. In the author's experience, some parameters measured in this project have actual experimental uncertainties somewhat smaller than those estimated by the propagation of errors method.

Chapter 4: Properties of Cross-linked Poly(ethylene oxide): Prior Work and Modification Strategies

4.1. Summary

In Section 4.2, previous work related to structure/property characteristics of cross-linked polymeric membranes containing poly(ethylene oxide), XLPEO, is reviewed. XLPEO was prepared through photopolymerization of poly(ethylene glycol) diacrylate (PEGDA) in the presence of varying amounts of water or functionalized monoacrylates (*i.e.,* poly(ethylene glycol) acrylate, *n*=7 (PEGA) or poly(ethylene glycol) methyl ether acrylate, *n*=8 (PEGMEA)) to obtain networks with similar chemical composition but varying cross-link density. High concentrations of ethylene oxide units within the network improve the separation of quadrupolar carbon dioxide gas from mixtures with other light gases such as H_2, N_2, and CH_4. Dynamic mechanical analysis was used to assess the cross-link density variation in the networks as a function of initial reaction composition and to elucidate the time-temperature characteristics of the glass transition as a function of network structure. Gas permeability and diffusivity in these polymers

---

Sections 4.1 and 4.2 has been adapted with permission from an article published in *Advanced Membrane Technology and Applications* entitled "Structure/Property Characteristics of Polar Rubbery Polymeric Membranes for Carbon Dioxide Removal from Mixtures with Light Gases" [3], originally written by the author.

are essentially insensitive to cross-link density, but they can be very sensitive to the fractional free volume, which can be tuned by varying the concentration of acrylate side groups present in the networks. For the PEGDA/PEGMEA copolymers, fractional free volume correlated linearly with glass transition temperature, and this relation can be used to correlate the diffusivity and permeability of the network to various gases. The relationship permits an estimation of the influence of temperature and gas partial pressure on diffusion coefficients. Carbon dioxide/light gas separation performance in XLPEO compares favorably with the separation performance of other commonly-used polymers and the 'upper-bound' reported in the literature.

Based on earlier work described in Section 4.2, Section 4.3 describes the rationale for the material selection for further XLPEO modification.

4.2. Structure/Property Characteristics of Cross-linked Poly(ethylene oxide) for Gas Separation

4.2.1. Viscoelastic Properties of Cross-linked PEO Networks

The glass-rubber relaxation characteristics of the cross-linked PEO networks were studied using dynamic mechanical analysis [74, 75]. Figure 4.1 shows representative results (storage modulus versus temperature) for cross-linked PEGDA (n=14) and the PEGDA/PEGA copolymers. The modulus curves indicate a modest decrease in glass transition temperature (T_α; 1 Hz) with increasing acrylate content that reflects insertion

of the non-reactive PEGA branches into the polymer network; a similar effect, with an even stronger negative shift in glass transition temperature, was observed for the PEGDA/PEGMEA copolymers (see summary of transition temperatures in Table 4.1). The rubbery plateau modulus displays a systematic decrease with increasing PEGA (*i.e.,* decreasing cross-linker content). Rubbery modulus (E_R) is plotted versus PEGDA content in Figure 4.2 for the PEGDA/PEGA and PEGDA/PEGMEA copolymer networks, as well as for networks formed via the photopolymerization of PEGDA in the presence of water diluent. For all three series, a single relationship is observed between rubbery modulus and cross-linker content, implying that effective cross-link density (υ_e) depends solely on the amount of PEGDA cross-linker present in the reaction mixture, even though the structural details of the resulting networks may differ. Notably, for the PEGDA/water networks, no change in glass transition temperature is observed with varying effective cross-link density [18]. For this particular cross-linker (n=14), the modification in network structure that occurs with reaction in the presence of diluent apparently does not lead to a significant change in the constraint experienced by the chain segments at the length scale associated with the glass transition. Although the observed variation in rubbery modulus clearly indicates a reduction in effective cross-link density, the formation of loops or wasted cross-links in the presence of water has little influence on the resulting value of T_g [75].

Table 4.1: Characteristics of cross-linked PEGDA (n=14) and copolymer networks: T_α, dynamic mechanical peak temperature for glass transition (1 Hz); T_g, calorimetric glass transition temperature; β_{KWW}, KWW distribution parameter for glass-rubber relaxation; *FFV*, fractional free volume based on density measurements.

Co-monomer	PEGDA wt%	T_α [°C] (1 Hz)	T_g [°C]	β_{KWW}	*FFV* [a]
---	100	-35	-40	0.30	0.118
PEGMEA	80	-41	-44	0.33	0.122
	50	-47	-52	0.34	0.127
	30	-52	-57	---	0.128
PEGA	80	-38	-40	0.34	0.112
	50	-41	-42	0.35	0.112
	30	-42	-44	0.38	0.110

[a] *FFV* as published in this table and chapter were calculated with data and assumptions of Lin et al. (ref. [32]), and are thus not directly comparable with the author's original work in subsequent chapters: see ref. [2], Section 3.4 and Table 5.2 for the refined method. PEGDA/PEGMEA *FFV* calculated with the new method are presented in Figure 6.2. This table was based on ref. [74].

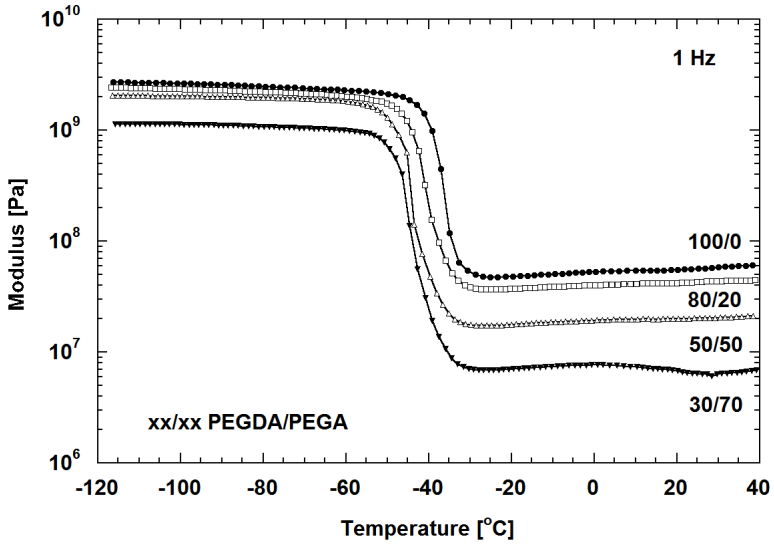

Figure 4.1: Storage modulus (E') versus temperature for PEGDA/PEGA copolymer networks with varying weight fraction PEGDA cross-linker. Composition in wt% PEGDA (from top to bottom): 100, 80, 50, 30. Frequency of 1 Hz; heating rate of 1°C/min. (Adapted with permission from [74])

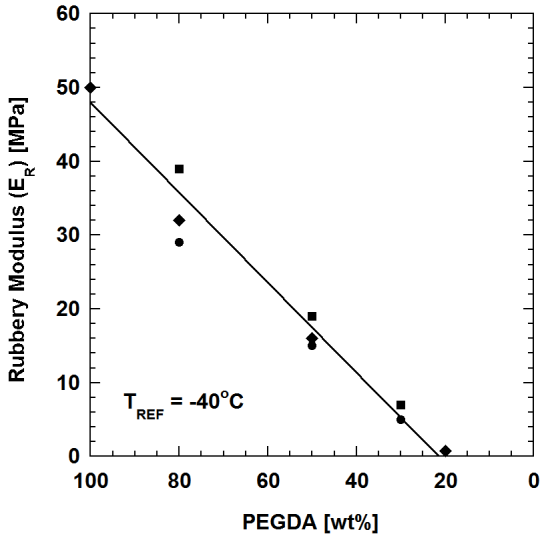

Figure 4.2: Rubbery modulus ($E_{R;}$ MPa) versus PEGDA cross-linker content for ●: PEGDA/PEGMEA, ■: PEGDA/PEGA, and ♦: PEGDA/water networks. E_R evaluated from time-temperature master curves at –40°C. (Adapted with permission from [74].)

Time-temperature superposition was used to establish master curves of storage modulus versus ωa_T, as shown in Figure 4.3 (for PEGDA/PEGA copolymer networks); the shift of the curves to higher frequency with PEGA content reflects a progressive decrease in relaxation time consistent with the observed trend in glass transition temperature. KWW curve fits (solid curves in Figure 4.3) indicate narrowing of the glass-rubber relaxation with decreasing overall cross-link density, as reflected in the value of the distribution parameter, β_{KWW}, which increases from 0.30 to 0.38 across the series; see Table 4.1. The relaxation narrowing suggests a reduction in the elastic constraint imposed by the cross-link junctions, leading to a more homogeneous relaxation environment at lower cross-link density. This result, which was also observed for the PEGDA/PEGMEA and

PEGDA/water series, is consistent with observations reported for comparable polymer networks of varying cross-link density [76-78, 103].

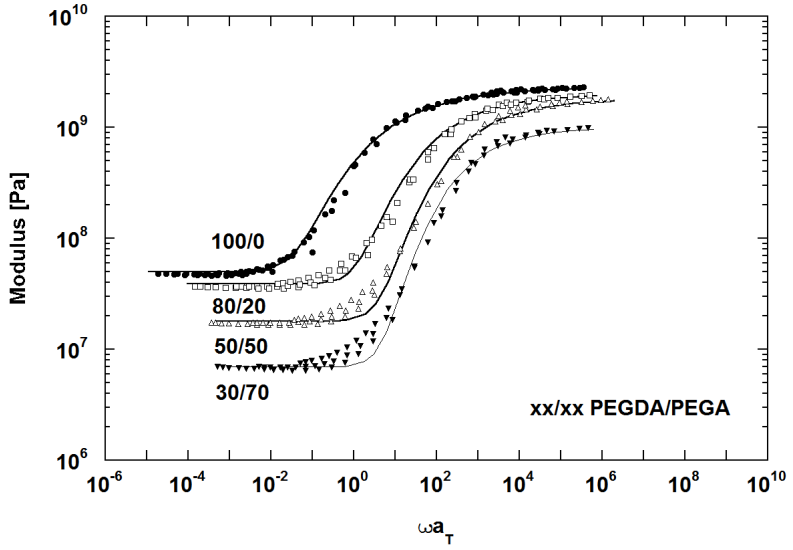

Figure 4.3: Time-temperature master curves for PEGDA/PEGA copolymer networks; T_{REF} = –40°C. Composition in wt% PEGDA (from top to bottom): 100, 80, 50, 30. Solid curves are KWW best fits (*cf.* Equation 2.19). (Adapted with permission from [74].)

An effective method for comparing the time-temperature relaxation characteristics of the networks is the construction of cooperativity plots [79], wherein the time-temperature shift factor is plotted as $\log(a_T)$ versus reciprocal temperature, expressed as T_α/T, where T_α is the dynamic mechanical glass transition temperature at 1 Hz. The cooperativity plot for the PEGDA/PEGA series is shown in Figure 4.4. The local slope of the individual curves reflects the activation energy associated with the glass transition process and indicates the relative intermolecular cooperativity inherent to the relaxation in each network. For the PEGDA copolymer networks, decreasing cross-link density leads to a

gradual reduction in apparent activation energy (*i.e.,* fragility), which is consistent with the relaxation of a less constrained network in which the underlying motional processes encompass a lower degree of intermolecular cooperativity [104, 105]. The observed behavior, which is characteristic of many homopolymer network systems with varying cross-link density, suggests that the glass-rubber relaxation process in the PEGDA copolymer networks is not substantially altered or impeded by the introduction of the pendant branches. In fact, the segmental motions occurring along the ethylene oxide segments in the pendant branches are likely to be very similar in character to those occurring across the PEGDA cross-link bridges; as such, the presence of branches does not significantly change the time-temperature character of the glass transition. The decrease in cooperativity that is evident in Figure 4.4 is due primarily to the net decrease in cross-link density with increasing branch content.

The presence of the pendant branches does, however, lead to a decrease in the glass transition temperature for the copolymer networks as measured by both dynamic mechanical and calorimetric methods (*cf.* Table 4.1), as the non-reactive chain ends opens up free volume in the network structure. This effect is more pronounced for the PEGDA/PEGMEA copolymers (–OCH_3 branch ends) as compared to the PEGDA/PEGA copolymers (–OH branch ends). For the PEGDA/PEGMEA copolymers, the decrease in T_g is accompanied by a progressive increase in fractional free volume (*FFV*) as determined using Equation 2.14, see Table 4.1. Interestingly, for the PEGDA/PEGA copolymers, a small *decrease* in *FFV* is observed with increasing PEGA branch content.

As will be shown in Sections 4.2.2 and 5.3.2, this relatively minor difference in network structure (–OCH_3 vs. –OH end group) strongly influences the gas transport properties of these rubbery networks.

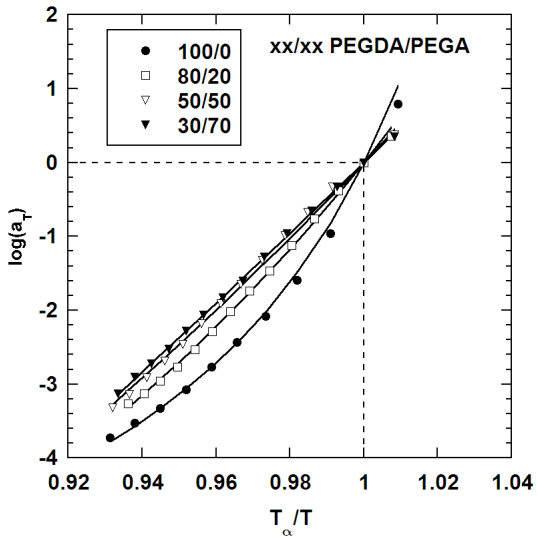

Figure 4.4: Cooperativity plots (log(a_T) vs T_α/T) for PEGDA/PEGA copolymer networks. Solid curves are WLF (Williams-Landel-Ferry) fits, as defined in reference [84]. (Adapted with permission from [74].)

4.2.2. Correlation of Structural Detail of the Membrane with Gas Transport Properties

To analyze the effect of cross-link density and structural details on the gas transport properties of XLPEO, samples with varying degrees of cross-linking were subjected to permeability measurements using selected gases. Figure 4.5a presents the CO_2 permeability at infinite dilution [32]. The infinite dilution permeability of the

PEGDA/PEGMEA network increased by more than 400%, from 110 to 580 barrer, as PEGDA content was decreased from 100 to 1.3 wt%. In contrast, the infinite dilution permeability of the PEGDA/PEGA network remained relatively constant (110 barrer) with varying PEGDA content. For comparison, samples of PEGDA diluted before photopolymerization with different amounts of water were tested: dilution reduced the effective cross-link density of the network, as shown in Figure 4.2. In this case, the permeability increased from 110 to 140 barrer as water content increased from 0 to 80 wt %, so cross-link density *per se* had only a minimal effect on the permeability of the polymer membranes.

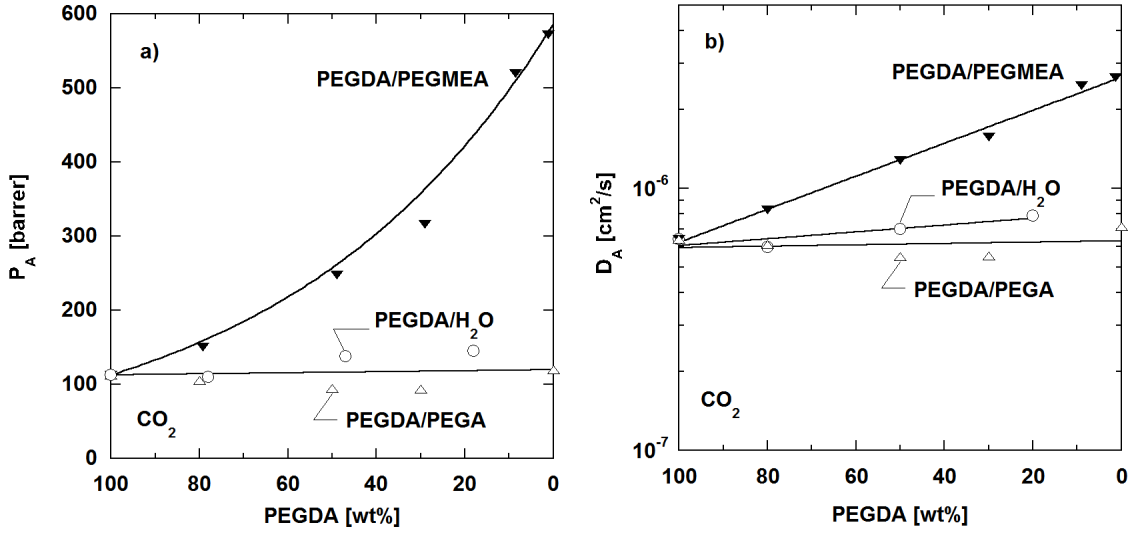

Figure 4.5: CO_2 infinite dilution (a) permeability and (b) diffusivity through XLPEO to downstream vacuum as a function of PEGDA content in the prepolymer solution; 35°C. D_A is calculated from P_A based on Equation 2.6. (Reprinted with permission from [32].)

To understand the effect of network structure on permeability, the diffusion coefficients for each system were calculated based on independent sorption studies, and the results are presented in Figure 4.5b. Comparison with Figure 4.5a reveals similar trends, such that the observed permeability variation can be attributed mostly to a change in penetrant diffusivity in the networks. In a homogeneous blend, gas transport properties (*X)* such as permeability or diffusivity are often modeled empirically as [106]:

$$\ln X = \varphi_1 \ln X_1 + \varphi_2 \ln X_2 \qquad (4.1)$$

where φ_i is the volume fraction of component *i*, and the subscripts *1* and *2* correspond to components *1* and *2*, respectively. The volume fractions were estimated as follows: $\varphi_1 = \rho_P w_1/\rho_1$, where w_1 is the weight fraction of component 1 in the copolymer, ρ_P is the density of the copolymer, and ρ_1 is the density of pure polymerized component 1; $\varphi_2 = 1 - \varphi_1$. This equation, represented as the solid curves in Figure 4.5a, satisfactorily predicts the change in gas permeability with varying PEGDA content; the equation takes into account only the correlation between permeability and composition of the polymer blends and copolymers, and does not account for cross-link density. Therefore, the changes in CO_2 permeability can be attributed mainly to the influence of the methoxy ($-OCH_3$) chain end groups on bulk density and not to variations in cross-link density. The presence of the methoxy chain end groups increases the polymer fractional free volume and, therefore, the diffusivity of gases through the network (see *FFV* values in Table 4.1); a detailed analysis of this result has been published separately [32, 88].

Since permeability of gases in these systems depends primarily on diffusivity, Equation 2.12 can be used to correlate the network selectivity (calculated from measured pure gas permeabilities) with *FFV* using previously calculated adjustable constants (Table 2.1) [43, 56]; the selectivity values for several CO_2/light gas systems are presented in Figure 4.6 and compared with model calculations as described below. The lines through the data points were calculated using the following free volume model derived from Equations 2.8 and 2.13:

$$\alpha_{A/B} = \frac{A_{P,A}}{A_{P,B}} \exp\left(\frac{B_B - B_A}{FFV}\right) \qquad (4.2)$$

which predicts that CO_2/light gas selectivity increases with increasing *FFV* if the light gas is smaller than CO_2, and that CO_2/light gas selectivity decreases with increasing *FFV* if the light gas is larger than CO_2. For the gas pairs shown in Figure 4.6, H_2 is smaller than CO_2, while N_2 and CH_4 have larger kinetic diameters. For each gas pair considered, the selectivity values indicate preferential permeation of CO_2 ($\alpha > 1$); in the case of CO_2 and H_2, CO_2/H_2 selectivity ranges from 7 to 12, showing that these networks have high permeability and high "reverse-selectivity".

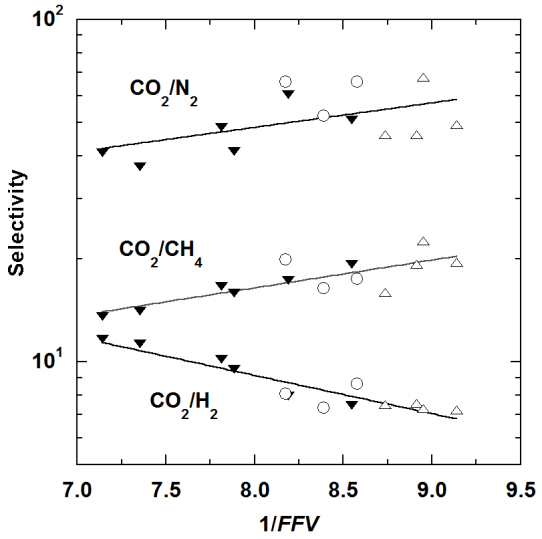

Figure 4.6: Correlation between pure gas selectivity and fractional free volume, *FFV*, for various XLPEO networks. Symbols correspond to those used in Figure 4.5. Permeability data used were as extrapolated to infinite dilution. (Reprinted with permission from [32].)

4.2.3. Temperature and Pressure Effects on the Transport Properties of XLPEO

Temperature plays an important role in determining the transport performance of any membrane. Usually, with increasing temperature, permeability of all penetrants increases, as described by the Van't Hoff-Arrhenius expression [1, 62]:

$$P_A = P_{A0} \exp\left(\frac{-E_P}{RT}\right) \qquad (4.3)$$

This behavior is demonstrated in Figure 4.7a, where CO_2 permeability data for selected PEGDA/PEGMEA copolymers are plotted against reciprocal temperature according to Equation 4.3. Higher temperatures and greater PEGMEA content lead to higher permeability.

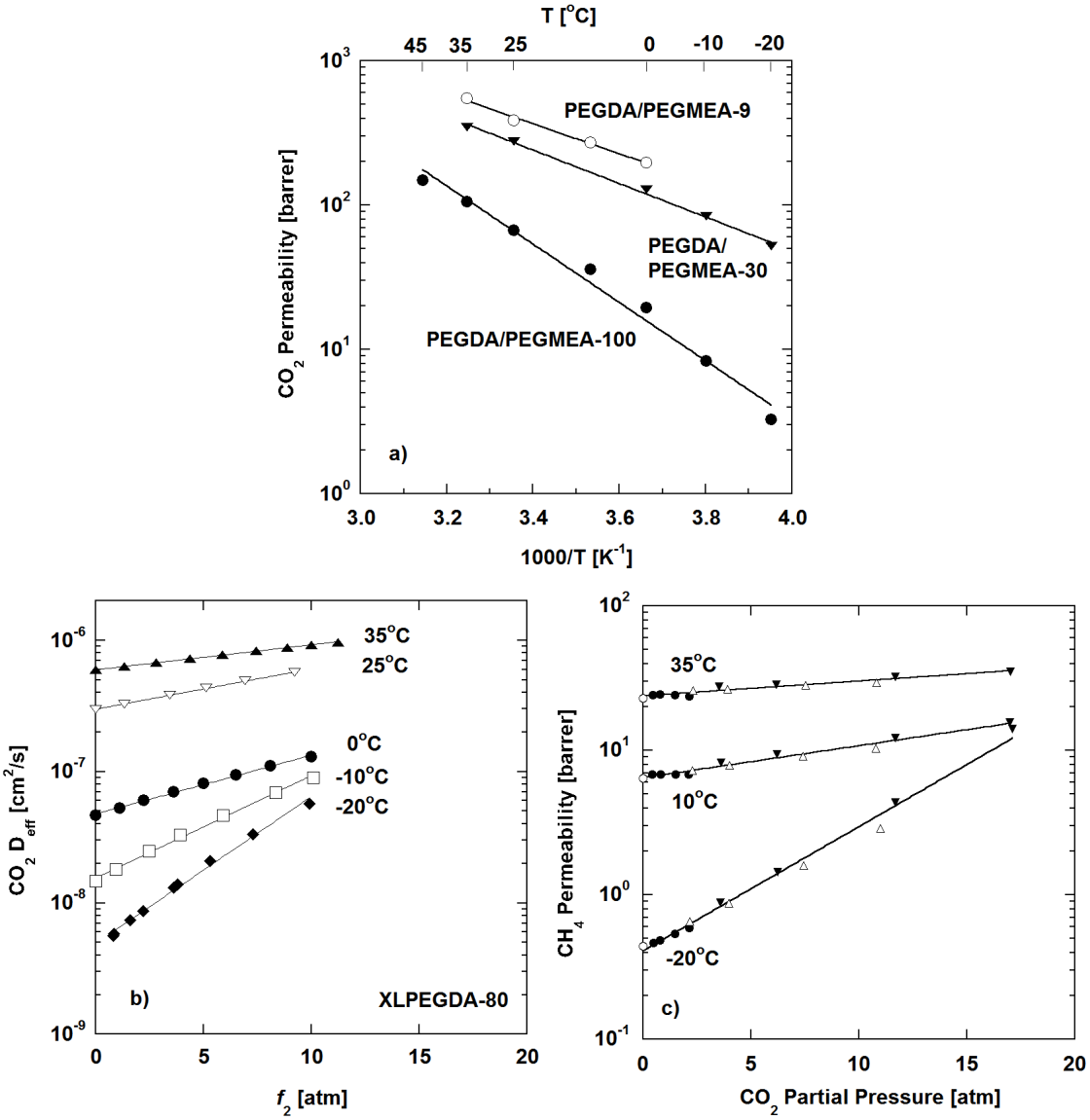

Figure 4.7: (a) Effect of temperature and polymer composition on CO_2 permeability for various PEGDA/PEGMEA networks. (b) Effect of pure CO_2 upstream fugacity and temperature on CO_2 diffusion coefficient in XLPEGDA-80. (c) Effect of CO_2 partial pressure on CH_4 permeability in PEGDA/PEGMEA-30 from CO_2/CH_4 gas mixtures. The different symbols denote different CO_2/CH_4 mixed gas compositions (○: pure CO_2, ●: 10% CO_2, Δ: 50% CO_2, and ▼: 80% CO_2). XX in PEGDA/PEGMEA-XX refers to the weight percent of PEGDA in the prepolymer mixture with PEGMEA, while XX in XLPEGDA-XX refers to the weight percent of PEGDA in the prepolymer mixture with water.

The influence of temperature on gas diffusion coefficients is presented in Figure 4.7b, which shows pure gas CO_2 diffusivity at various temperatures as a function of CO_2 fugacity for cross-linked PEO prepared by photopolymerization of PEGDA cross-linker in the presence of 20 wt% water. As indicated by these data, diffusivity increases as temperature increases.

In this series of experiments, CO_2 diffusivity increases much more strongly with fugacity at lower temperatures than at higher temperatures. For example, from Figure 4.7b, CO_2 diffusivity increases from 6×10^{-7} cm^2/s to 9×10^{-7} cm^2/s as fugacity increases from 0 to 10 atm at 308 K; in contrast, at 253 K, diffusivity increases by a full order of magnitude, from 6×10^{-9} cm^2/s to 6×10^{-8} cm^2/s, over a similar fugacity range. This difference can be attributed to the plasticization effect of sorbed CO_2 in the polymer, leading to an increase in fractional free volume and in turn, gas diffusivity [44]. Because CO_2 sorption increases as temperature decreases [56], the plasticization effect of CO_2 on diffusivity is more pronounced at lower temperatures.

Figure 4.7c presents the influence of CO_2 partial pressure on CH_4 permeability in CO_2/CH_4 mixed gas permeation experiments. In this case, the presence of CO_2 strongly increases the permeability of CH_4. This effect is believed to be linked to plasticization of the polymer matrix by CO_2, which would act to increase the *FFV* and, in turn, CH_4 permeability. This effect is more pronounced at lower temperature since, at a given partial pressure of CO_2, the thermodynamic activity of CO_2 (and, therefore, the CO_2

concentration in the polymer) is higher. CH_4 is much less soluble than CO_2, so the permeation properties of both CO_2 and CH_4 are essentially independent of CH_4 partial pressure [56]. For the so-called "reverse-selective" separations such as the removal of CO_2 from H_2, plasticization by CO_2 actually *improves* separations performance by increasing gas permeability without loss of selectivity in rubbery XLPEO, which does not depend on size-sieving ability to achieve good separation performance [44].

4.2.4. Modified Free Volume Model

The general relationship between permeability and fugacity, as given in Equation 2.10, can be substituted into Equation 2.5 to estimate diffusion coefficients as a function of temperature and penetrant concentration [16, 59]. However, because $P_{A,o}$ and $m_{P,E}$ values are required for each gas at each temperature of interest, a large number of empirical parameters are needed to characterize diffusivity in a particular material [43]. To address this shortcoming, a model based on free volume theory was used to correlate the data, as described below.

An increase in the concentration of methoxy ($-OCH_3$) chain end groups in the PEO copolymers leads to an increase in diffusivity and permeability due to enhanced polymer *FFV*. This result was confirmed by Positron Annihilation Lifetime Spectroscopy (PALS) measurements: as the concentration of methoxy chain end groups in the PEGDA/PEGMEA networks rises, the *FFV* as probed by PALS increases [43]. In addition, the glass transition temperature as measured by the calorimetric method (T_g) in

these polymers decreases as the methoxy chain end group concentration (*i.e.*, PEGMEA concentration) increases. T_g has been correlated with *FFV* in rubbery PEO according to the following expression [107, 108]:

$$FFV = FFV(T_g) + \alpha_r (T - T_g) \qquad (4.4)$$

where $FFV(T_g)$ is the apparent fractional free volume at T_g (also known as the Simha-Boyer isofree volume [109]) and α_r is the thermal expansion coefficient of the fractional free volume. This equation assumes that the volume occupied by the polymer above its T_g remains constant with temperature, which is an approximation [17, 107]. Figure 4.8 presents this correlation for a series of PEGDA/PEGMEA copolymers with varying concentrations of methoxy chain end groups. Assuming that α_r is independent of copolymer composition, Equation 4.4 can be used to fit the data, as per the straight line shown in Figure 4.8. Based on this result, $FFV(T_g)$ is 0.055 ± 0.001, and α_r is (8.4 ± 2.6) × 10^{-4} K^{-1} [44]. These values were obtained by taking T = 35°C while using polymer density data taken at ambient temperature. For the sake of consistency, these assumptions are employed in the calculations of free volume correlation with T_g throughout this project. The value of $FFV(T_g)$ agrees with "universal" values estimated for other polymeric materials [107]: 0.113, according to Simha and Boyer [109], and 0.025, as the result of the WLF (Williams-Landel-Ferry) equation [84, 110]. Likewise, the value of α_r is similar to the magnitude of the thermal expansion coefficient of amorphous PEO chains as estimated from dilatometry measurements on poly(ethylene oxide) dimethyl ether (M_w = 1000); the reported value is 7.8 × 10^{-4} K^{-1} [111].

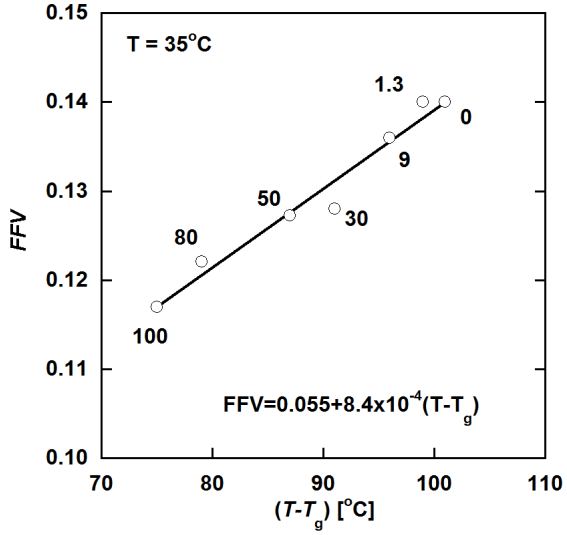

Figure 4.8: Correlation of *FFV* and (T - T_g) based on Equation 4.4 for various PEGDA/PEGMEA networks [17]. The numbers above each data point indicate the weight percent of PEGDA in the prepolymerization mixture with PEGMEA.

The correlation between *FFV* and (T - T_g) as defined in Equation 4.4 can be combined with the Fujita-modified Cohen-Turnbull model (Equation 2.12) to obtain an equation relating diffusivity to temperature and $FFV(T_g)$ [43]:

$$D_{eff} = A_D \exp\left(\frac{-B}{0.055 + 8.4\times10^{-4}(T - T_g)}\right) \qquad (4.5)$$

This model is then used in Figure 4.9a to correlate CO_2 infinite dilution diffusivity at 35°C in various PEGDA/PEGMEA networks; the experimental results are provided to illustrate the fit, which appears to provide a reasonable description of these PEO-containing materials at 35°C. The adjustable parameters found are given in Table 2.1. In Figure 4.9b, the model is used to describe infinite dilution diffusivity of CO_2 in similar systems at different temperatures. Thus, the model can be generalized to correlate CO_2 diffusivity within similar PEO-containing systems across a range of temperatures.

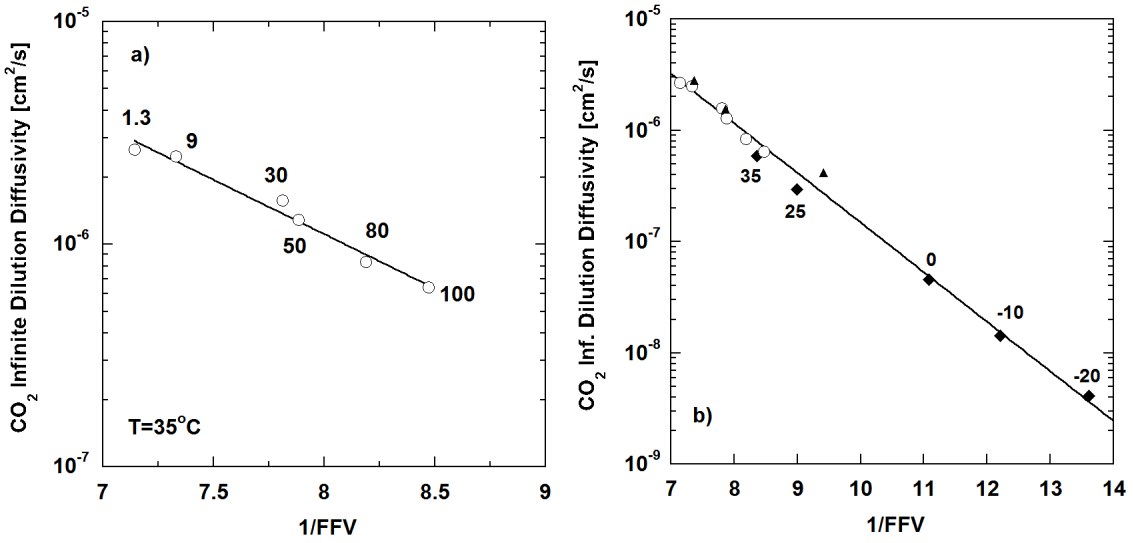

Figure 4.9: Infinite dilution diffusivity of CO_2 as function of 1/*FFV* for several PEGDA/ PEGMEA networks at (a) 35°C and (b) several temperatures, showing the general application of Equation 4.5. The numbers above each data point in Figure 4.9a indicate the weight percent of PEGDA (*i.e.*, cross-linker) in the prepolymerization mixture with PEGMEA. In Figure 4.9b, ○ represents PEGDA/PEGMEA at 35°C with various compositions, ▲ represents PEGDA/PEGMEA-9 (contained 9% PEGDA in prepolymer mixture) at various temperatures, and ♦ represents XLPEGDA-80 (prepared using 80% by weight PEGDA in prepolymer mixture with water) at various temperatures, denoted above the data points in [°C].

The free volume model can be extended beyond infinite dilution in the case of strongly sorbing components like CO_2. As CO_2 sorbs into the polymer matrix, the polymer swells, resulting in enhanced segmental mobility and a depression in T_g, and, therefore, an increase in diffusivity as indicated by Equation 4.5 [112]. Chow proposed an expression relating T_g depression to diluent concentration [113]:

$$\ln\frac{T_g}{T_{g0}} = \beta[(1-\theta)\ln(1-\theta)+\theta\ln\theta] \qquad (4.6)$$

where

$$\theta = \frac{M_p}{z M_d} \frac{w_2}{1 - w_2} \qquad w_2 = \frac{C_2 M_d}{C_2 M_d + 22414 \rho_p} \qquad \beta = \frac{z R}{M_p \Delta C_{pp}}$$

Here T_{g0} and T_g are the glass transition temperatures of pure polymer and the polymer-diluent mixture, respectively, when the diluent weight fraction is w_2. M_p and M_d are the molecular weights of the polymer repeat unit (taken as 44 g/mole, the molecular weight of an ethylene oxide moiety, in this study) and diluent, respectively. ρ_p is the polymer density. ΔC_{pp} is the change in heat capacity of the pure polymer at its glass transition, 0.99 J/(g °C), which was obtained from differential scanning calorimetry (DSC) experiments [43]. Lin et al. combined Equation 4.6 with Equation 4.5 to predict the quantitative effect of CO_2 concentration on diffusivity as a function of temperature and CO_2 partial pressure [43, 88]. This "modified free volume" model uses a single parameter (*FFV*) and two adjustable parameters, A_D and B in Equation 4.5, to describe the effect of temperature and pressure on gas diffusion coefficients.

Based on this model, Figure 4.10a presents the effect of temperature and pressure on CO_2 diffusivity in two different cross-linked PEO materials. The permeation properties of CH_4, a co-permeant in gas mixtures with CO_2, may also be correlated with *FFV* using this model. Unlike CO_2, CH_4 experiences little solubility changes with temperature [56], so CH_4 permeability can be plotted directly against $1/FFV$ at different temperatures and partial pressures of CO_2, as shown in Figure 4.10b. Again, there is good agreement between the model and the experimental results.

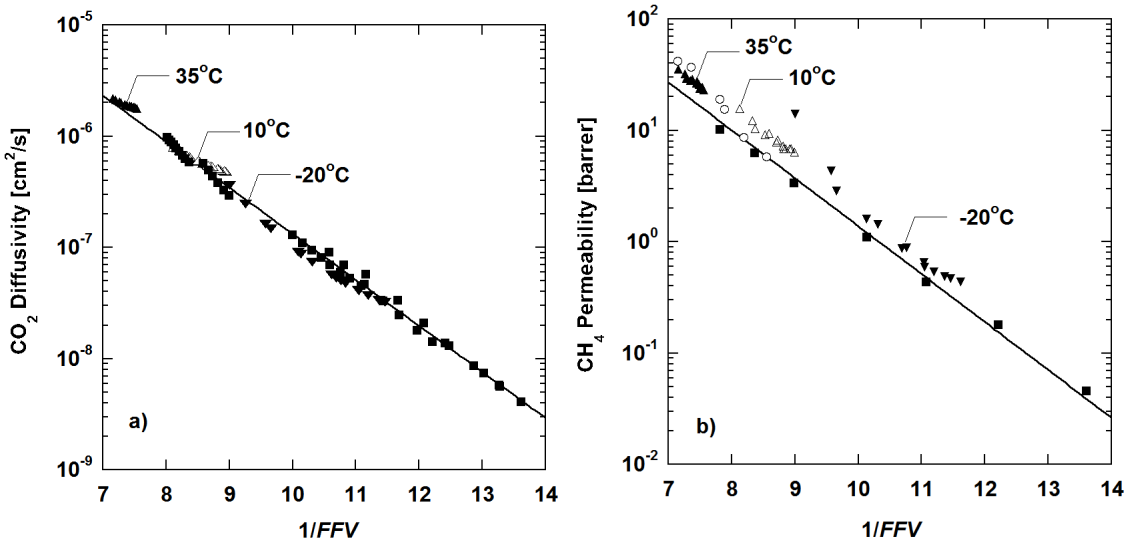

Figure 4.10: (a) Diffusivity of CO_2 as a function of 1/*FFV* for PEGDA/PEGMEA networks, and (b) mixed gas permeability of CH_4 as a function of 1/*FFV* for several PEGDA/PEGMEA networks, at several temperatures and partial pressures of CO_2, showing the general application of Equation 4.5. (■ denotes PEGDA/PEGMEA-100, ▲▼Δ denote PEGDA/PEGMEA-30 at various designated temperatures, and ○ denotes PEGDA/PEGMEA-1.3)

4.2.5. Performance of XLPEO Relative to the Upper Bound

The performance of XLPEO for CO_2 removal compares favorably to other polymers in terms of permeability and selectivity, quantities that are often plotted against each other as a basis of comparison between various materials. A characteristic trade-off is observed between permeability and selectivity for polymeric membranes: more permeable polymers are generally less selective, and vice versa. This trade-off was first described empirically by Robeson [114] in examining the selectivity of several gas pairs in glassy polymers at 35°C, and was later determined to be a function of factors such as the ratio of the kinetic diameters of the penetrants, expressed as [36]:

$$\ln \alpha_{A/B} = -\left[\left(\frac{d_B}{d_A}\right)^2 - 1\right] \ln P_A + \left\{\ln\left(\frac{S_A}{S_B}\right) - \left[\left(\frac{d_B}{d_A}\right)^2 - 1\right] \times \left(b - f\left(\frac{1-a}{RT}\right) - \ln S_A\right)\right\} \quad (4.7)$$

where d_A and d_B are the kinetic diameters of the penetrants, a and b are gas species-independent parameters where a has a universal value of 0.64 and b has a value of $-\ln(10^{-4}\ \mathrm{cm^2/s}) = 9.2$ for all rubbery polymers [115, 116], and f is a polymer-dependent parameter related to the average distance between polymer chains. For rubbery polymers, f may be set to zero as a first approximation [36]. The selectivity of CO_2 relative to various gases of interest is plotted against CO_2 permeability in the cross-linked PEO family of materials in Figure 4.11 and compared to other previously studied materials.

Figure 4.11a compares the separation characteristics of XLPEO to those of cellulose acetate (CA) [45]. Mixed gas CO_2/CH_4 selectivity values in XLPEO and in CA are similar, but XLPEO is more than an order of magnitude more permeable to CO_2. At 253 K, the separation performance of XLPEO at high CO_2 partial pressure exceeds the Robeson upper bound limit [114]. Similar performance can be observed in Figures 4.11b and 4.11c for CO_2/N_2 and CO_2/O_2, respectively. In these cases, the performance of cross-linked PEO generally exceeds the upper bound within the limits of our studies. In Figure 4.11d, CO_2/H_2 separation performance, based on mixed gas studies in the case of XLPEO, is compared with the performance of other materials. Since the kinetic diameter of H_2 is smaller than that of CO_2 (2.89 Å as opposed to 3.3 Å, see Table 2.2), the upper

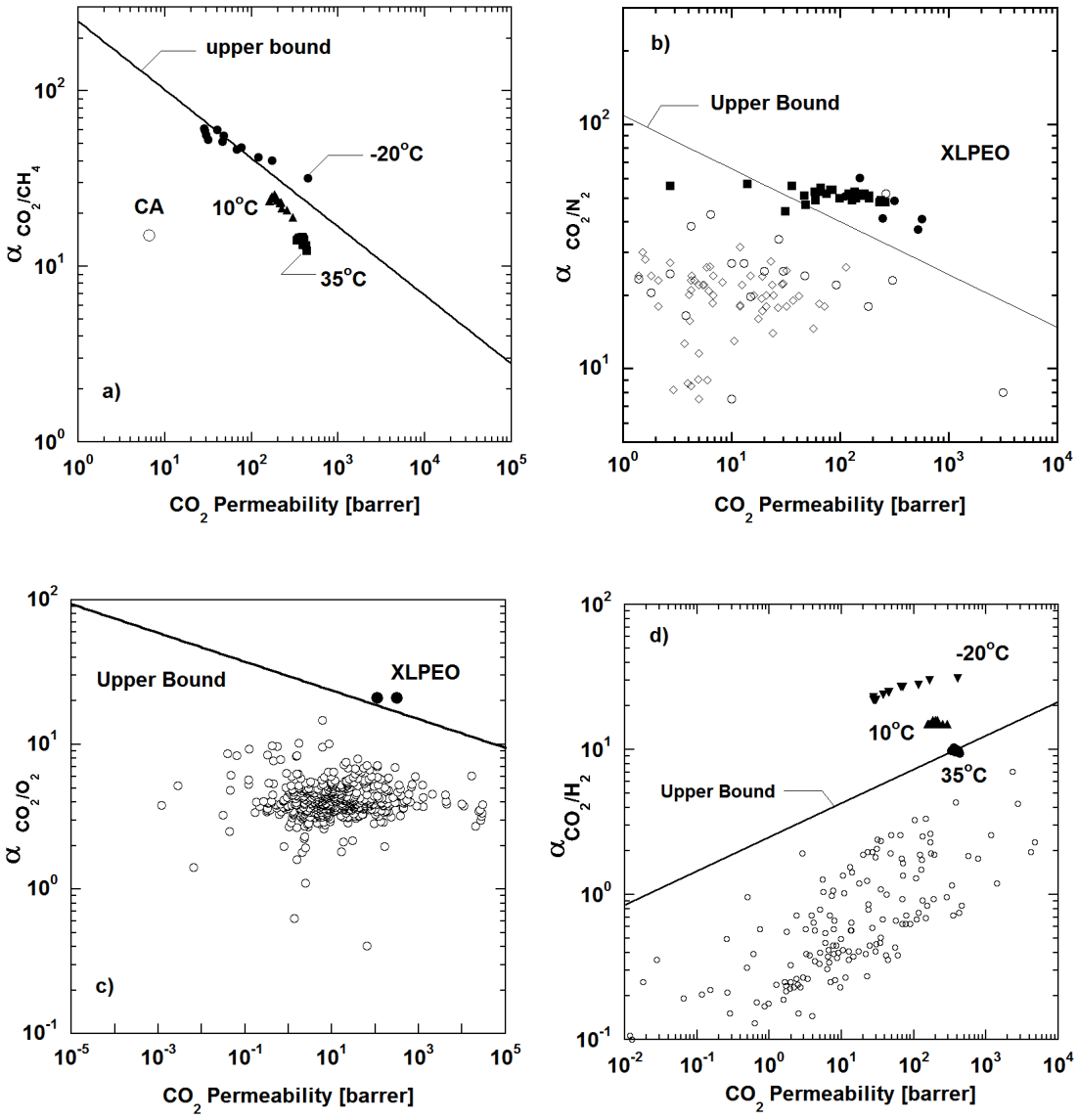

Figure 4.11: Permeability/selectivity performance map of XLPEO for (a) CO_2/CH_4, (b) CO_2/N_2, (c) CO_2/O_2, and (d) CO_2/H_2, showing the upper bound calculated by Equation 4.7 [36] or defined by Robeson [114]. Comparisons with cellulose acetate (CA) and other previously studied systems are provided wherever available [114, 117]. PEO-based materials are depicted as solid symbols.

bound line constructed in Figure 4.11d has a positive slope, as per Equation 4.7. Therefore, unlike separation based on strong size-sieving ability (which always results in

a distinct trade-off between permeability and selectivity), high CO_2 permeability and high CO_2/H_2 selectivity can be realized simultaneously with reverse-selective membranes: increased permeability in the rubbery polymer networks is achieved by increasing *FFV* and corresponding diffusivity for all penetrants, thus reducing sieving effects and unfavorable selectivity based on relative size. Indeed, the materials exhibit excellent separation performance for CO_2/H_2 mixtures, and lowering the temperature moves the separation performance above the defined upper bound.

4.3. Cross-linked Poly(ethylene oxide) Modification Strategies

Polymers based on PEGDA (n=14) copolymerized with either PEGMEA or PEGA represent a small subset of cross-linked poly(ethylene oxide) copolymers. Due to the versatility and reactivity of the acrylate polymerization, almost any acrylate or methacrylate functionalized co-monomer can be considered for polymerization. It is important, therefore, to identify basic molecular design rules to direct the selection of co-monomers that will most improve transport properties, *i.e.*, increasing gas permeability and/or increasing CO_2/light gas selectivity.

Gas permeability can be increased through diffusivity, which is generally considered a strong function of *FFV* (*cf*. Equation 2.13). This relationship was demonstrated by PEGMEA copolymerization with PEGDA (*cf*. Figure 4.5), indicating that mono-functional acrylates with certain functional non-polar endgroups (such as $-OCH_3$) may increase local free volume. Similar results are anticipated for polymers terminated with

longer alkoxy groups, *e.g.*, ethoxy (-OC_2H_5) groups. As the current longest commercially available EO-bearing ethoxy-terminated monoacrylate contains only two ethylene oxide repeat units per molecule (*i.e.*, DEGEEA), a more direct comparison may be made with one methoxy-terminated and one hydroxy-terminated co-monomers of shorter ethylene oxide length. This strategy has the added advantage of elucidating the effect of modifying the side-chain length of the co-monomer on polymer properties, by comparison with PEGA and PEGMEA. The comparison of 2-HEA, EGMEA and 2-EEA as co-monomers (*cf*. Table 3.2) is given in Chapter 5, and incorporation of DEGEEA as a co-monomer is explored in Chapters 6 and 7.

In a similar vein, *FFV* can be increased by introducing a co-monomer with certain other bulky non-polar end-groups that may also increase local free volume. Commercially-available phenoxy-based co-monomers (-OC_6H_5) are easily incorporated into PEGDA; the study of these copolymers is also given in Chapter 6. In addition, a co-monomer with bulky end-group has been synthesized in the course of soft contact lens material research [118]; this co-monomer (popularly known as TRIS) contains bulky trimethylsilyl groups attached by flexible siloxane bonds to the methacrylate functional group. An acrylate analog of this molecule (TRIS acrylate, or TRIS-A) has been copolymerized with PEGDA, and the results are reported in Chapter 7.

CO_2/light gas selectivity can be increased by modifying the chemical properties of the polymer to increase carbon dioxide affinity with the matrix. Intuitively, this is achieved

by increasing the ethylene oxide (EO) content of the constituent monomers. PEGDA (n=14) already contains a significant amount of EO (nominally 82 wt% by molecular weight) [18], with the co-monomers PEGA and PEGMEA containing similar amounts of EO by weight. While many acrylate-functionalized PEGDA materials with different EO chain lengths are available commercially, there are shortcomings in using some of these cross-linkers. As shown in Figure 4.12, PEGDA (n=23), for instance, begins to exhibit significant crystallization of the EO chains, consistent with prior observation of crystallization in straight chain PEO with molecular weight above 600 Daltons [21, 119]. Although the EO content increases, the potential gains in selectivity may be offset by the loss of permeability associated with crystal structure formation. On the other hand, decreasing the PEGDA chain length may lead to increased cross-link density and better mechanical properties (as characterized by rubbery modulus [75]). However, these benefits are countered by the decreased EO content and subsequent loss in CO_2-favoring selectivity [120]. In addition, decreasing chain length between cross-links also leads to greater chain stiffness and associated loss of permeability due to higher activation energy for diffusion. In the extreme case, cross-linked PEGDA (n=3) loses its rubbery character altogether at 35°C due to its high cross-link density, indicated by inhomogeneous broadening of the glass transition regime [75, 77] (*cf*. Figure 4.12). Patel et al. noted that CO_2 permeability in XLPEGDA (n=3) is approximately an order of magnitude below that in XLPEGDA (n=14) [120]. FTIR analysis also shows that this polymer cannot achieve 100% acrylate conversion due to vitrification during the reaction [34, 75], which impedes the diffusion of unreacted monomer for further reaction propagation [35].

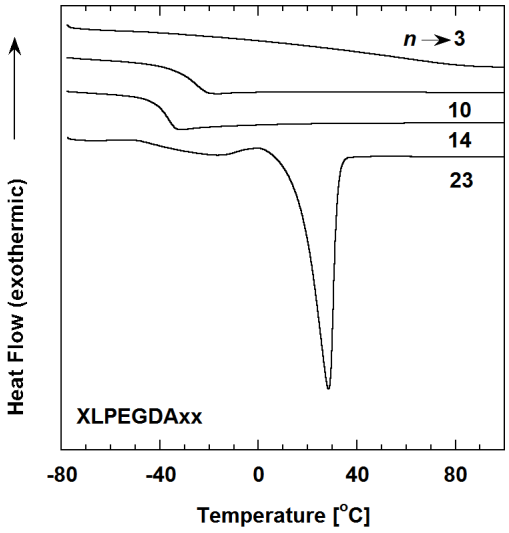

Figure 4.12: Second scan heating curve of cross-linked PEGDA with various EO chain length as obtained by the DSC, with heating rate of 10°C/min. Crystallization is observed in XLPEGDA23. The thermograms have been displaced vertically for clarity. *n* is the number of ethylene oxide units in the PEGDA.

An interesting strategy for monomer modification is inserting a bulky functional group to interrupt the continuous chain of ethylene oxide moieties, thus keeping EO content high while simultaneously preventing crystallization. A commercially available diacrylate series, bisphenol-A ethoxylate diacrylate (BPAEDA), is essentially a PEGDA analog with the EO chain symmetrically interrupted by a bisphenol-A group (*cf*. Table 3.1). The properties of a few BPAEDA-based copolymers are reviewed in Chapter 8. The bisphenol-A group successfully suppresses crystallization in BPAEDA (n=15), in particular, despite the presence of 30 EO moieties between the diacrylate groups.

Other modification strategies are discussed in Chapter 9, as part of the recommendations arising from the results of this project.

Chapter 5: Influence of Chemical Structure of Short Chain Pendant Groups on Gas Transport Properties of Cross-linked Poly(ethylene oxide) Copolymers

5.1. Summary

Three series of amorphous cross-linked poly(ethylene oxide) (XLPEO) rubbers were prepared by photopolymerization of prepolymer solutions containing poly(ethylene glycol) diacrylate (PEGDA) cross-linker and one of three structurally similar short chain acrylate co-monomers: 2-hydroxyethyl acrylate (2-HEA), ethylene glycol methyl ether acrylate (EGMEA) and 2-ethoxyethyl acrylate (2-EEA). Copolymerization with the mono-functional acrylates led to the insertion of short side branches along the network backbone, terminated by either hydroxy, methoxy or ethoxy functional groups. Permeability measurements for the copolymers (35°C) are presented for CO_2, H_2, CH_4, O_2 and N_2; corresponding solubility and diffusivity data are presented for CO_2 and CH_4. The side branches significantly influenced the thermal and gas transport properties of the polymers: methoxy and ethoxy terminated side-branches modestly increased free volume and gas permeability. This effect was pronounced by the introduction of ethoxy-terminated 2-EEA, while the presence of hydroxy terminated 2-HEA side-branches

This chapter has been adapted with permission from an article published in the *Journal of Membrane Science* under the same title [2], originally written by the author.

reduced free volume, resulting in a strong decrease in gas permeability with increasing co-monomer content. In each case, gas diffusivity correlated with polymer fractional free volume, while gas solubility was a function of both free volume characteristics and the corresponding concentration and accessibility of polar groups within the networks. The resulting selectivity ratios reflected variations in penetrant affinity and size discrimination as a function of copolymer composition. This chapter highlights the significant changes in various XLPEO properties that can be achieved by making small changes to its network structure.

5.2. Introduction

Variations in the XLPEO chemical structure can be achieved by copolymerizing PEGDA with other acrylate-functionalized PEO oligomers, and these structural variations influence both the transport properties [18, 32] and chain flexibility [74, 86] of the resulting cross-linked network. In Chapter 4, XLPEO samples were synthesized from mixtures of PEGDA with one of two monoacrylate co-monomers with similar chemical composition and ethylene oxide content: PEGA or PEGMEA (*cf.* Table 3.2) [32]. As the amount of -OCH_3 terminated PEGMEA increased, gas permeability rose significantly. For instance, CO_2 permeability (35°C) increased from 110 barrer to 510 barrer with addition of 90 wt% PEGMEA to PEGDA (*cf.* Figure 4.5). Adding PEGMEA branches increased polymer free volume, lowered glass transition temperatures and, in turn, increased gas diffusivity and permeability [32]. In contrast, copolymerization of -OH terminated PEGA with PEGDA did not strongly affect gas transport properties. It was

speculated that the -OH terminal groups on PEGA might hydrogen bond with the polar network, constraining chain motion and preventing an increase in overall free volume that might otherwise be expected to accompany the introduction of PEG branches into the network [74].

This chapter focuses on the introduction of short chain branches into XLPEO, obtained by copolymerizing PEGDA with shorter analogues of PEGA or PEGMEA. The monomers considered are 2-hydroxyethyl acrylate (2-HEA) and ethylene glycol methyl ether acrylate (EGMEA), each of which has one ethylene oxide repeat unit. Copolymers of PEGDA with 2-ethoxyethyl acrylate (2-EEA) are also examined. The chemical structures are shown in Table 3.2, and a representative schematic of XLPEO is provided in Figure 5.1. 2-EEA is terminated by a $-OC_2H_5$ functional group, which is bulkier than the $-OCH_3$ functional group. A companion study (Borns et al. [95]) summarized the changes in the network properties using thermal analysis, whereas this chapter focuses on transport properties of the materials. The three co-monomers have roughly the same molecular weight and ethylene oxide content (according to chemical structure, 38 wt% EO in 2-HEA, 34 wt% in EGMEA and 31 wt% in 2-EEA). For comparison, the EO content in the PEGDA cross-linker used is 82 wt% [18]. Pure gas permeability data are reported for CO_2, CH_4, H_2, O_2 and N_2 at 35°C, along with pure gas solubility data for CO_2 and CH_4, also at 35°C. Gas diffusion coefficients are calculated from the permeability and solubility data where available.

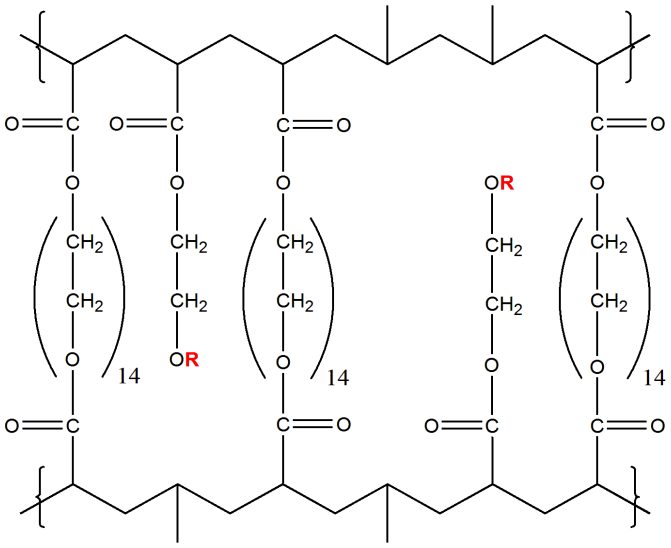

Figure 5.1: Scheme of representative network elements in XLPEO, with **R** representing functional end-group of monoacrylate co-monomer (**R** = H for 2-HEA, CH_3 for EGMEA, CH_2CH_3 for 2-EEA).

5.3. Results and Discussion

5.3.1. Physical Characterization

In this chapter, PEGDA was copolymerized with various amounts of 2-HEA, EGMEA or 2-EEA. The FTIR-ATR spectra of a representative sample from each monomer subgroup are compared with the spectra of the respective pure monomers, shown in Figure 5.2. Consistent with the results for PEGDA/PEGA and PEGDA/PEGMEA [32], all polymers in this chapter underwent essentially complete reaction of the monomers and cross-linker, as evidenced by the absence of the acrylate double bond peaks highlighted in the figure. The change in polymer weight before and after purification by extraction in ultrapure water was less than 1 wt%. Consequently, the polymerized film composition is taken to be essentially that of the corresponding prepolymer solution.

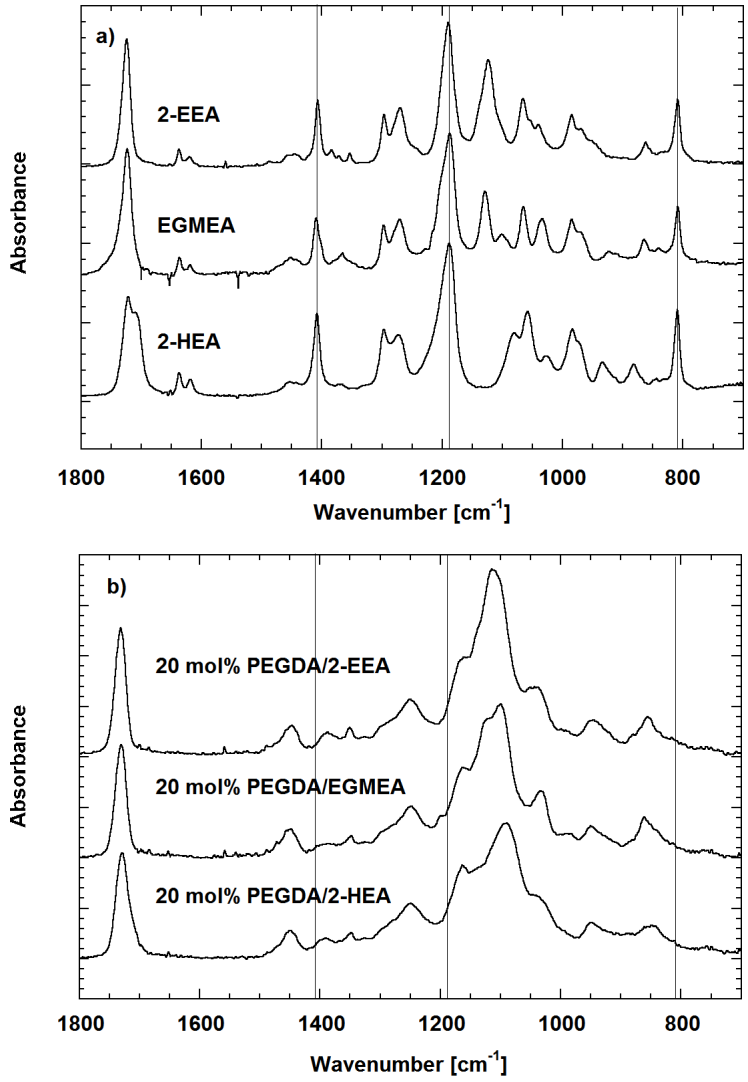

Figure 5.2: FTIR-ATR spectra of a) pure unpolymerized 2-HEA, EGMEA, and 2-EEA, and b) 20 mol% PEGDA copolymerized with 2-HEA, EGMEA and 2-EEA. The spectra have been displaced vertically for clarity. The characteristic acrylate peaks (810, 1190 and 1410 cm^{-1}) are marked by vertical lines (see Section 3.5).

Table 5.1: Physical properties of PEGDA/2-HEA, PEGDA/EGMEA and PEGDA/2-EEA copolymers.

Co-monomer	PEGDA mol%	PEGDA wt%	PEGDA vol%	T_g [°C]	ρ_P [g/cm^3]	*FFV*
---	100	100	100	-37 ± 1	1.190 ± 0.004	0.120 ± 0.003
2-HEA	79.8	96.0	96.3	-35 ± 1	1.194 ± 0.004	0.119 ± 0.003
	59.5	89.9	90.9	-33 ± 1	1.203 ± 0.004	0.117 ± 0.003
	39.8	79.9	81.4	-28 ± 1	1.212 ± 0.004	0.118 ± 0.003
	19.9	59.9	62.4	-18 ± 1	1.239 ± 0.004	0.113 ± 0.003
	10.1	40.3	42.8	-9 ± 1	1.265 ± 0.004	0.110 ± 0.003
EGMEA	79.8	95.5	95.3	-36 ± 1	1.188 ± 0.003	0.123 ± 0.002
	59.6	88.8	88.9	-36 ± 1	1.192 ± 0.005	0.121 ± 0.004
	39.4	78.8	78.7	-35 ± 1	1.189 ± 0.003	0.126 ± 0.002
	19.9	57.4	57.3	-35 ± 1	1.187 ± 0.003	0.133 ± 0.002
	9.11	37.7	37.5	-34 ± 1	1.185 ± 0.003	0.137 ± 0.002
2-EEA	78.7	94.7	94.5	-37 ± 1	1.188 ± 0.003	0.121 ± 0.002
	60.0	88.0	87.4	-37 ± 1	1.182 ± 0.003	0.125 ± 0.002
	40.1	76.5	75.4	-38 ± 1	1.173 ± 0.003	0.132 ± 0.002
	19.9	54.8	53.5	-38 ± 1	1.162 ± 0.003	0.140 ± 0.002
	9.98	35.0	33.8	-39 ± 1	1.148 ± 0.002	0.150 ± 0.002

Note: Uncertainties associated with density measurements were estimated using the propagation of errors method [102]. Uncertainties associated with *FFV* were estimated only from range of density values.

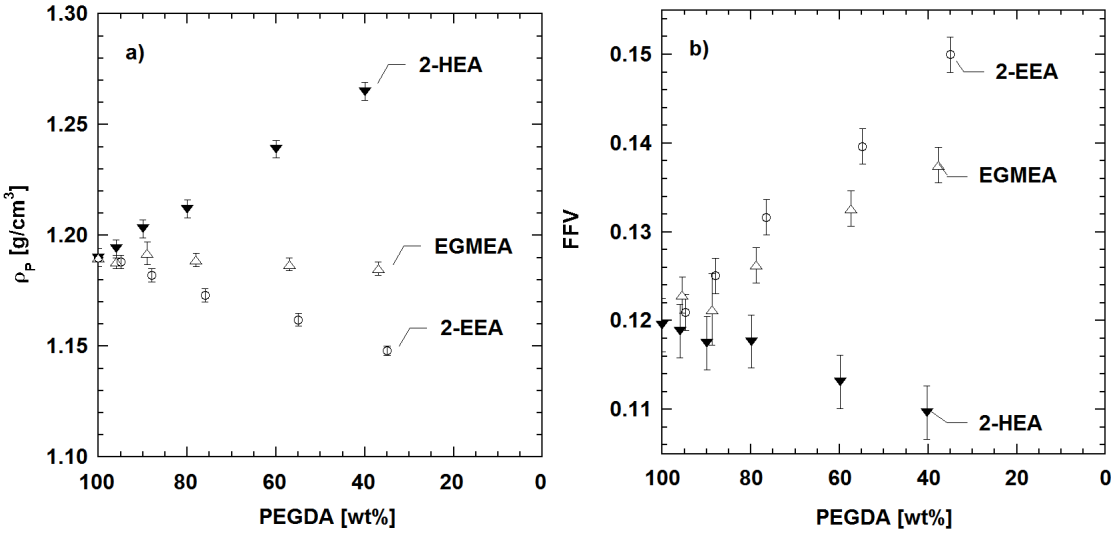

Figure 5.3: Effect of PEGDA content in the prepolymer solution on: a) dry film density and b) fractional free volume at room temperature. The co-monomers are ▼: 2-HEA, Δ: EGMEA and ○: 2-EEA. The uncertainty in each data point was estimated by the propagation of errors method [102].

Table 5.1 presents representative physical properties (density and glass transition temperature; calculated fractional free volume) of all XLPEO films prepared for this chapter. The density results are plotted in Figure 5.3a. As was the case with PEGDA/PEGMEA [32], copolymerization of PEGDA with increasing amounts of 2-EEA decreases the density of the resulting copolymer network. In contrast, there is a considerable density increase as the amount of 2-HEA in the film increases. Copolymerization with EGMEA has little influence on polymer density.

Fractional free volume (*FFV*) calculated for the various samples is plotted as a function of network composition in Figure 5.3b. For the co-monomers examined in this chapter, the component values used to estimate *FFV* in the group contribution method (as

described in Section 2.3) are given in Table 5.2; the structural group breakdown for the repeat unit of PEGDA is provided as an example. Some assumptions with regards to individual v_w values were changed from previous work as given in references [17, 18, 32, 43-45, 88], Chapter 4 (*cf*. Table 4.1), and especially the companion study by Borns et al. [95], leading to slightly different estimates for the *FFV* of these copolymers.

Table 5.2: Copolymer repeat unit structural groups for fractional free volume calculations.

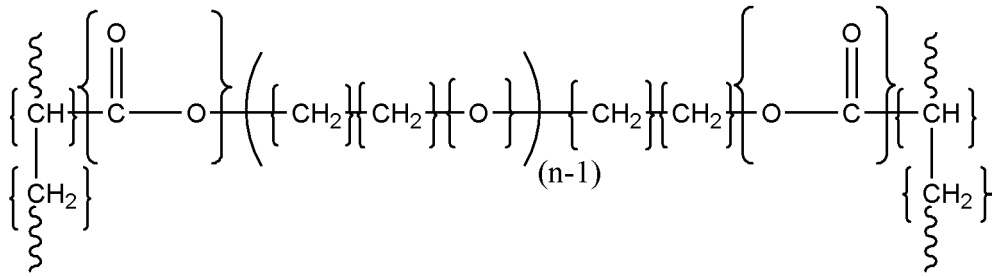

Structural groups of PEGDA repeat unit (n=14)

Moiety	M_w [g/mol]	v_w [cm^3/mol]	Number of moiety in structure			
			PEGDA	2-HEA	EGMEA	2-EEA
-CH_2-	14.03	10.23	30	3	3	4
-O-	16.00	5.5	13	0	1	1
>CH-	13.02	6.8	2	1	1	1
-COO-	44.01	15.2	2	1	1	1
-CH_3	15.03	13.67	0	0	1	1
-OH	17.01	8.0	0	1	0	0

Note: The van der Waals volume values are given by van Krevelen [71].

The validity of the group contribution method depends on the absence of strong inter-chain interactions, *e.g.*, hydrogen bonding [72]. H-bonding interactions between the -OH terminal groups in 2-HEA and other polar moieties in the network have the potential to distort individual bonds and alter the measured free volume of the network relative to the predictions described above.

Fractional free volume increases with EGMEA or 2-EEA content, with the latter showing a more pronounced effect. Since a similar trend was observed across the PEGDA/PEGMEA copolymer series [32], the *FFV* increases appear to be attributable to the presence of mobile EGMEA or 2-EEA co-monomer pendant chains within the polar network. Moreover, the ethoxy ($-OC_2H_5$) terminal group of 2-EEA is bulkier and has a lower density of polar groups than does the methoxy ($-OCH_3$) terminal group of EGMEA and thus should have fewer/weaker interactions with the other polar units in the network. As a result, 2-EEA based copolymers form networks with higher *FFV* than those prepared from EGMEA at comparable composition.

In contrast, *FFV* decreases with increasing 2-HEA content. For comparison, in the PEGDA/PEGA networks [32], *FFV* did not change with increasing PEGA content, even though the pendant chains were of similar length to PEGMEA. The -OH terminated PEO side-chains may interact with the polar network via hydrogen bonding [74], thus preventing the network from adopting a more open structure (*i.e.*, higher *FFV*) despite decreasing overall cross-link density. The 2-HEA-derived side-chains, which, like

PEGA, are also terminated by -OH functional groups, may similarly be expected to form hydrogen bonds within the network. However, because 2-HEA is much shorter than PEGA, any such interactions will likely have a greater impact on network properties, leading to stronger coupling between the -OH terminal group and the cross-linked network backbone. This effect is manifested in the observed trend in *FFV*, as well as by a marked increase in glass transition temperature with increasing 2-HEA concentration.

Figure 5.4 examines the influence of co-monomer structure and concentration on glass transition temperature. The lines in this figure represent the Fox equation for the glass transition temperature of random copolymers [107]:

$$\frac{1}{T_g} = \sum_i \frac{w_i}{T_{gi}} \qquad (5.1)$$

where w_i is the weight fraction of each component in the prepolymer solution, and T_{gi} is the glass transition temperature of the pure polymerized component, as obtained experimentally using DSC. Only modest changes in glass transition temperature are observed for networks containing EGMEA (consistent with the results of Borns et al. [95]) or 2-EEA. Adding these short co-monomer chains does not appear to markedly alter overall chain mobility as reflected by T_g. On the other hand, glass transition temperatures increase significantly when 2-HEA is added (again consistent with the findings of Borns et al. [95]), indicating the presence of additional interactions within the network that reduce available free volume and corresponding motional freedom as compared to 100% cross-linked PEGDA, as well as the PEGDA/EGMEA and PEGDA/

2-EEA copolymers. On this basis, the presence of -OH terminal groups in the PEGDA/ 2-HEA networks appears to correlate with a strong decrease in chain mobility, which is consistent with these groups interacting, perhaps via hydrogen bonding, with surrounding chain elements.

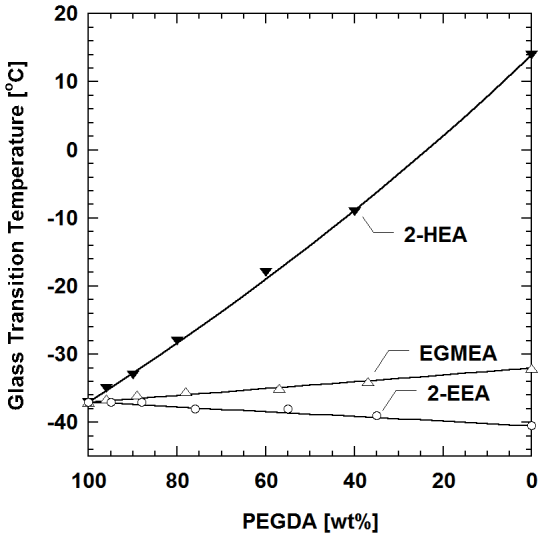

Figure 5.4: Effect of PEGDA content in the prepolymer solution on glass transition temperature. The co-monomers are ▼: 2-HEA, Δ: EGMEA and ○: 2-EEA. The lines are drawn based on Equation 5.1.

Figure 5.5 presents the relations between T_g and *FFV* for each polymer series (*cf.* Equation 4.4). Systematic variations of T_g with *FFV* are evident for each copolymer series, but no universal correlation is observed. In general, the introduction of short pendant groups along the network backbone has the potential to hinder chain motion, imparting a stiffer character to the polymer. At the same time, the relatively non-polar terminal ends associated with these branches can expand the polar network, increasing

local free volume. This would appear to be the situation when PEGDA is copolymerized with EGMEA or 2-EEA, where the respective -OCH_3 and -OC_2H_5 end groups are unlikely to display strong dispersive interactions with the surrounding polar matrix, and *FFV* increases with increasing co-monomer content. The measured T_g reflects segmental mobility as influenced both by the nature of the side groups present and by the resultant free volume. In the case of PEGDA/EGMEA and PEGDA/2-EEA copolymers, only a modest variation in T_g is observed across each series, reflecting a trade-off between increasing free volume and impediments to large-scale motion posed by the presence of the relatively short branches. A similar outcome has been observed for short-branch copolymers based on cross-linked poly(propylene glycol) diacrylate (PPGDA), wherein T_g remains nearly constant with expanding free volume owing to the insertion of an increasing fraction of bulky pendants along the network backbone [121]. With longer side chains (*e.g.*, PEGDA/PEGMEA series), the flexible pendants facilitate chain motion, and a strong reduction in T_g is observed with increasing *FFV* [17]. Finally, in the case of the PEGDA/2-HEA copolymers, the local dispersive interactions associated with the -OH terminal groups are responsible for both a stiffening of the backbone and an increase in polymer density, and these factors contribute to the measured increase in T_g of nearly 30°C with addition of 60 wt% 2-HEA.

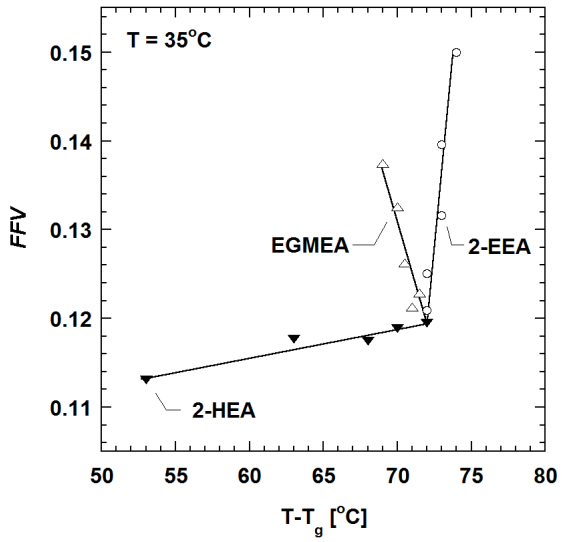

Figure 5.5: Correlation of fractional free volume of XLPEO prepared from ▼: PEGDA/ 2-HEA, Δ: PEGDA/EGMEA and ○: PEGDA/2-EEA with ($T - T_g$), where T = 35°C and T_g is the glass transition temperature of the corresponding copolymer. The lines are drawn based on Equation 4.4.

5.3.2. Permeability, Solubility and Diffusivity

Figure 5.6 presents the fugacity dependence of gas permeability for two representative polymers studied – one from the PEGDA/2-HEA series and one from the PEGDA/2-EEA series. The permeability coefficients of the permanent gases (hydrogen, oxygen and nitrogen), as well as methane, were essentially independent of fugacity for the copolymer network series, whereas the permeability coefficients for carbon dioxide increased with increasing fugacity [32]. This behavior is consistent with gas permeation properties in rubbery polymers in general [59], and specifically in XLPEO [18, 32, 43], as carbon dioxide and other condensable penetrants have higher solubility at higher fugacity, leading to plasticization of the polymer and, consequently, higher permeability [59].

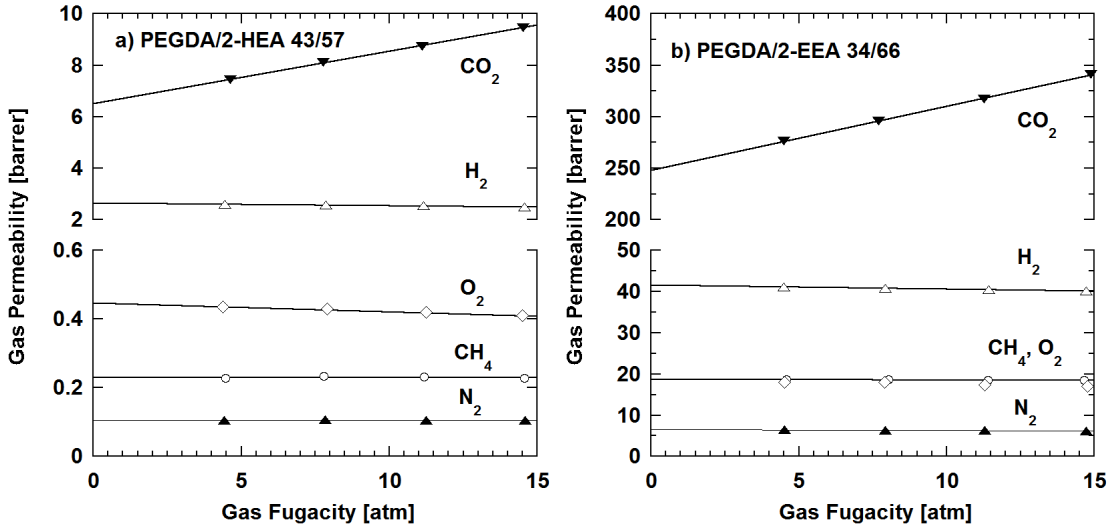

Figure 5.6: Effect of upstream gas fugacity on pure gas permeability coefficients at 35°C in: a) 43 vol% PEGDA/57 vol% 2-HEA and b) 34 vol% PEGDA/66 vol% 2-EEA. The gases are: ▼: CO_2, Δ: H_2, ○: CH_4, ◊: O_2 and ▲: N_2. The lines are drawn based on Equation 2.10.

To compare the permeability values of carbon dioxide with permeability values for other gases, the data may be extrapolated to infinite dilution (*i.e.*, an upstream fugacity of zero) from several permeability measurements performed at various fugacities, using Equation 2.10. Figure 5.7 and Table 5.3 present the infinite dilution permeability for CO_2, CH_4, H_2, O_2 and N_2 as a function of co-monomer content in the polymer for the three systems studied. The permeability trends are systematic for all gases used: gas permeability increases with increasing EGMEA or 2-EEA content, while gas permeability significantly decreases as the amount of 2-HEA increases in the copolymer. The order of gas permeability across all three copolymer series is: $CO_2 > H_2 > O_2 \geq CH_4 > N_2$. Carbon dioxide has the highest permeability due, presumably, to its favorable interaction with the polar ether oxygen groups in the network, coupled with its strong condensability and

fairly small size (kinetic diameter of 3.3 Å [67], also refer to Table 2.2). The relatively high permeability of hydrogen should be due primarily to its small molecular diameter (kinetic diameter of 2.89 Å). Methane, which is larger in size (3.8 Å) than the permanent gases and carbon dioxide, displays higher permeability than does nitrogen (3.64 Å), and permeability approximately equal to that of oxygen (3.46 Å), owing to its high condensability (*i.e.*: critical temperature of CH_4 as compared to that of O_2 or N_2). The observed order of permeability values among the various gases is consistent with comparable transport measurements performed for the PEGDA/PEGMEA and PEGDA/PEGA network series ([32]; also refer to Chapter 4), as well as semi-crystalline PEO [16].

Changes in permeability with co-monomer composition have been correlated using Equation 4.1. With $X = P_A$, $P_{A,1}$ was determined by direct experimental measurement of 100% PEGDA polymer. A lack of structural integrity for the pure polymerized monoacrylates precludes direct measurement of $P_{A,2}$, so it was estimated by applying Equation 4.1 to the sample with the least amount of PEGDA in each series. The correlation is illustrated in Figure 5.7 and, in all cases, provides a satisfactory description of the data.

Table 5.3: Infinite dilution gas permeability and solubility of PEGDA/2-HEA, PEGDA/EGMEA and PEGDA/2-EEA copolymers at 35°C, determined experimentally.

Co-monomer	PEGDA vol%	Permeability [barrer]					Solubility [cm^3(STP)/cm^3 atm]	
		CO_2	H_2	CH_4	O_2	N_2	CO_2	CH_4
---	100	110 ± 6	15 ± 0.8	5.5 ± 0.3	5.1 ± 0.3	1.9 ± 0.1	1.30 ± 0.06	0.075 ± 0.03
2-HEA	96.3	90 ± 5	14 ± 0.7	4.6 ± 0.2	4.4 ± 0.2	1.6 ± 0.1	1.27 ± 0.06	0.067 ± 0.03
	90.9	78 ± 4	13 ± 0.7	4.0 ± 0.2	4.6 ± 0.3	1.4 ± 0.1	1.25 ± 0.06	0.056 ± 0.03
	81.4	49 ± 3	9.3 ± 0.5	2.3 ± 0.1	2.4 ± 0.1	0.79 ± 0.04	1.20 ± 0.04	0.051 ± 0.03
	62.4	20 ± 1	5.5 ± 0.3	0.90 ± 0.06	1.1 ± 0.06	0.36 ± 0.02	1.10 ± 0.06	0.064 ± 0.03
	42.8	6.5 ± 0.4	2.7 ± 0.2	0.23 ± 0.02	0.45 ± 0.03	0.11 ± 0.007	---	---
EGMEA	95.3	110 ± 6	16 ± 0.9	5.6 ± 0.3	5.5 ± 0.3	2.0 ± 0.1	1.32 ± 0.06	0.073 ± 0.03
	88.9	120 ± 6	18 ± 0.9	6.4 ± 0.4	5.2 ± 0.3	1.9 ± 0.1	1.35 ± 0.04	0.072 ± 0.03
	78.7	140 ± 8	19 ± 1.0	6.9 ± 0.4	6.7 ± 0.4	2.8 ± 0.2	1.40 ± 0.05	0.095 ± 0.03
	57.3	150 ± 8	23 ± 1.2	7.8 ± 0.4	7.3 ± 0.4	2.8 ± 0.2	1.46 ± 0.06	0.10 ± 0.03
	37.5	160 ± 9	26 ± 1.4	9.2 ± 0.5	9.2 ± 0.5	3.4 ± 0.2	1.57 ± 0.06	0.10 ± 0.03
2-EEA	94.5	120 ± 6	17 ± 0.9	6.0 ± 0.3	5.3 ± 0.3	2.0 ± 0.1	1.34 ± 0.05	0.083 ± 0.03
	87.4	140 ± 7	20 ± 1.1	7.3 ± 0.4	6.6 ± 0.4	2.6 ± 0.1	1.36 ± 0.06	0.085 ± 0.03
	75.4	160 ± 8	24 ± 1.3	8.9 ± 0.5	8.2 ± 0.4	3.6 ± 0.2	1.42 ± 0.06	0.091 ± 0.03
	53.5	190 ± 10	31 ± 1.7	13 ± 0.7	12 ± 0.7	5.2 ± 0.3	1.52 ± 0.04	0.10 ± 0.03
	33.8	250 ± 13	42 ± 2.2	19 ± 1.0	19 ± 1.0	6.6 ± 0.4	1.60 ± 0.04	0.12 ± 0.03

Note: All uncertainties are estimated using the propagation of errors method [102].

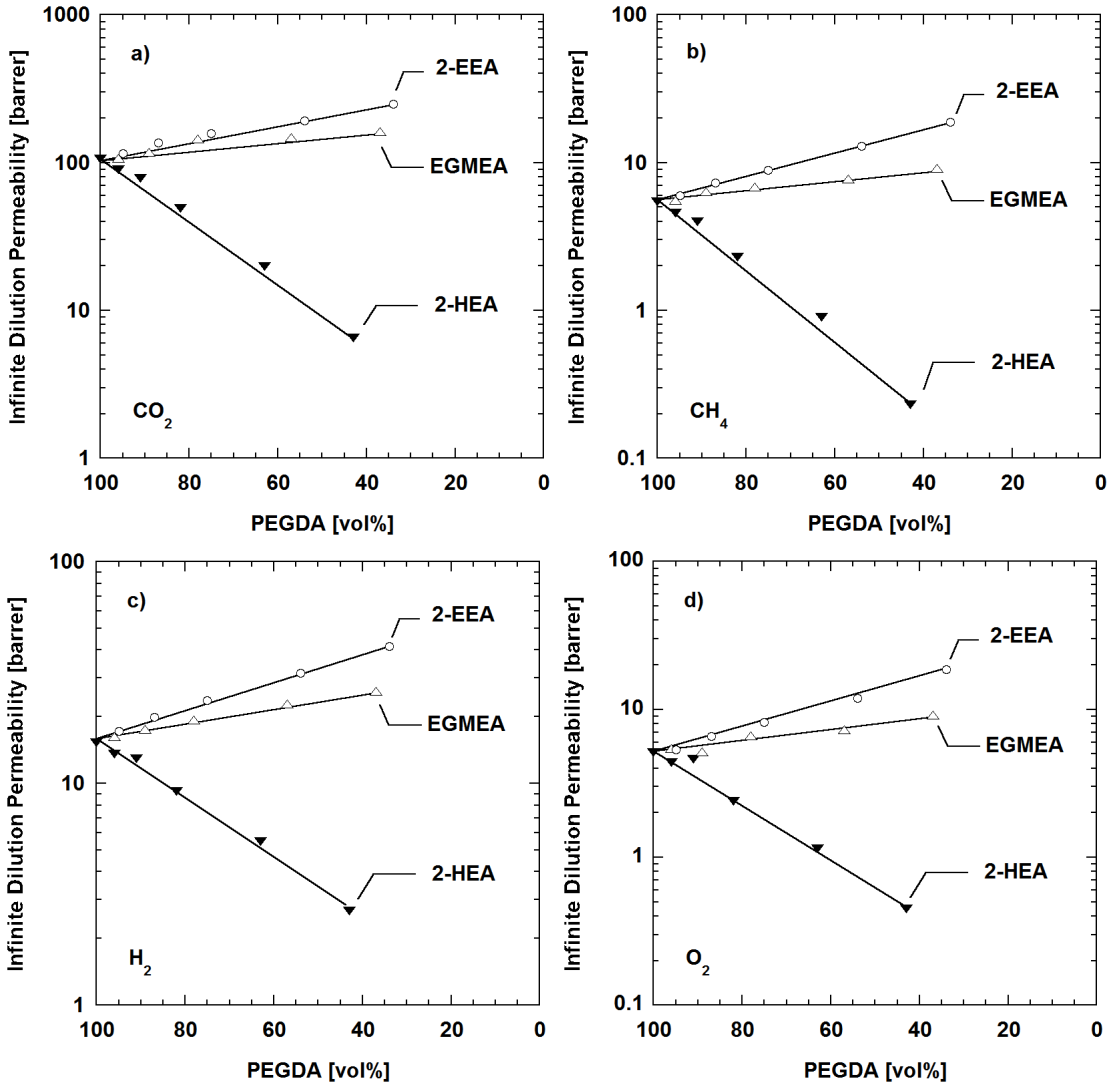

Figure 5.7: Effect of PEGDA content on infinite dilution gas permeability at 35°C. The lines through the data are drawn based on Equation 4.1. The gases are a) CO_2, b) CH_4, c) H_2, d) O_2, and e) N_2. The co-monomers are ▼: 2-HEA, Δ: EGMEA and ○: 2-EEA.

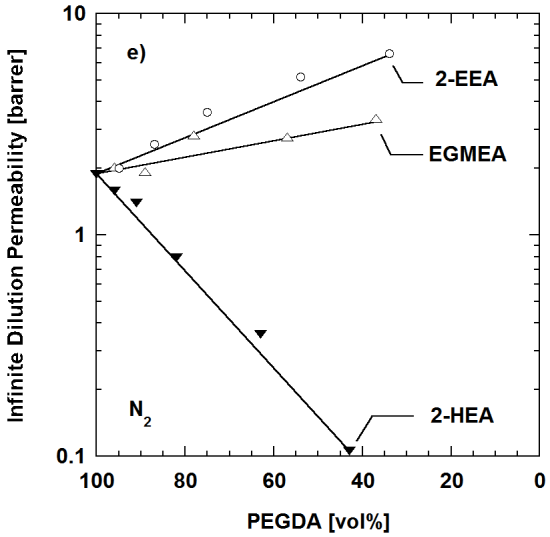

Figure 5.7 (*continued*)**:** Effect of PEGDA content on infinite dilution gas permeability at 35°C. The lines through the data are drawn based on Equation 4.1. The gases are a) CO_2, b) CH_4, c) H_2, d) O_2, and e) N_2. The co-monomers are ▼: 2-HEA, Δ: EGMEA and ○: 2-EEA.

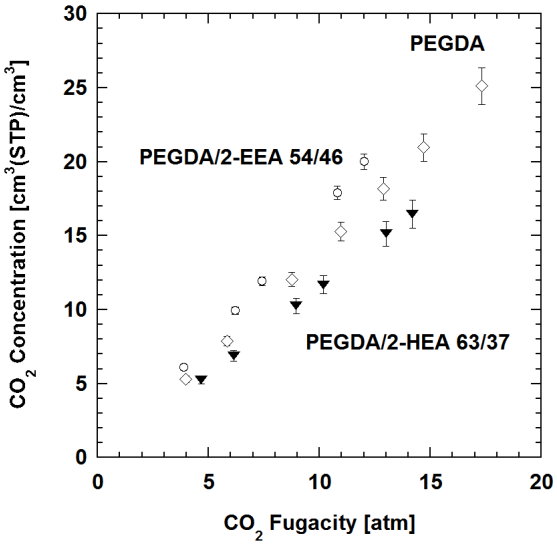

Figure 5.8: CO_2 sorption isotherms of XLPEO prepared from ◊: 100% PEGDA, ▼: 63 vol% PEGDA/37 vol% 2-HEA and ○: 54 vol% PEGDA/46 vol% 2-EEA.

To better understand the transport mechanism and interpret the results presented in the previous section, the individual contributions of gas solubility and diffusivity to the permeability of gases through a polymer may be separated. Gas diffusivity can be calculated using Equation 2.6 from experimental measurements of permeability and solubility. This study limits solubility measurements to carbon dioxide and methane, owing to the low solubilities of other non-polar permanent gases in polar rubbers [41] such as XLPEO, and the correspondingly high uncertainty associated with their determination. Sorption isotherms can be obtained by measuring the concentration of CO_2 or CH_4 in the polymer as a function of fugacity. Figure 5.8 presents representative CO_2 sorption isotherms for the various polymer series considered in this chapter. CO_2 solubility is only very slightly fugacity-dependent, a result that is consistent with the findings of Lin et al. [18, 56] (also see: Figure 2.1). Thus, CO_2 and CH_4 solubility at a particular fugacity can be found from the sorption isotherms using Henry's law approximation (Equation 2.11) [41]. Infinite dilution solubility can then be calculated in a similar fashion as Equation 2.10 from these fugacity-dependent solubility values.

Infinite dilution solubility of carbon dioxide in the previously-studied PEGDA/PEGMEA series of copolymer networks increased slightly from approximately 1.3±0.1 cm^3(STP)/(cm^3 atm) for 100% PEGDA to 1.6±0.1 cm^3(STP)/(cm^3 atm) for the network containing only 1.3 wt% PEGDA cross-linker [32]. Similar trends in CO_2 and CH_4 solubility were observed for the PEGDA/EGMEA and PEGDA/2-EEA networks, with solubility increasing with decreasing cross-linker content for both series; see Figure 5.9 and Table

5.3. For the PEGDA/2-HEA copolymers, however, the opposite trend was evident: solubility decreased with increasing 2-HEA concentration.

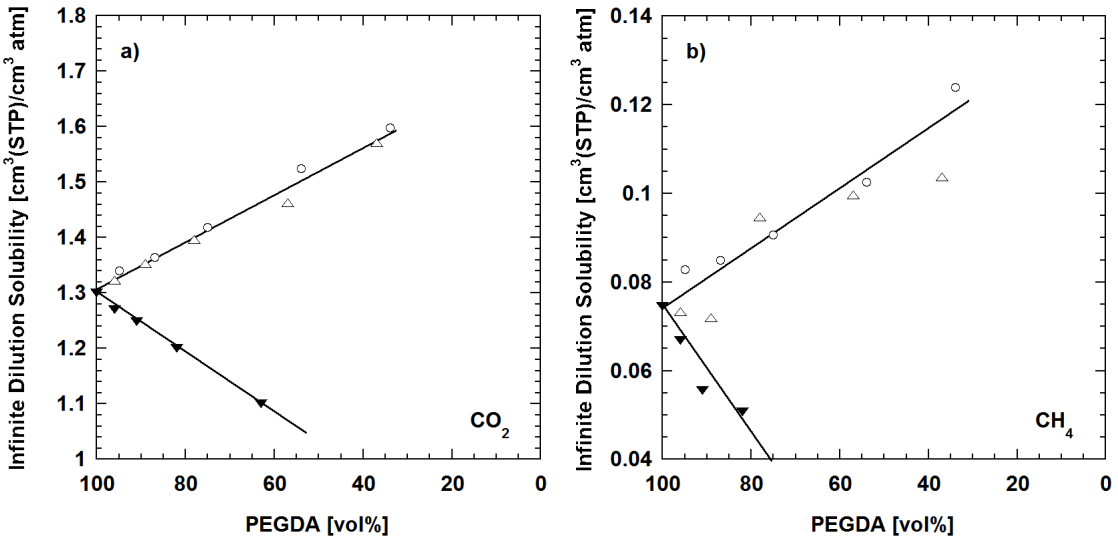

Figure 5.9: Effect of PEGDA content on infinite dilution gas solubility at 35°C, a) CO_2 and b) CH_4. The co-monomers are ▼: 2-HEA, Δ: EGMEA and ○: 2-EEA. The lines are drawn to guide the eye.

Several factors may account for the observed gas solubility trends with varying network composition. By increasing the amount of 2-HEA in the PEGDA/2-HEA system, the concentration of polar -OH terminal groups along the network backbone is increased. Typically, an increase in available polar groups would be expected to produce a decrease in the solubility of non-polar penetrants in the polymer and a corresponding increase in the solubility of polar or quadrupolar penetrants (such as carbon dioxide), as has been observed when non-polar butadiene is copolymerized with polar acrylonitrile [41]. Consequently, the measured decrease in carbon dioxide solubility with increasing 2-HEA

concentration (*cf*. Figure 5.9) may seem counterintuitive, as it suggests less favorable interaction of carbon dioxide molecules with the increasingly polar polymer. On the other hand, the ether linkages in XLPEO materials have been identified as contributing to high CO_2 solubility in these polymers [17]. Perhaps the 2-HEA hydroxyl groups, due to their hydrogen-bonding ability, effectively compete with CO_2 for ether oxygen interactions, with higher concentrations of -OH pendant groups limiting the ether linkages available to enhance CO_2 solubility in the polymer matrix. In essence, the strong association between the -OH groups and the polar ether oxygens within these networks may reduce the accessibility of ether oxygen groups to CO_2 molecules. This effect has been observed in diphenylsulfone polyamides, where the polar diphenylsulfone units along the polymer backbone interact in a similar manner with the polar amide groups present in the polymer, effectively lowering CO_2 solubility below the level expected for the number of polar groups possessed by the polyamide [122]. An additional factor that may contribute to the observed results is that gas solubility, from rather straightforward thermodynamic considerations, is expected to decrease with increasing polymer polarity, all other factors being equal. The energy required to open a gap in a polymer matrix to accommodate a penetrant molecule is higher if the polymer matrix is more polar, due to the increase in cohesive energy density, and this energy penalty acts to reduce gas solubility [41, 107].

A different trend is observed in the PEGDA/EGMEA and PEGDA/2-EEA copolymer series, where the short-chain branches are terminated with $-OCH_3$ and $-OC_2H_5$ groups,

respectively. In these polymers, the presence of less polar side chains presumably favors increased methane solubility but renders the polar ether oxygen groups more accessible to interaction with carbon dioxide, as a result of higher *FFV* in the materials, leading to the observed increase in CO_2 solubility (*cf*. Figure 5.9). The increase in *FFV* due to the presence of the non-polar branch ends essentially weakens internal interactions between polar ether oxygens, allowing for stronger interaction with CO_2 [122].

The value of the infinite dilution solubility of methane in polymerized 100% PEGDA reported in this chapter, 0.075±0.03 cm^3(STP)/(cm^3 atm), is lower than that reported by Lin et al., 0.11±0.02 cm^3(STP)/(cm^3 atm) [18]. The discrepancy arises from an experimental improvement introduced into the current work that eliminates the influence of dissolved water vapor from the atmosphere on the determination of polymer mass (as much as 2 wt% difference) and corresponding density, as described in Section 3.4. The correction factor is small, but the effect on the measurement of methane sorption is significant due to low methane uptake in these polymers. Carbon dioxide solubility is less sensitive to this effect, as it is an order of magnitude higher than methane solubility. Consequently, the infinite dilution carbon dioxide solubility in 100% PEGDA reported here, 1.30±0.06 cm^3(STP)/(cm^3 atm), is equal to the value reported by Lin et al. [18, 32, 56].

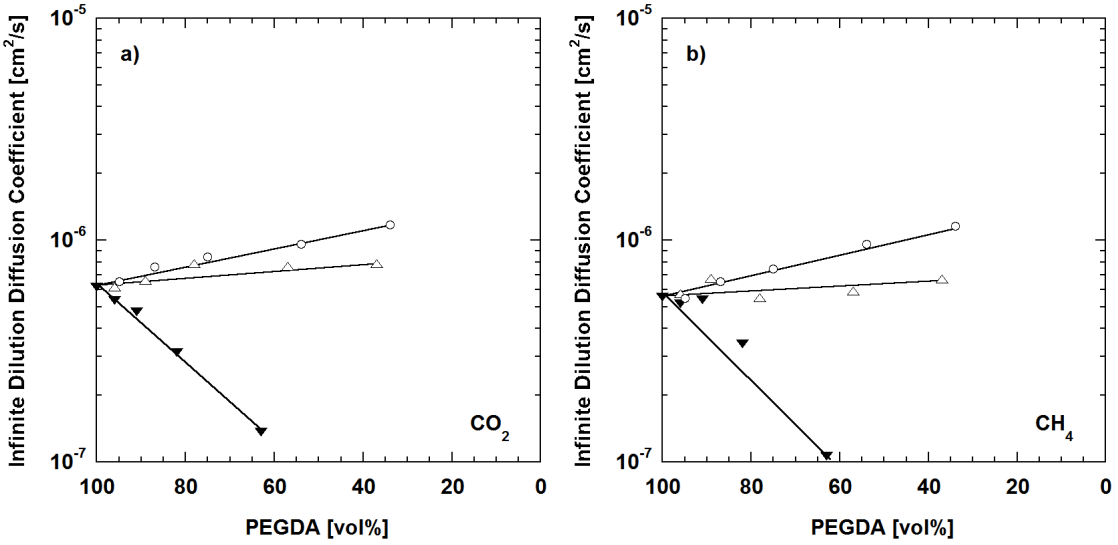

Figure 5.10: Effect of PEGDA content on infinite dilution gas diffusivity at 35°C, a) CO_2 and b) CH_4. The co-monomers are ▼: 2-HEA, Δ: EGMEA and ○: 2-EEA. The lines are drawn based on Equation 4.1.

Having obtained infinite dilution solubility coefficients for carbon dioxide and methane, the infinite dilution diffusion coefficients of the aforementioned gases through the polymers can be determined using Equation 2.6, and they are presented in Figure 5.10. Both gases display very systematic trends for the PEGDA/2-HEA, PEGDA/EGMEA and PEGDA/2-EEA networks. The diffusion coefficients increase with increasing amounts of EGMEA or 2-EEA in the network, although the effect is more pronounced with 2-EEA than with EGMEA. Conversely, the diffusion coefficients decrease significantly with increasing 2-HEA content. From the comparison between permeability trends shown in Figure 5.10 and those shown in Figure 5.7, the changes in permeability due to variations in co-monomer content can be attributed mainly to changes in diffusivity.

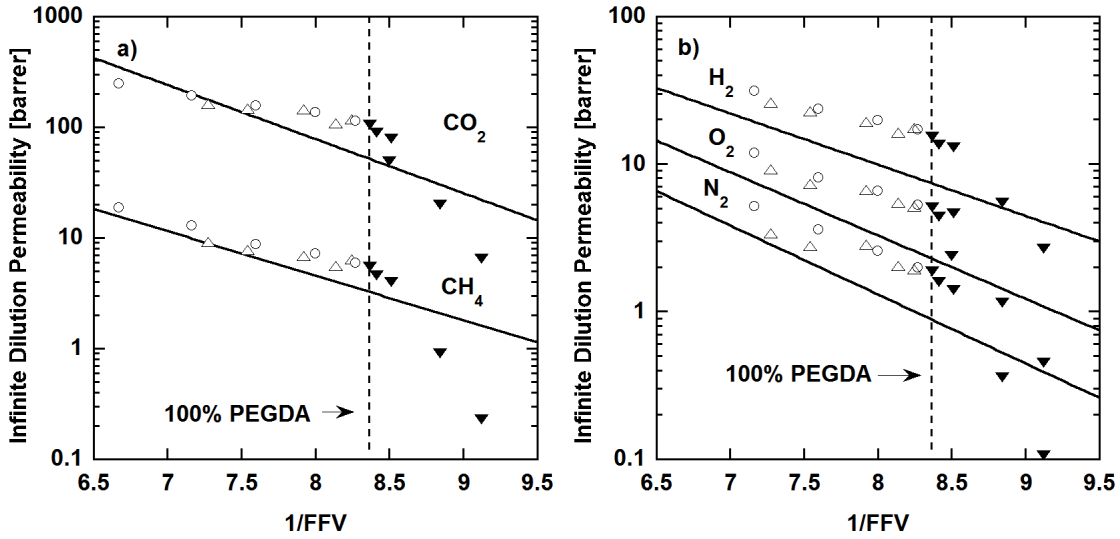

Figure 5.11: Comparison between experimental and predicted infinite dilution permeability based on the free volume model, with model parameters given in Table 2.1. From top to bottom: a) CO_2 and CH_4, b) H_2, O_2 and N_2. The dashed line indicates the free volume of a polymer prepared from 100% PEGDA in the prepolymer solution. The co-monomers are ▼: 2-HEA, Δ: EGMEA and ○: 2-EEA, with increasing content of co-monomer being represented by points further away from the dashed line.

Traditionally, cross-link density has been considered to significantly influence gas permeability, based mainly on classical studies involving natural rubber [123]. However, for the polymers considered here, cross-link density does not appear to be a decisive factor in determining transport properties. In each copolymer series examined, cross-link density decreases with decreasing PEGDA content [95]. Because the diffusivity trend for PEGDA/2-HEA is opposite those of the other two series (*cf.* Figure 5.10), the role of cross-link density in determining diffusivity is clearly minimal relative to other aspects of network architecture and short-branch composition discussed above. This result is consistent with the data on various XLPEO polymers reported by Lin et al., where diffusivity was correlated most strongly with *FFV*, and was essentially independent of

cross-link density [18, 32, 43, 56, 88] (also see Section 4.2.2). The correlation is expressed using Equation 2.12 or 2.13, the Fujita-modified Cohen-Turnbull relationship.

The values of A_P and B in Equation 2.13 were determined for XLPEO by Lin et al. based on the transport properties of cross-linked PEGDA that had been diluted with 20 wt% water in the prepolymer [32]; these values (provided in Table 2.1) have been used successfully to predict the transport properties of PEGDA/PEGMEA and PEGDA/PEGA networks solely as a function of fractional free volume [88]. As shown in Figure 5.11, the correlation established by these parameters compares favorably with the data obtained for the alkoxy-terminated copolymers, PEGDA/EGMEA and PEGDA/2-EEA, despite small differences in the *FFV* calculation method relative to the original study (see Section 2.3). However, the PEGDA/2-HEA copolymers do not follow the same relation: with increasing 2-HEA, gas permeability decreases more strongly than predicted by the *FFV* correlation. This seemingly anomalous result can be explained by noting that the van der Waals volumes used to calculate *FFV* are valid only in the absence of strong inter-chain interactions, which can distort bond lengths. The addition of 2-HEA introduces -OH moieties that have the potential to form strong hydrogen bonds within the network, thereby altering *FFV* relative to the predicted value. Another possible explanation for the phenomenon is that addition of 2-HEA may change the distribution of free volume elements in the polymer, which cannot be accounted for by an average fractional free volume calculation alone [124].

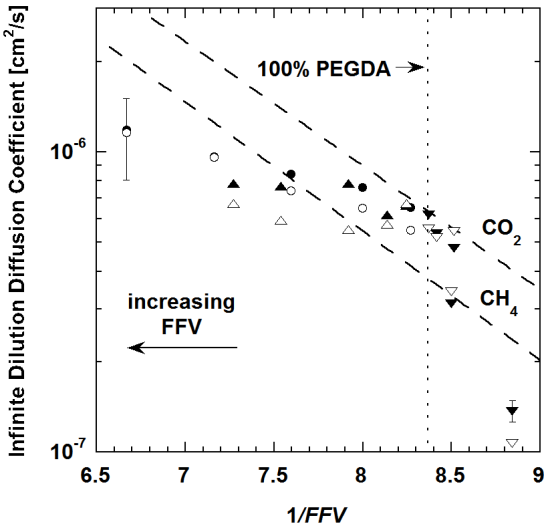

Figure 5.12: Correlation between infinite dilution gas diffusivity at 35°C and polymer free volume. The data shown are for both CO_2 (▼: PEGDA/2-HEA, ▲: PEGDA/EGMEA and ●: PEGDA/2-EEA) and CH_4 (corresponding open symbols). The vertical dashed line indicates the free volume of polymer prepared from 100% PEGDA. For comparison, the model parameters reported by Lin et al. [43] and shown in Table 2.1 were used to prepare the dashed lines. Representative error bars are shown.

Figure 5.12 presents the relationship between carbon dioxide and methane diffusivity and fractional free volume. The data in Figure 5.12 are compared to the model predictions (based on Equation 2.12) from Lin et al. [43]. The parameters from Lin et al. are provided in Table 2.1. These model lines were generated based on experimental data of the influence of temperature on gas diffusivity in cross-linked PEGDA ([43], also *cf.* Figure 4.10). As such, this model may not necessarily accurately predict the influence of polymer chemical structure on diffusivity at a single temperature. As illustrated by the PEGDA/2-HEA series and described in the previous paragraph, other factors that may affect adherence to this general model include changes in chain mobility or distribution of free volume elements.

5.3.3. Selectivity

Figure 5.13 presents the pure gas selectivity values for the series of materials considered in this chapter. The trends for CO_2/CH_4 and CO_2/N_2 selectivity are similar: addition of 2-HEA increases selectivity, EGMEA modestly decreases selectivity, and 2-EEA decreases selectivity more strongly. There is a uniform trend of decreasing CO_2/O_2 selectivity with increasing co-monomer content in all three series. For CO_2/H_2, the selectivity decrease is much more pronounced in the PEGDA/2-HEA networks than in the other two series, where selectivity does not change appreciably. The selectivities of the other gases (e.g. H_2/N_2; O_2/N_2) do not change appreciably with changes in polymer composition, with the exception of the PEGDA/2-HEA series. Selectivity ratios favoring smaller molecules increase as 2-HEA content increases (the kinetic diameter of molecules increases in the following order: $H_2 < CO_2 < O_2 < N_2 < CH_4$; also see Table 2.2) [67]. This result may arise from decreasing polymer chain mobility (as indicated by T_g, *cf*. Figure 5.4) due to increasing interaction between the polymer chains through hydrogen bonding. Since greater activation energy is required to open diffusion paths [125] as chain mobility decreases, the activation energy required for diffusion of a larger molecule increases more than that for smaller molecules. However, as shown by Figure 5.14, the solubility selectivity is the primary determinant for the separation ability of these XLPEO polymers.

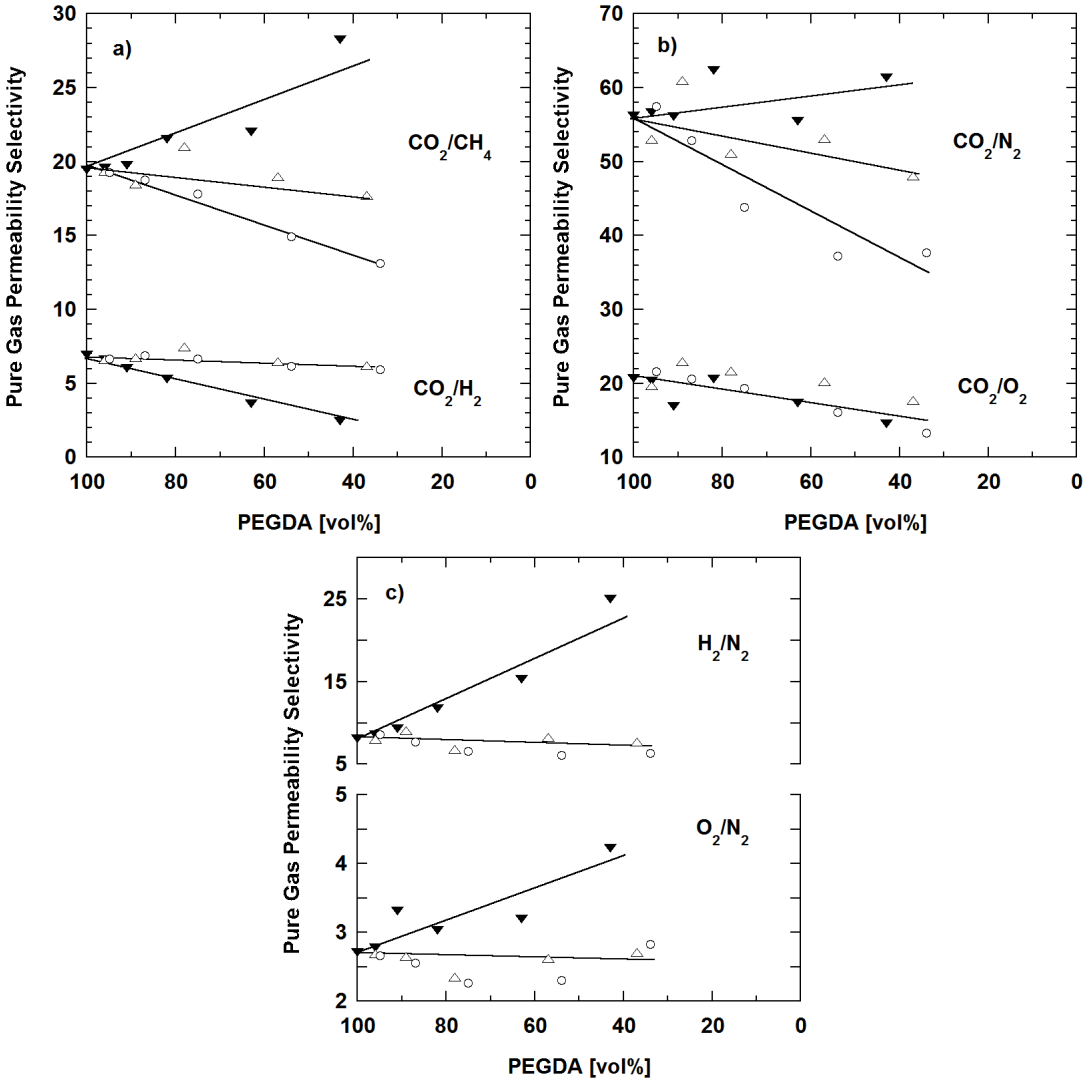

Figure 5.13: Effect of PEGDA content on infinite dilution gas selectivity at 35°C. The solid lines through the data are drawn to guide the eye. The selectivity data presented are for: a) CO_2/CH_4 and CO_2/H_2, b) CO_2/N_2 and CO_2/O_2, c) H_2/N_2 and O_2/N_2. The co-monomers are ▼: 2-HEA, Δ: EGMEA and ○: 2-EEA.

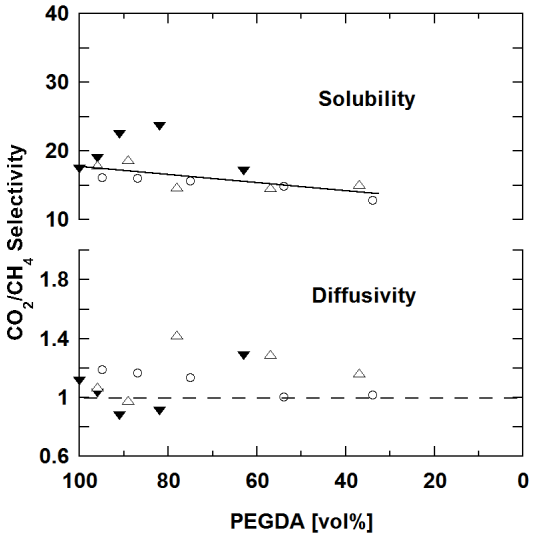

Figure 5.14: Effect of PEGDA content on infinite dilution CO_2/CH_4 solubility and diffusivity selectivity. The co-monomers are ▼: 2-HEA, Δ: EGMEA and ○: 2-EEA. The dashed line indicates α=1, or no separation.

Finally, Figure 5.15 provides comparisons of the carbon dioxide separation performance of the copolymers in this chapter with other polymers from the literature [44, 45] and the PEGDA/PEGMEA series (*cf.* Figure 4.11) [32, 44, 45]. The upper bound line given in Figure 5.15a is drawn as described in ref. [44], and it provides an estimate of the highest possible pure gas selectivity for a given permeability in polymer-based materials at 25°C. Unlike Figure 4.11, the upper bound line given in Figure 5.15b is drawn based on the most recent upper bound curves at 35°C [126]. Because adding the co-monomers selected in this chapter into PEGDA reduces the overall concentration of polar ether oxygen groups in the resulting polymers, they do not exhibit the same strong carbon dioxide separation performance demonstrated by the PEGDA/PEGMEA copolymer series. Of the three co-monomers in this chapter, 2-EEA yields the best performance in

terms of permeability and selectivity of interest, because these branches are more effective in increasing fractional free volume than are EGMEA or 2-HEA at similar concentration.

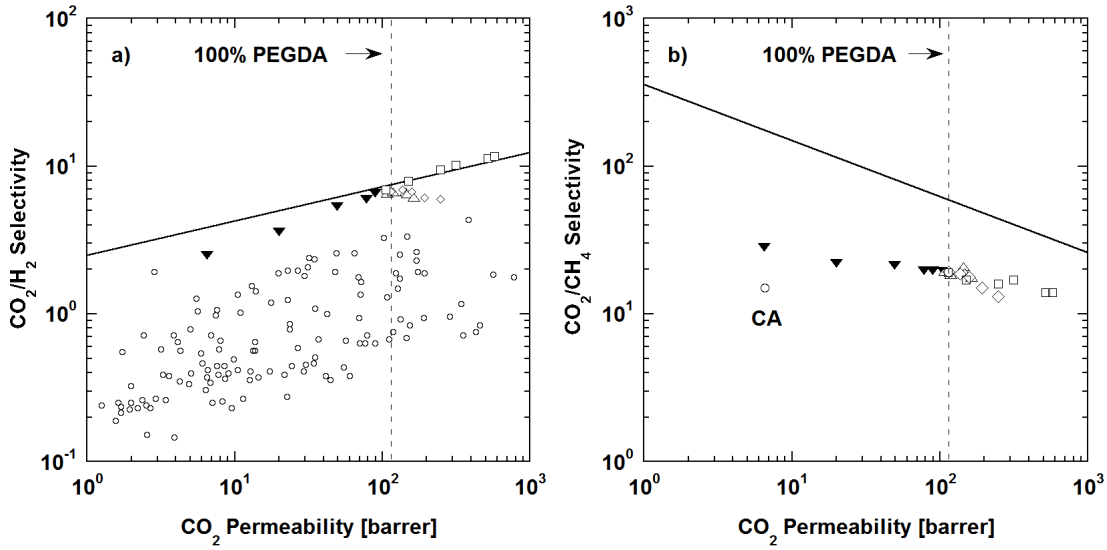

Figure 5.15: Permeability/selectivity map for: a) CO_2/H_2 and b) CO_2/CH_4 separations. The copolymers considered in this chapter are ▼: PEGDA/2-HEA, Δ: PEGDA/EGMEA and ◊: PEGDA/2-EEA, and the data for these materials are presented at 35°C and infinite dilution. The dashed line indicates the permeability of 100% PEGDA. PEGDA/PEGMEA results are provided for comparison (□). All other points in Figure 5.15a are provided from the literature [44]. In Figure 5.15b, a comparison with cellulose acetate (CA) is provided [45].

5.4. Conclusions

This chapter examined the effect of copolymerizing poly(ethylene glycol) diacrylate (PEGDA) with one of three co-components: 2-hydroxyethyl acrylate (2-HEA), ethylene glycol methyl ether acrylate (EGMEA), or 2-ethoxyethyl acrylate (2-EEA), resulting in

the insertion of short branches with different chemical properties into the cross-linked polymer network. The goal was to determine the effectiveness of these branches in enhancing fractional free volume and facilitating favorable CO_2 interaction with the networks, in order to improve transport properties for CO_2 separation. Addition of EGMEA or 2-EEA, terminated by $-OCH_3$ or $-OC_2H_5$ functional groups, respectively, was effective in increasing gas permeability through an increase in gas diffusivity. This increase was due to the ability of these functional groups, especially $-OC_2H_5$, to increase local free volume as well as the accessibility of the polar ether oxygens to the CO_2 penetrant. The introduction of 2-HEA in PEGDA, however, produced the opposite effect. The -OH terminated 2-HEA branches appeared to form hydrogen bonds with other polar moieties in the network, resulting in lower fractional free volume and fewer opportunities for carbon dioxide to interact with the polar ether oxygen groups. Gas diffusivity in the PEGDA/EGMEA and PEGDA/2-EEA networks was correlated with fractional free volume in agreement with the Fujita-modified Cohen-Turnbull equation, using correlation parameters established in an earlier study. While diffusivity in the PEGDA/2-HEA networks could be similarly correlated with fractional free volume, the parameters required to describe this correlation were different from those reported previously. This observation suggested that additional chain interactions through hydrogen bonding played an important role in determining the free volume characteristics and corresponding diffusivities of the PEGDA/2-HEA networks relative to the other two copolymer systems. Further, changes in the free volume characteristics had the potential to influence the relative affinities of the various gases for the modified

networks, as manifested in the trends observed in gas solubility, and ultimately, gas selectivity. By providing a direct comparison of the physical and transport properties of short-branch networks containing distinctly different branch-end terminal groups, the work described in this chapter further elucidates the synthetic strategies necessary for the optimization of gas separation performance in cross-linked poly(ethylene oxide) networks.

Chapter 6: Influence of Phenoxy-Terminated Short Chain Pendant Groups on Gas Transport Properties of Cross-linked Poly(ethylene oxide) Copolymers

6.1. Summary

In this chapter, gas transport properties of rubbery cross-linked poly(ethylene oxide) films containing short phenoxy-terminated pendant chains are reported. Poly(ethylene glycol) diacrylate (PEGDA) was UV-polymerized with poly(ethylene glycol) phenyl ether acrylate co-monomers of two different ethylene oxide unit repeat lengths: n=2 (DEGPEA) and n=4 (PEGPEA). Although fractional free volume increased with increasing co-monomer concentration, gas permeability did not rise accordingly. For instance, while *FFV* increased from 0.120 to 0.135 in both series of copolymers, CO_2 permeability went from 110 barrer to 35 barrer (DEGPEA) or to 100 barrer (PEGPEA). At the same time, glass transition temperature increased from -37°C to -12°C (DEGPEA) or to -28°C (PEGPEA). The observed decrease in chain mobility with phenoxy-terminated co-monomer content indicated by increasing glass-rubber transition temperature apparently had a stronger influence on gas transport properties than the increase in fractional free volume.

This chapter has been adapted with permission from an article published in the *Journal of Membrane Science* under the same title [90], originally written by the author.

6.2. Introduction

In the previous chapter, incorporation of ethoxy (-OC_2H_5) terminal groups into XLPEO was found to be potentially even more effective than -OCH_3 terminal groups in increasing gas permeability. Further permeability increase in XLPEO seems achievable by introducing bulky, non-polar, non-interacting terminal groups into the copolymer networks to expand local free volume and increase overall polymer fractional free volume (*FFV*). To assess this hypothesis, this chapter reports the physical and transport properties of cross-linked PEGDA prepared with two phenoxy-terminated co-monomers of different chain lengths. PEGDA copolymers prepared with a flexible, ethoxy-terminated co-monomer of comparable length are explored for comparison.

The two phenoxy-terminated co-monomers are di(ethylene glycol) phenyl ether acrylate (DEGPEA) and poly(ethylene glycol) phenyl ether acrylate (n=4) (PEGPEA), containing 37 wt% EO and 54 wt% EO, respectively. The ethoxy-terminated co-monomer in this chapter is di(ethylene glycol) ethyl ether acrylate (DEGEEA); like DEGPEA, it contains two ethylene oxide moieties per monomer. In DEGEEA, the concentration of ethylene oxide (47 wt% EO) is higher than that of the ethoxy-terminated co-monomer studied in Chapter 5 (2-ethoxyethyl acrylate (2-EEA); 31 wt% EO). Chemical structures are given in Table 3.2, and a schematic of XLPEO synthesized from these co-monomers is provided in Figure 6.1. Characterization of the as-prepared copolymer networks included bulk density measurement for the estimation of fractional free volume, as well

as thermal analysis studies for the elucidation of the glass transition and overall polymer chain mobility. Transport properties of the corresponding copolymer networks were established based on experimental determination of pure gas permeability (CO_2, CH_4, H_2, O_2 and N_2) and pure gas solubility (CO_2 and CH_4) at 35°C.

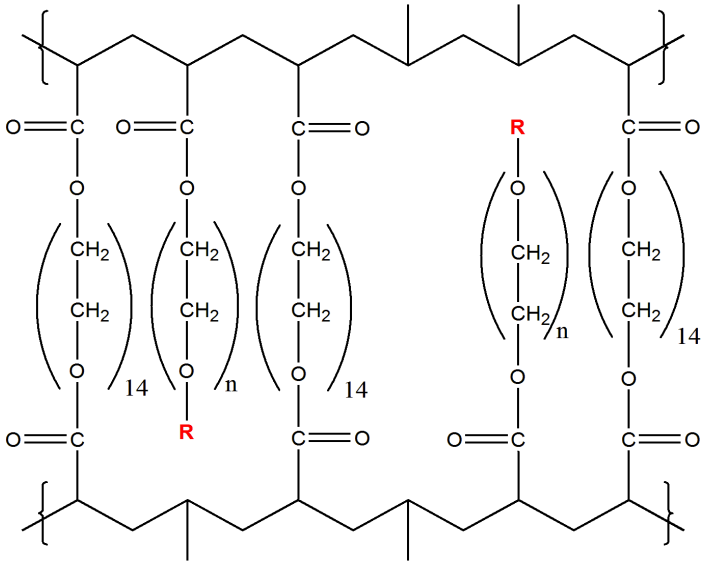

Figure 6.1: Scheme of representative network elements in XLPEO, with **R** representing the functional end-group of the monoacrylate co-monomer (**R** = CH_2CH_3 for DEGEEA, C_6H_5 for DEGPEA and PEGPEA) and *n* representing the average number of ethylene oxide group repeat units (*n* = 2 for DEGEEA and DEGPEA, 4 for PEGPEA).

6.3. Results and Discussion

6.3.1. Fractional Free Volume and Chain Mobility

Density, glass transition temperature and fractional free volume (*FFV*) data for the copolymer films prepared in this chapter are presented in Table 6.1. Increasing the amount of phenoxy-terminated ($-OC_6H_5$) co-monomers (DEGPEA or PEGPEA) in the cross-linked PEGDA networks leads to a systematic increase in *FFV*. Similar to the

methoxy- or ethoxy-terminated monomers, such as PEGMEA, 2-EEA and DEGEEA (*cf.* Chapters 4 and 5), the bulky, non-polar phenoxy groups at the end of the flexible pendant chains appear to be responsible for the observed increase in local free volume in the networks. As illustrated in Figure 6.2, the increases in *FFV* across the PEGDA/DEGPEA and PEGDA/PEGPEA network series appear to be similar, despite the difference in pendant chain length. However, these *FFV* increases are lower than the trend observed for the PEGDA/DEGEEA networks (*cf.* Table 6.1).

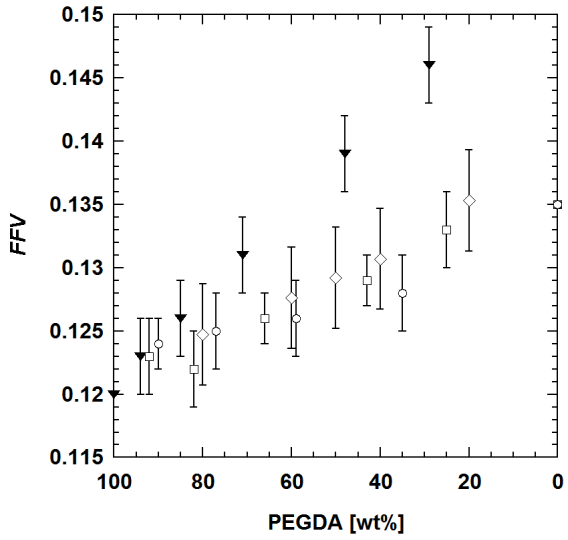

Figure 6.2: Fractional free volume of PEGDA copolymers as a function of PEGDA content in prepolymer solution. The co-monomers are ▼: DEGEEA, ◊: PEGMEA, □: DEGPEA and ○: PEGPEA. Free volume for PEGMEA was calculated using density data measured by the author according to assumptions detailed in Section 2.3 and Table 5.2.

Table 6.1: Physical properties of PEGDA/DEGEEA, PEGDA/DEGPEA and PEGDA/PEGPEA copolymers.

Co-monomer	PEGDA mol%	PEGDA wt%	T_g [°C]	ρ_P [g/cm^3]	*FFV*
---	100	100	-37 ± 1	1.190 ± 0.004	0.120 ± 0.003
DEGEEA	80	94	-38 ± 1	1.184 ± 0.004	0.123 ± 0.003
	60	85	-39 ± 1	1.180 ± 0.004	0.126 ± 0.003
	40	71	-41 ± 1	1.171 ± 0.004	0.131 ± 0.003
	20	48	-44 ± 1	1.159 ± 0.004	0.139 ± 0.003
	10	29	-46 ± 1	1.148 ± 0.004	0.146 ± 0.003
DEGPEA	80	92	-35 ± 1	1.188 ± 0.004	0.123 ± 0.003
	60	82	-32 ± 1	1.193 ± 0.004	0.122 ± 0.003
	40	66	-29 ± 1	1.195 ± 0.004	0.126 ± 0.002
	20	43	-23 ± 1	1.199 ± 0.002	0.129 ± 0.002
	10	25	-17 ± 1	1.201 ± 0.004	0.133 ± 0.003
	0	0	-12 ± 1	1.209 ± 0.003	0.135 ± 0.002
PEGPEA	80	90	-37 ± 1	1.185 ± 0.002	0.124 ± 0.002
	60	77	-35 ± 1	1.186 ± 0.003	0.125 ± 0.003
	40	59	-33 ± 1	1.188 ± 0.004	0.126 ± 0.003
	20	35	-31 ± 1	1.190 ± 0.004	0.128 ± 0.003
	0	0	-28 ± 1	1.186 ± 0.004	0.135 ± 0.003

The glass transition temperature provides an indication of the overall copolymer chain mobility. Representative DSC scans for the PEGDA/PEGPEA copolymers are shown in Figure 6.3. Figure 6.4 compares the glass transition temperatures of the PEGDA/DEGPEA and PEGDA/PEGPEA copolymers to those of the PEGDA/DEGEEA, PEGDA/2-EEA and PEGDA/PEGMEA networks (*cf.* Tables 4.1 and 5.1). The glass transition temperatures follow a random copolymer model as given by the Fox equation (Equation 5.1) [107]. For the XLPEGDA copolymer networks containing phenoxy-terminated side chains, an increase in glass transition temperature is observed with increasing co-monomer content, the effect being stronger in copolymers containing shorter DEGPEA pendant groups. The increase in T_g is presumably due to the bulky character of the phenoxy terminal group, which introduces considerable steric hindrance to segmental motions associated with the glass-rubber transition. The glass transition temperatures of the DEGEEA-based copolymers, in contrast, decrease with increasing co-monomer content, and fall between those of PEGDA/2-EEA and PEGDA/PEGMEA. This result appears to be primarily a reflection of side-chain length, as determined by the number of flexible repeat units within the respective co-monomers [107].

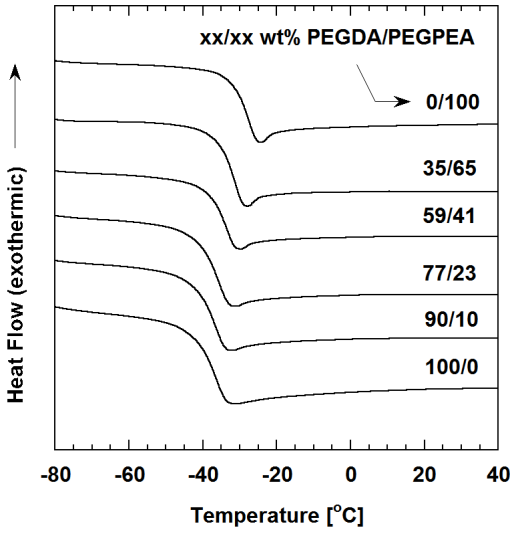

Figure 6.3: Second scan DSC thermograms for PEGDA/PEGPEA copolymers. The heating rate was 10°C/min. The thermograms have been displaced vertically for clarity.

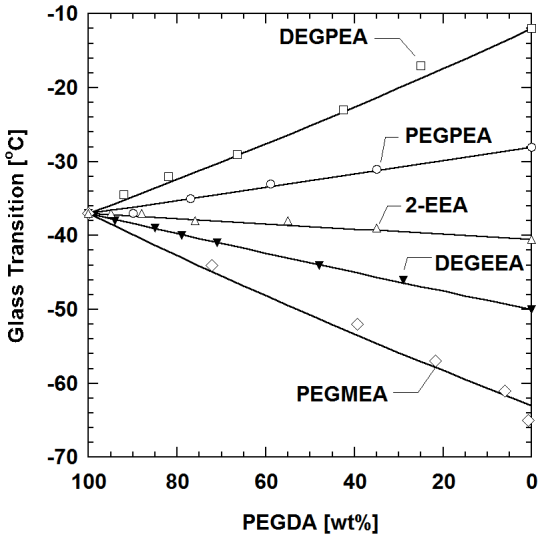

Figure 6.4: Effect of PEGDA content in the prepolymer solution on glass transition temperature determined by DSC. The co-monomers are Δ : 2-EEA,▼: DEGEEA, ◊: PEGMEA, □: DEGPEA and ○: PEGPEA. The model lines are drawn according to Equation 5.1 (Fox equation). Data for PEGMEA are reproduced from Figure 4.8, and those for 2-EEA are from Figure 5.4. The uncertainty is ±1°C.

As shown in the previous chapter, while changes in *FFV* can be correlated with overall polymer chain mobility and T_g (see Equation 4.4), such correlations are not necessarily universal across various copolymer series (*cf*. Figure 5.5). Both the length of the co-monomer side chains and the nature of the side chain terminal groups can significantly affect the glass transition temperature and free volume characteristics of the resulting networks (see previous chapter) [32, 74, 95]. *FFV*-T_g correlations for the copolymers considered in this chapter are shown in Figure 6.5. In all cases, the introduction of the PEG-based side chains produces an increase in *FFV* with increasing co-monomer content. For PEGDA/DEGEEA, the relatively flexible, compact DEGEEA pendants lead to a progressive reduction in T_g with increasing branch concentration, a trend that is consistent with the results for the PEGDA/PEGMEA series. However, for networks containing the phenoxy-terminated side chains, the steric hindrance introduced by the terminal phenyl group drives T_g upwards with increasing branch content, an effect that is especially pronounced for the shorter DEGPEA pendant, which is spatially more strongly correlated to the network backbone. The outcome is distinct *FFV*-T_g relations that appear to independently reflect the influence of co-monomer repeat length, and the relative bulk and chemical nature of the side-chain terminal groups. As such, increased *FFV* in the phenoxy-terminated copolymer series does not reflect increased polymer chain flexibility.

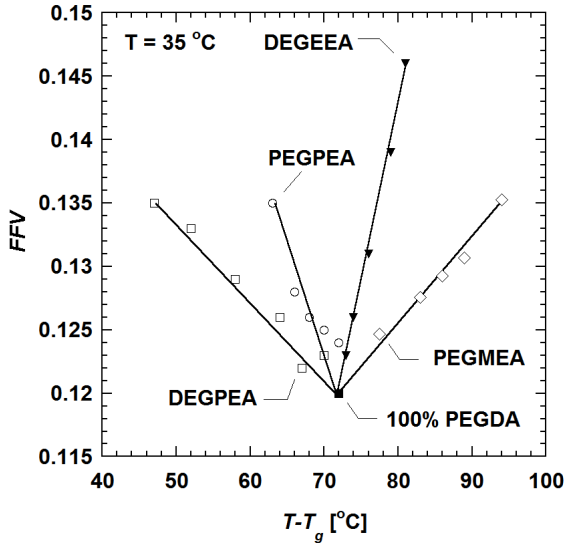

Figure 6.5: Fractional free volume of XLPEO versus ($T - T_g$), where $T = 35°C$ and T_g is the glass transition temperature of the corresponding copolymer. T_g data are obtained from Figure 6.4 and plotted against *FFV* from Figure 6.2. The lines are drawn based on Equation 4.4. ■: 100% PEGDA, ▼: PEGDA/DEGEEA, ◊: PEGDA/PEGMEA, □: PEGDA/DEGPEA and ○: PEGDA/PEGPEA.

Additional insights into the structure and relaxation properties of the copolymer networks were obtained via dynamic mechanical and dielectric spectroscopy measurements; these results complement detailed dynamic studies on XLPEGDA networks reported previously. Representative dynamic mechanical data for the PEGDA/PEGPEA copolymer series are shown in Figure 6.6, and demonstrate the influence of increasing co-monomer content on the glass-rubber relaxation. Similar data for the PEGDA/DEGEEA series were presented earlier in the study by Borns et al. [95]. With increasing PEGPEA co-monomer, the glass transition temperature shifts to higher values consistent with the calorimetric results; the associated peak temperatures (T_α, based on peak in tan δ at 1 Hz) are reported in Table 6.2. The observed increase in relaxation

intensity with co-monomer content is primarily a reflection of the stoichiometrically-controlled decrease in cross-link density across the copolymer series.

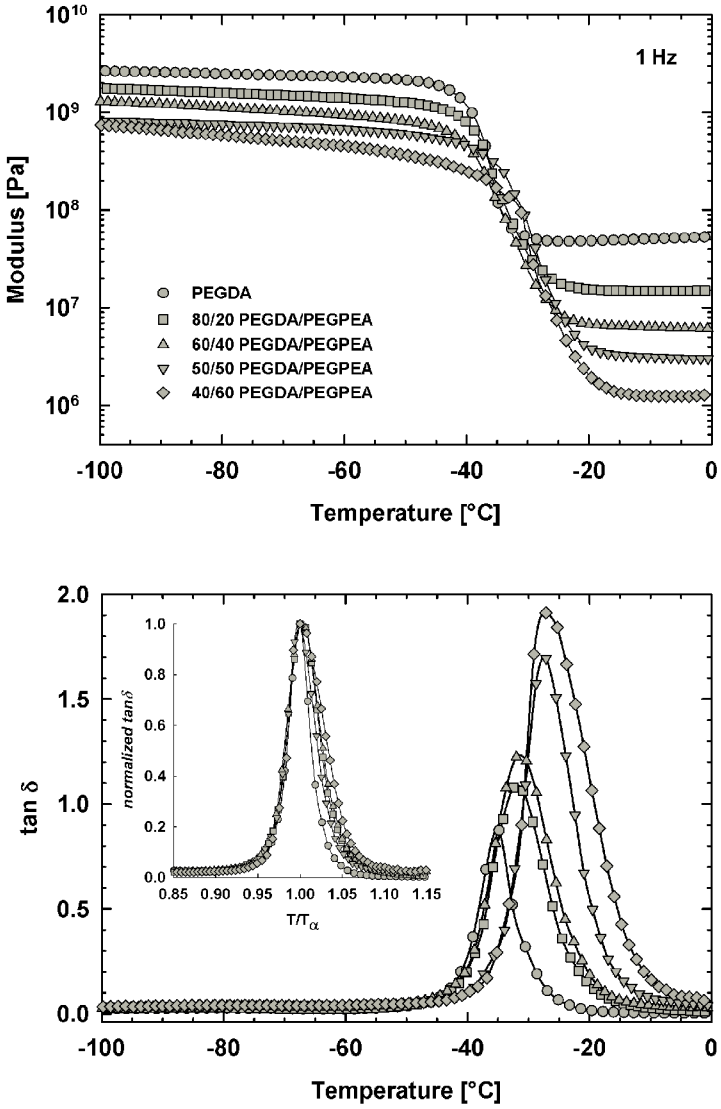

Figure 6.6: a) Dynamic mechanical storage modulus (*E'*) [Pa] and b) tan δ vs. temperature [°C] for PEGDA/PEGPEA copolymers at 1 Hz; all compositions expressed on a wt% basis. *Inset on b):* normalized tan δ vs. T/T_α for PEGDA/PEGPEA copolymers. Symbols are defined in Figure 6.6a.

Table 6.2: Characteristics of PEGDA/DEGEEA and PEGDA/PEGPEA as determined via dynamic mechanical analysis (DMA)

Co-monomer	PEGDA [wt%]	T_α (1 Hz) [°C]	β_{KWW}
---	100	-35	0.30
DEGEEA*	80	-36	0.29
	60	-38	0.33
	50	-38	0.32
PEGPEA	80	-32	0.23
	60	-31	0.21
	50	-27	0.20
	40	-27	0.19

Note: T_α [°C] is the dynamic mechanical peak temperature at 1 Hz; β_{KWW} is the Kohlrausch-Williams-Watts distribution parameter [85]. *PEGDA/DEGEEA data are taken from Borns et al. [95].

Time-temperature superposition was used to establish storage modulus master curves for each copolymer composition, consistent with prior studies [74, 75]. The resulting master curves were fit using the Kohlrausch-Williams-Watts (KWW) stretched-exponential function (Equation 2.19), with the corresponding exponent designated as β_{KWW} [85]. The exponent determined for the XLPEGDA homopolymer network, β_{KWW} = 0.30 [75]. Across the highly-flexible PEGDA/PEGMEA series, the glass-rubber relaxation was observed to narrow with increasing co-monomer content and correspondingly lower cross-link density [74]. For the PEGDA/PEGPEA series studied here, however, the introduction of bulky side pendants leads to a broadening of the relaxation and a progressive decrease in the β_{KWW} exponent, despite the reduced cross-link constraint associated with increasing co-monomer content (see Table 6.2). The inset to Figure 6.6b

(normalized tan δ vs. normalized relaxation temperature) indicates that most of this broadening occurs on the high-temperature side of the glass-rubber relaxation.

Dielectric measurements performed on the PEGDA/PEGPEA copolymers provide information with respect to the intensity and time-temperature behavior of both the sub-glass and glass-rubber relaxations. Dielectric studies on crystalline PEO and the XLPEGDA homopolymer indicate two local sub-glass relaxations (β_1 and β_2), as well as the glass-rubber relaxation (α) with increasing temperature [87]; the influence of co-monomer content on the dielectric dispersion characteristics of various PEGDA copolymers has been reported in detail [86, 95]. An Arrhenius plot (f_{MAX} vs. 1000/T) for the PEGDA/PEGPEA copolymers studied here is shown in Figure 6.7, where $f_{MAX} = [2\pi\tau_{MAX}]^{-1}$ and τ_{MAX} is the relaxation peak time. For both sub-glass processes, a linear result is obtained, consistent with the localized, essentially non-cooperative character of these relaxations. The data are independent of copolymer composition, with corresponding activation energies identical to the 100% XLPEGDA result: $E_A(\beta_1) = 41$ kJ/mol, and $E_A(\beta_2) = 65$ kJ/mol [87]. This comparison indicates that despite their bulky nature, the presence of the phenoxy-terminated side chains does not alter the time-temperature character of the sub-glass transitions. Across the glass-rubber relaxation, the data indicate a non-Arrhenius process that is cooperative in character, and which can be described by the Williams-Landel-Ferry (WLF) relation (see solid curves in Figure 6.7) [84]. The relative position of each copolymer data set reflects the progressive increase in T_g (or relaxation time) with increasing co-monomer content.

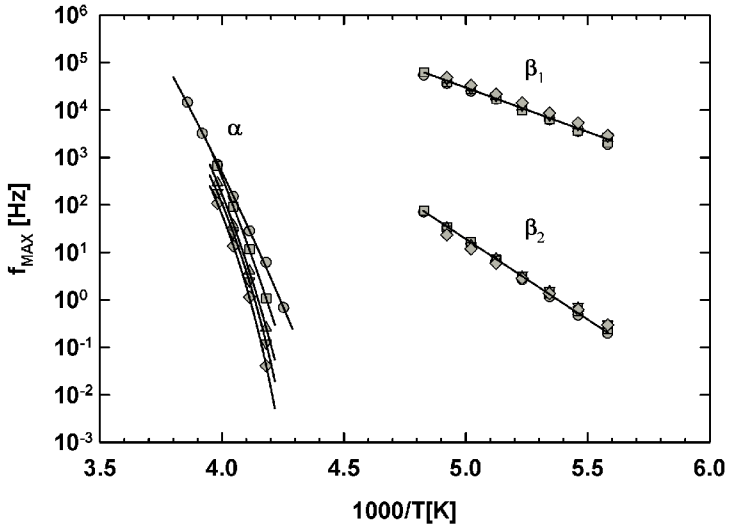

Figure 6.7: Arrhenius plot of f_{MAX} [Hz] vs. 1000/T [K] for PEGDA/PEGPEA copolymers based on dielectric measurements. Symbols are defined in Figure 6.6a.

The dielectric relaxation response characteristics of the PEGDA/PEGPEA copolymers are similar in many respects to the results obtained for the model PEGDA/PEGMEA series, and are not detailed here in the interest of brevity. For more information regarding the dielectric relaxation behavior of the XLPEGDA copolymers, the reader is referred to ref. [86].

6.3.2. Gas Transport Properties

The gas permeability data were interpolated to infinite dilution (*i.e.*, an upstream fugacity of zero) from several measurements performed at various fugacities and 35°C [63] (*cf.* Equation 2.10). Figure 6.8 and Table 6.3 present gas permeability as a function of co-monomer content. The order of the gas permeability values is: $CO_2 > H_2 > O_2 \geq CH_4 > N_2$ [2, 32] (also see section 5.3.2). The data obey the random binary copolymer model given

in Equation 4.1 [106]. Given the relatively small variations in density encountered across each polymer series, the resulting volume fraction values are nearly identical to the wt% figures reported in Table 6.1. $P_{A,1}$ in Equation 4.1 was determined by experimental measurement of 100% PEGDA polymer. For the DEGPEA and PEGPEA series, $P_{A,2}$ was determined by direct experimental measurement of the polymerized acrylate monomer. However, for the DEGEEA series, $P_{A,2}$ could not be determined directly due to a lack of structural integrity for the pure polymerized DEGEEA film. In this case, $P_{A,2}$ was estimated instead by applying Equation 4.1 to the sample polymerized with the least amount of PEGDA.

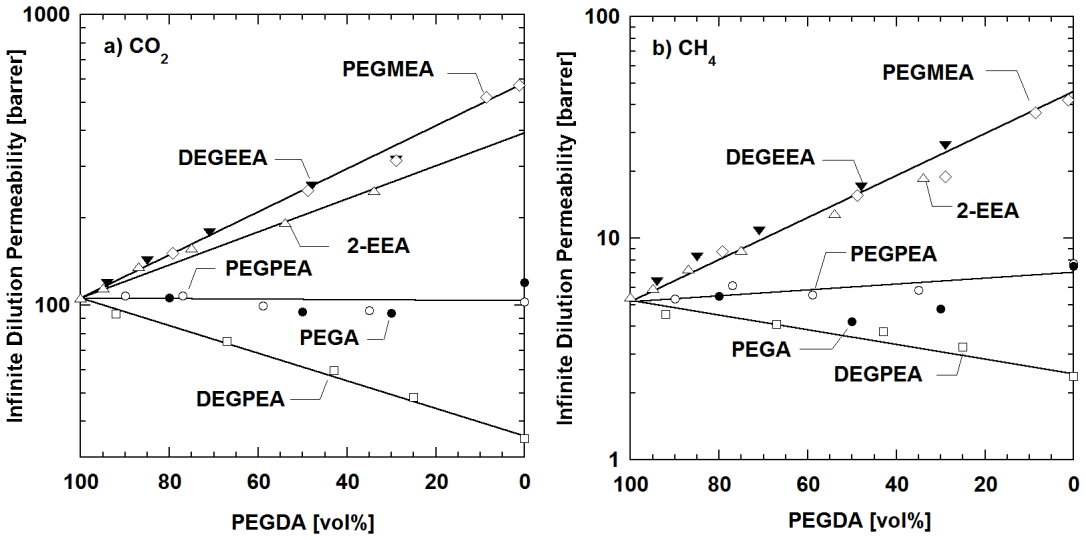

Figure 6.8: Effect of PEGDA content on infinite dilution gas permeability at 35°C. The lines through the data are based on Equation 4.1. The gases are a) CO_2, b) CH_4, c) H_2, d) O_2 and e) N_2. The co-monomers are ▼: DEGEEA, ◊: PEGMEA, Δ : 2-EEA, □: DEGPEA, ○: PEGPEA, ●: PEGA. PEGMEA and PEGA data were reproduced from Figure 4.5 and 2-EEA data from Figure 5.7. The average uncertainty is ± 6% of the permeability value.

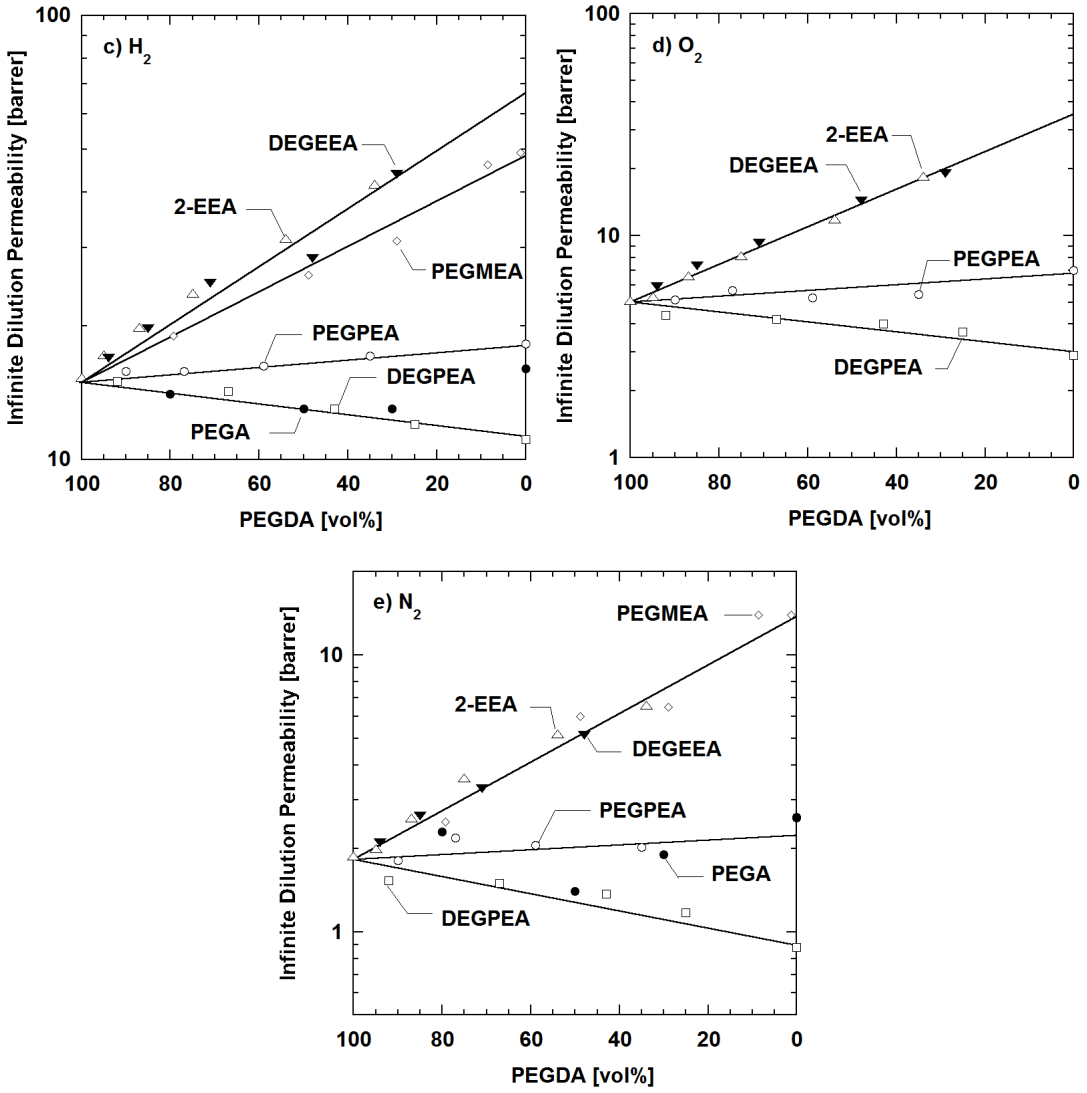

Figure 6.8 (*continued*)**:** Effect of PEGDA content on infinite dilution gas permeability at 35°C. The lines through the data are based on Equation 4.1. The gases are a) CO_2, b) CH_4, c) H_2, d) O_2 and e) N_2. The co-monomers are ▼: DEGEEA, ◊: PEGMEA, Δ : 2-EEA, □: DEGPEA, ○: PEGPEA, ●: PEGA. PEGMEA and PEGA data were reproduced from Figure 4.5 and 2-EEA data from Figure 5.7. The average uncertainty is ± 6% of the permeability value.

Table 6.3: Infinite dilution gas permeability and solubility of PEGDA/DEGEEA, PEGDA/DEGPEA and PEGDA/PEGPEA copolymers at 35°C, determined experimentally.

Co-monomer	PEGDA vol%	Permeability [barrer]					Solubility [cm^3(STP)/cm^3 atm]	
		CO_2	H_2	CH_4	O_2	N_2	CO_2	CH_4
---	100	110 ± 6	15 ± 0.8	5.5 ± 0.3	5.1 ± 0.3	1.9 ± 0.1	1.30 ± 0.06	0.075 ± 0.03
DEGEEA	94	120 ± 7	17 ± 1.0	6.4 ± 0.4	5.9 ± 0.4	2.1 ± 0.1	1.34 ± 0.04	0.078 ± 0.03
	85	140 ± 9	20 ± 1.2	8.3 ± 0.5	7.4 ± 0.4	2.6 ± 0.2	1.37 ± 0.06	0.10 ± 0.03
	71	180 ± 11	25 ± 1.5	11 ± 0.6	9.3 ± 0.6	3.3 ± 0.2	1.42 ± 0.06	0.094 ± 0.03
	48	260 ± 15	28 ± 1.7	17 ± 1.0	14 ± 0.9	5.2 ± 0.3	1.52 ± 0.05	0.11 ± 0.04
	29	320 ± 19	44 ± 2.6	26 ± 1.6	19 ± 1.1	---	1.59 ± 0.06	0.11 ± 0.04
DEGPEA	92	94 ± 5.6	15 ± 0.9	4.5 ± 0.3	4.4 ± 0.3	1.5 ± 0.1	1.21 ± 0.06	0.094 ± 0.04
	67	76 ± 4.5	14 ± 0.9	4.1 ± 0.2	4.2 ± 0.2	1.5 ± 0.1	1.18 ± 0.04	0.083 ± 0.03
	43	60 ± 3.6	13 ± 0.8	3.8 ± 0.2	4.0 ± 0.2	1.4 ± 0.1	1.12 ± 0.06	0.091 ± 0.05
	25	48 ± 2.9	12 ± 0.7	3.2 ± 0.2	3.7 ± 0.2	1.2 ± 0.1	1.02 ± 0.03	0.077 ± 0.02
	0	35 ± 2.1	11 ± 0.7	2.4 ± 0.1	2.9 ± 0.2	0.88 ± 0.05	0.94 ± 0.03	0.089 ± 0.03
PEGPEA	90	110 ± 6	16 ± 0.9	5.3 ± 0.3	5.2 ± 0.3	1.8 ± 0.1	1.28 ± 0.03	0.073 ± 0.02
	77	110 ± 6	16 ± 0.9	6.1 ± 0.4	5.7 ± 0.3	2.2 ± 0.1	1.25 ± 0.05	0.091 ± 0.05
	59	100 ± 6	16 ± 1.0	5.6 ± 0.3	5.3 ± 0.3	2.0 ± 0.1	1.22 ± 0.04	0.095 ± 0.04
	35	100 ± 6	17 ± 1.0	5.8 ± 0.4	5.4 ± 0.3	2.0 ± 0.1	1.15 ± 0.03	0.086 ± 0.03
	0	100 ± 6	18 ± 1.1	7.7 ± 0.5	7.0 ± 0.4	2.6 ± 0.2	1.09 ± 0.05	0.085 ± 0.04

Note: All uncertainties are estimated using the propagation of errors method [102].

In general, permeability of all gases increases with DEGEEA co-monomer content in XLPEGDA, which is consistent with the results obtained for 2-EEA and PEGMEA. According to Equation 2.13, permeability should increase as *FFV* increases. Therefore, the observed *FFV* increase with increasing DEGEEA content appears to account for the observed increase in gas permeability. The increase in permeability for light gases other than CO_2 is nearly the same in PEGDA/DEGEEA as in PEGDA/2-EEA and is attributable to the comparable structure of the two short-chain ethoxy-terminated co-monomers, leading to similar *FFV* and gas diffusivity at the same monomer concentrations. DEGEEA, however, contains an additional ethylene oxide group and this ethylene oxide unit results in increased CO_2 affinity with the polymer and, in turn, higher CO_2 permeability in PEGDA/DEGEEA as compared to PEGDA/2-EEA. The CO_2 permeability increase in PEGDA/DEGEEA with increasing co-monomer content nearly matches the increase observed in the PEGDA/PEGMEA system, despite the lower EO content of DEGEEA.

Given the *FFV* increase encountered upon increasing PEGPEA or DEGPEA concentration in the XLPEO networks, which was similar to that encountered in PEGDA/PEGMEA, one might anticipate an increase in gas permeability of these materials. However, this result is not observed. Instead, gas permeability of the PEGDA/PEGPEA series varies little with PEGPEA content, increasing only slightly for penetrants other than CO_2. Gas permeability decreases significantly with addition of the

shorter DEGPEA co-monomer. For example, CO_2 permeability decreases from 110 barrer for pure XLPEGDA to 35 barrer for polymerized DEGPEA.

Pure gas ideal selectivity data are presented in Figure 6.9. The gas selectivity trends in XLPEO primarily result from the changing gas affinity due to changes in polymer chemical properties (in the case of CO_2), and changes in the size-sieving ability of the polymer due to changes in free volume and chain stiffness (see previous chapter). An increase in size-sieving ability favors the transport of gases with smaller kinetic diameter, and can be illustrated by considering the selectivity of permanent gases [2, 44]. Selectivity comparisons for the permanent gases (*i.e.*, H_2/N_2 and O_2/N_2) are presented in Figure 6.9a. For these gas pairs, any changes in permanent gas selectivity should be due mainly to size differences: H_2 (2.89 Å) vs. N_2 (3.64 Å), and O_2 (3.46 Å) vs. N_2 (3.64 Å) (*cf*. Table 2.2) [67]. As shown in Figure 6.9a, changes in permanent gas selectivity as a result of changing polymer size-sieving characteristics for PEGDA/DEGEEA, PEGDA/ DEGPEA and PEGDA/PEGPEA series are not significant within the measurement uncertainty.

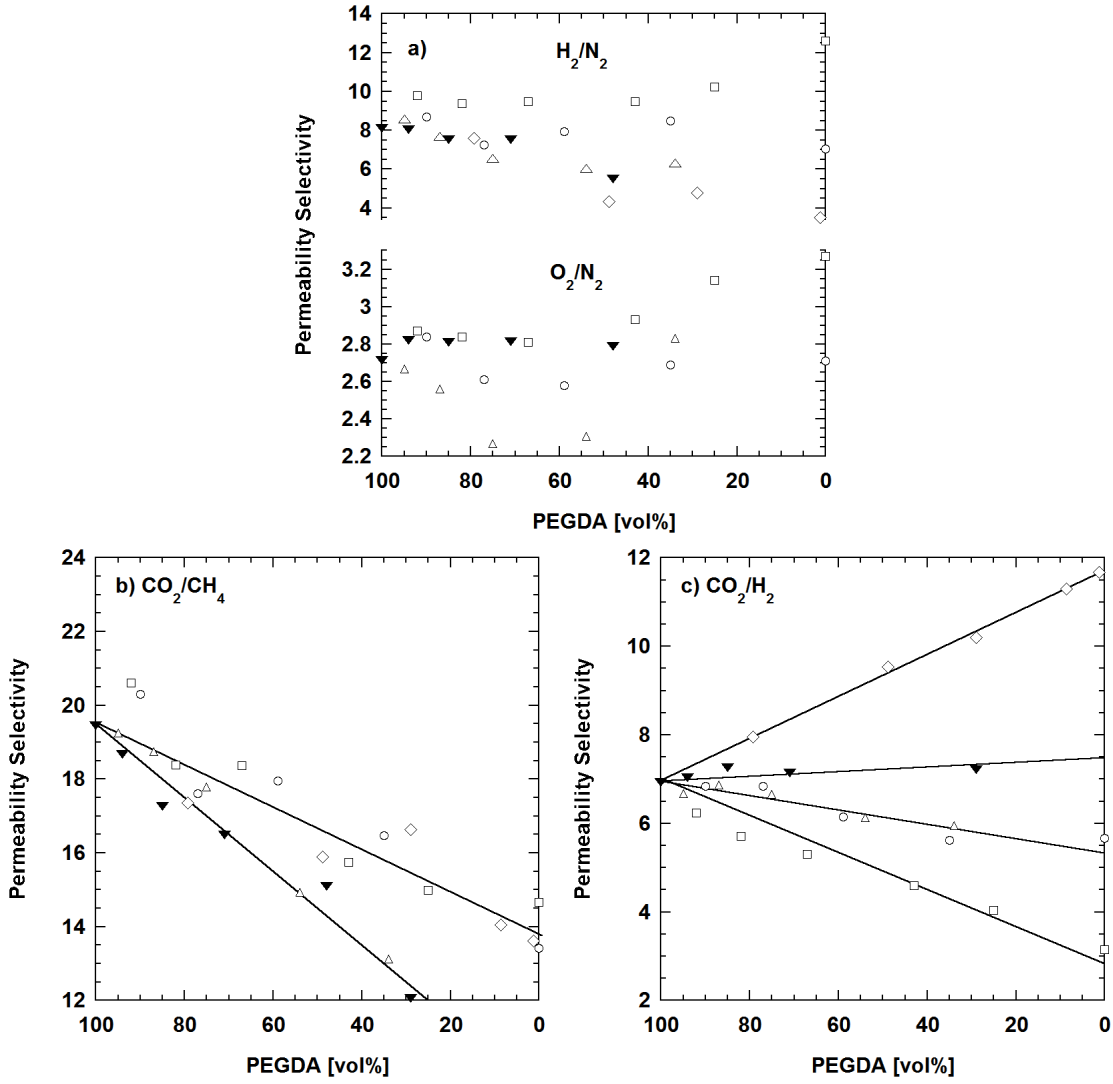

Figure 6.9: Effect of PEGDA content on infinite dilution gas selectivity at 35°C. The solid lines are drawn to guide the eye. The selectivities are a) H_2/N_2 and O_2/N_2, b) CO_2/CH_4, and c) CO_2/H_2. The co-monomers are ▼: DEGEEA, ◊: PEGMEA, Δ : 2-EEA, □: DEGPEA, ○: PEGPEA. The average uncertainty is ± 8% of the selectivity value.

Figures 6.9b and c shows selectivity values for CO_2/CH_4 and CO_2/H_2. Across each series, the overall EO content of the network decreases with increased DEGEEA, DEGPEA or PEGPEA concentration. In Figure 6.9b, CO_2/CH_4 selectivity generally decreases with

increasing co-monomer content regardless of the co-monomer, even the ones containing high EO content such as PEGMEA. As such, the relative affinity of CO_2 and CH_4 for the polymer does not appear to play a significant role in differentiating the selectivity trends for each series. In contrast, H_2 molecules are much smaller and less condensable than CH_4. Apparently, the combined effects of size discrimination, however minimal, and the change in CO_2 affinity for the polymer network compared to H_2 were sufficient to produce more distinct trends in CO_2/H_2 selectivity for the various copolymers, as shown in Figure 6.9c.

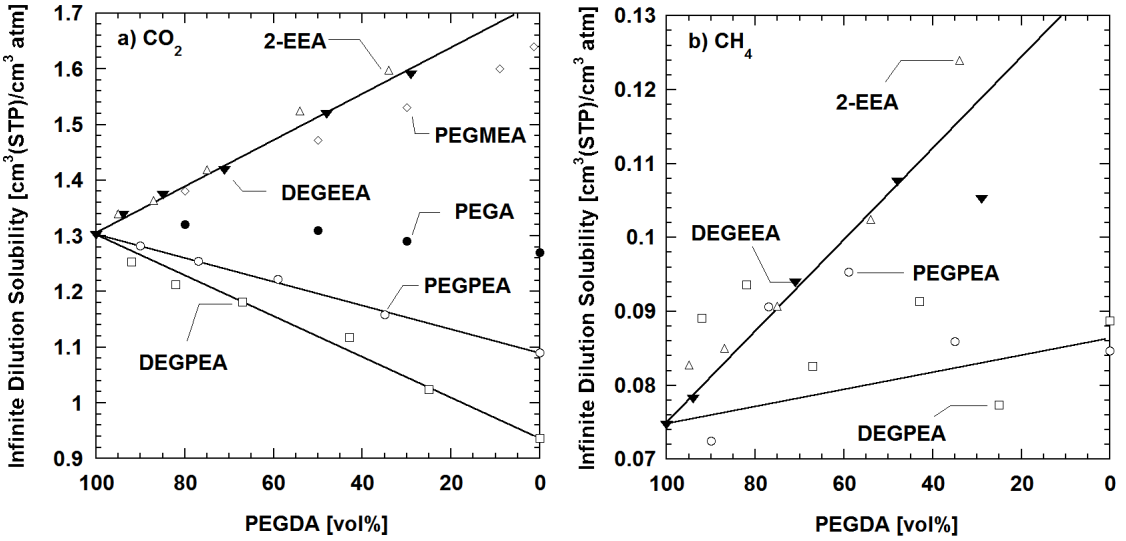

Figure 6.10: Effect of PEGDA content on infinite dilution gas solubility at 35°C, a) CO_2 and b) CH_4. The co-monomers are ▼: DEGEEA, ○: PEGPEA and □: DEGPEA. The lines are drawn to guide the eye. Comparison data with ◊: PEGMEA, Δ : 2-EEA, and ●: PEGA are given where available (ref. [32] and Figure 5.9). The average uncertainty is ± 0.04 $cm^3(STP)/cm^3$ atm (*cf.* Table 6.3 for actual values).

In order to directly assess CO_2 and CH_4 affinity for the polymer networks, sorption isotherms were obtained by measuring gas uptake in the polymer at equilibrium as a function of fugacity. The isotherms were linear in all cases, so solubility coefficients are reported as Henry's law coefficients (*cf.* Equation 2.11) [41]. The solubilities of permanent gases in XLPEO were too low to measure. The infinite dilution solubility coefficients are plotted as a function of copolymer composition in Figure 6.10 and are tabulated in Table 6.3.

The CO_2 solubility coefficients tend to increase with increasing DEGEEA content, consistent with trends previously observed in 2-EEA and PEGMEA [32, 127]. Addition of DEGEEA, like 2-EEA, introduces branches with relatively non-polar ends and lower EO content as compared to PEGDA, and thus increasing the amount of DEGEEA tends to lower overall polar content while simultaneously reducing cross-link density. Given the reduction in EO content with increasing DEGEEA, CO_2 solubility would be expected to decrease with increasing DEGEEA concentration [41]. However, as observed in Figure 6.10a, the CO_2 solubility coefficients in PEGDA/DEGEEA copolymers increase with increasing DEGEEA content. As DEGEEA concentration increases, the lower polar content in the polymer will lead to a decrease in overall polymer cohesive energy density and a reduction in the energy required to open a gap in the polymer matrix of sufficient size to accommodate a penetrant molecule [2, 41]. This reduction in cohesive energy density would be expected to act to increase solubility of all gases, and in the case of CO_2, it is apparently strong enough to counter a lower affinity to CO_2 that presumably

accompanies the reduction in polar group content as DEGEEA concentration increases. Additionally, the reduction in cross-link density with increasing DEGEEA content would act to increase solubility as well.

In contrast, the CO_2 solubility in both phenoxy-terminated copolymer systems decreases with increasing co-monomer content. The phenyl terminal groups of the DEGPEA or PEGPEA branches are less polar than the alkoxy end groups on 2-EEA, DEGEEA or PEGMEA. Lower polar content in the PEGDA/DEGPEA and PEGDA/PEGPEA networks, due to lower ethylene oxide content and the addition of phenoxy groups, may be the decisive factor with respect to CO_2 solubility for these series, particularly for PEGDA/DEGPEA (n=2 EO in side chains). A decrease in CO_2 solubility has also been observed in hydroxy-terminated PEGDA/2-HEA copolymer system (*cf*. Figure 5.9), where strong hydrogen bonds led enhanced inter-chain interactions, possibly contributing to increased cohesive energy density.

Infinite dilution diffusion coefficients can be calculated from permeability and solubility data using Equation 2.2; these results are shown in Figure 6.11. As in the other XLPEO systems studied in Chapters 4 and 5, the gas diffusivity follows the trends in permeability to a substantial degree. Both CO_2 and CH_4 diffusivity increases with increasing DEGEEA concentration: gas diffusivity tends to be slightly higher in the PEGDA/DEGEEA copolymers than in PEGDA/2-EEA at similar co-monomer content owing to the higher chain mobility (*i.e.*, lower T_g) imparted by the longer, more flexible

DEGEEA branches. As shown in Figures 6.12 and 6.13, the permeability and diffusivity coefficients in the PEGDA/DEGEEA series are well-described by the Cohen-Turnbull model (*cf.* Equations 2.12 and 2.13). Good agreement with the model is observed when adjustable parameters given in Table 2.1 are applied, consistent with results reported previously for the PEGDA/PEGMEA series [43] and the analogous series with shorter alkoxy-terminated co-monomers, PEGDA/EGMEA and PEGDA/2-EEA (*cf.* Figures 4.10, 5.11 and 5.12).

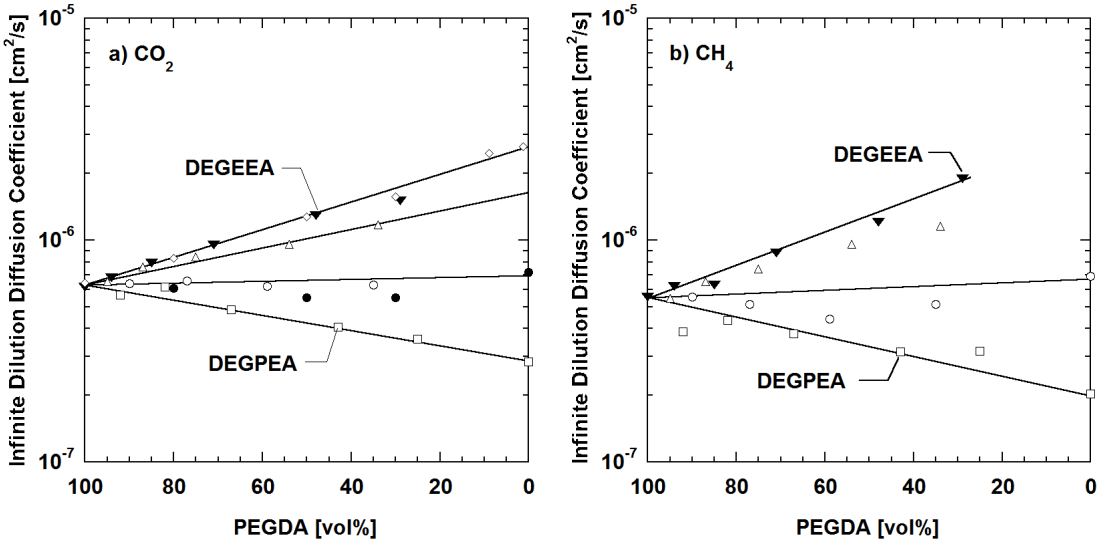

Figure 6.11: Effect of PEGDA content on infinite dilution gas diffusivity at 35°C, a) CO_2 and b) CH_4. The lines are drawn to guide the eye. The co-monomers are ▼: DEGEEA, ◊: PEGMEA, Δ : 2-EEA, ○: PEGPEA, □: DEGPEA, ●: PEGA. The average uncertainty is ± 7% the CO_2 diffusivity and between ± 30% and ± 40% of the CH_4 diffusivity.

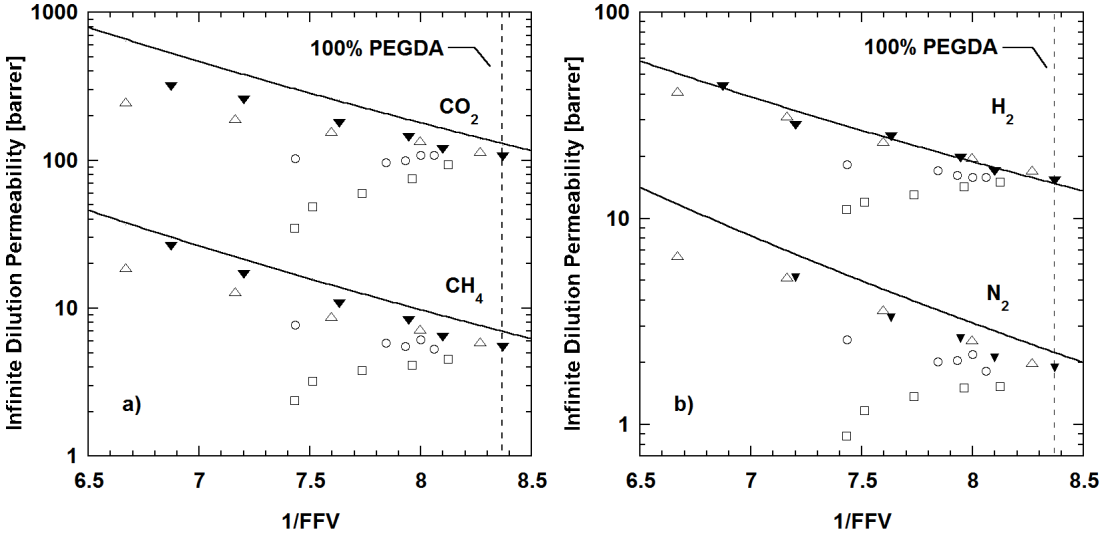

Figure 6.12: Comparison between experimental and predicted infinite dilution permeability based on the free volume model, with model parameters given in Table 2.1, for (from top to bottom) a) CO_2 and CH_4, b) H_2 and N_2. The dashed line indicates the free volume of polymer cast from 100 wt% PEGDA in the prepolymer solution. The co-monomers of PEGDA are ▼: DEGEEA, Δ : 2-EEA, □: DEGPEA and ○: PEGPEA, with increasing content of co-monomer further away from the dashed line.

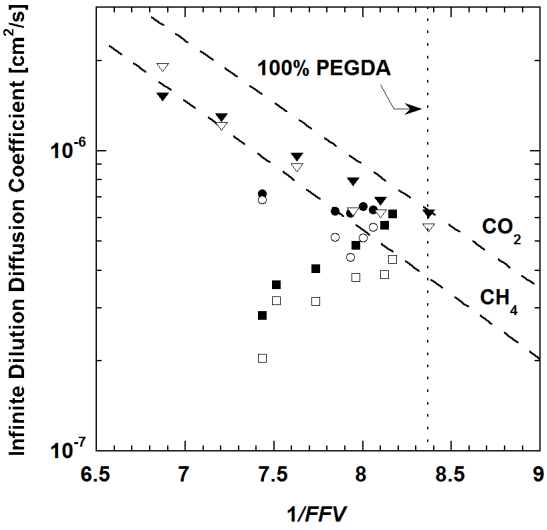

Figure 6.13: Correlation between infinite dilution gas diffusivity at 35°C and polymer free volume. The data shown are for CO_2 (▼: PEGDA/DEGEEA, ■: PEGDA/DEGPEA and ●: PEGDA/PEGPEA) and CH_4 (analogous open symbols). The vertical dashed line indicates the free volume of polymer prepared from 100% PEGDA. The model parameters are from Table 2.1.

Conversely, the gas diffusivity does not change appreciably with co-monomer content for the PEGPEA series and decreases for the DEGPEA series, again despite the apparent increase in estimated *FFV* as co-monomer content increases in both sets of copolymers. Consequently, as shown in Figures 6.12 and 6.13, gas diffusivity of the phenoxy-terminated copolymers does not follow the expected trends as predicted by the Cohen-Turnbull model.

An explanation for the gas diffusion behavior in phenoxy-terminated networks with respect to *FFV* may lie in the polymer chain mobility, as reflected in T_g. van Amerongen found that the logarithm of gas diffusion coefficients of permanent gases in a variety of rubbery polymers depended nearly linearly on ($T - T_g$) (*i.e.*, the difference between the measurement temperatures and the glass transition) [41]. Certainly, in the case of the PEGDA/DEGPEA and PEGDA/PEGPEA copolymers, (T - T_g) appears to be a stronger correlating factor for gas diffusivity as compared to free volume. Lin et al. accounted for chain mobility effects in the PEGDA/PEGMEA system by noting that *FFV* was positively correlated with ($T - T_g$) using Equation 4.4 [43]. For the PEGDA/DEGPEA and PEGDA/PEGPEA copolymer systems, this correlation is not obeyed, *i.e.*, *FFV* has a negative correlation with ($T - T_g$). While insertion of the bulky phenoxy-terminated side-chains seems to increase *FFV*, at the same time it also increases steric hindrance for chain motion and reduces chain mobility, as characterized by increasing T_g (*cf.* Figure 6.5).

In a sense, the copolymers containing phenoxy-terminated side-chains exhibit behavior reminiscent of glassy polymers, where insertion of functional groups into the polymer structure simultaneously increases chain stiffness and *FFV* [128, 129]. For example, amongst substituted glassy polysulfones, tetramethyl bisphenol-A polysulfone (TMPSF) exhibits a T_g that is ~55°C higher than that of bisphenol-A polysulfone (PSF); TMPSF also has higher *FFV* than PSF. Transport measurements indicate gas diffusivities that are greater in TMPSF as compared to PSF [128]. In these glassy polymers, the macromolecular chains are already highly hindered, such that gas diffusivity may be influenced more strongly by increasing *FFV*, rather than by the observed variation in chain stiffness. In rubbery XLPEO with phenoxy-terminated branches, the polymer chains are fairly mobile, and the decrease in chain mobility that is a result of increasing branch content may have a stronger impact on diffusivity relative to the observed increase in *FFV*. A similar contrast is encountered when comparing the gas diffusion characteristics of (rubbery) polyethylene [PE] versus (glassy) poly(ethylene terephthalate) [PET]. In PE, gas diffusion coefficients in the amorphous phase are substantially reduced by the presence of impermeable crystalline domains, which impose constraints on chain movement that persist into the amorphous regions [23]. In semicrystalline PET, the inherently rigid character of the PET backbone appears to be the controlling factor for chain mobility, and increasing levels of crystallinity do not significantly perturb the mobility of the amorphous phase chains [130]. As such, the gas diffusivity ascribed to the amorphous phase remains essentially constant in PET, independent of crystallinity.

An alternative explanation for the potentially disparate trends in diffusivity and permeability with *FFV* in the PEGDA/DEGPEA and PEGDA/PEGPEA systems would be that the assumptions in the *FFV* calculation for these copolymer systems are not strictly valid. Bondi's group contribution method, which was used to estimate *FFV* in this work, assumes the absence of strong non-covalent inter-chain interactions for van der Waals volume calculations [71-73]. Certain interactions, such as hydrogen bonding between polar groups (*e.g.*, in PEGDA/2-HEA copolymers) were observed to influence the *FFV*-diffusivity correlation (*cf.* Figure 5.12). One possible interaction in the polymers containing phenoxy groups is localized stacking of the terminal phenyl rings as a result of π-π bond interactions, as has been proposed for the phenyl rings in benzene [131] or polystyrene [132]. In this regard, even slight differences in van der Waals volume estimates of individual functional groups could produce significant changes in the *FFV* trends [73, 133]. Further, localized stacking of terminal phenyl rings could account for the decreased chain mobility that is observed, especially for the shorter DEGPEA branches. An experimental exploration of free volume characteristics in the phenoxy-terminated co-monomers may be performed using, for example, Positron Annihilation Lifetime Spectroscopy (PALS), but such studies were beyond the scope of this investigation.

6.4. Conclusions

This chapter presented the influence of phenoxy-terminated side chains on the transport properties of cross-linked poly(ethylene oxide) (XLPEO) networks. Poly(ethylene

glycol) diacrylate, n=14 (PEGDA) was UV-polymerized with poly(ethylene glycol) phenyl ether acrylate co-monomers encompassing two different ethylene oxide repeat lengths: DEGPEA (n=2) or PEGPEA (n=4). These copolymer systems were compared with PEGDA networks prepared using an ethoxy-terminated co-monomer, *i.e.*, di(ethylene glycol) ethyl ether acrylate (DEGEEA). While the introduction of phenoxy-terminated branches in XLPEGDA increased the calculated polymer fractional free volume, it did not increase gas permeability; instead, gas permeability decreased with increasing DEGPEA content and remained essentially constant at all PEGPEA concentrations. Possible explanations for these results were provided in the context of polymer chain mobility and network structure. Dynamic mechanical studies of PEGDA/ PEGPEA revealed an increase in the glass transition temperature and substantial relaxation broadening with increasing PEGPEA content, despite an overall decrease in cross-link density. The PEGDA/DEGPEA networks also exhibited reduced overall chain mobility with increasing DEGPEA content, as indicated by a strong positive shift in the glass transition temperatures of the copolymers. At the same time, dielectric measurements showed that the inclusion of phenoxy groups did not fundamentally change the local mobility of the ethylene oxide moieties. Ultimately, steric hindrance due to the phenoxy groups strongly impedes longer-range segmental motion in the PEGDA/PEGPEA and PEGDA/DEGPEA materials, which was decisive in reducing gas diffusivity in these polymers. This behavior was in contrast to the PEGDA/DEGEEA networks, where fractional free volume, chain mobility and gas permeability all increased simultaneously.

Chapter 7: Influence of a TRIS-based Co-monomer on Structure and Gas Transport Properties of Cross-linked Poly(ethylene oxide)

7.1. Summary

In this chapter, 3-[tris-(trimethylsiloxy)silyl] propyl acrylate (TRIS-A) was investigated as a co-monomer for UV cross-linked poly(ethylene glycol) diacrylate. The resulting homogeneous copolymers were characterized based on their physical and light gas (CO_2, CH_4, H_2, O_2 and N_2) transport properties. Introduction of TRIS-A led to increased polymer fractional free volume and strong broadening of the glass-rubber relaxation without a significant shift in glass transition temperature for up to 80 wt% TRIS-A. Along with these trends, a significant increase in gas permeability was observed as compared to cross-linked PEGDA: for instance, addition of 80 wt% TRIS-A increased CO_2 permeability from 110 to 800 barrer. The strongly non-polar character of TRIS-A, however, resulted in progressively lower CO_2 affinity for the polymer network with increasing TRIS-A content, leading to decreased CO_2/light gas selectivity.

This chapter has been adapted with permission from an article to be published as part of the special issue of the *Journal of Membrane Science* on "Membrane Technology for CO_2 Separation" under the same title [91], originally written by the author.

7.2. Introduction

The permeability values exhibited by XLPEO networks studied in Chapters 4 through 6, while generally higher than semicrystalline high M_w PEO, are still an order of magnitude below the most permeable rubbery polymer currently known, poly(dimethylsiloxane) (PDMS) [59, 61, 134, 135]. PDMS consists of highly flexible siloxane linkages with high segmental mobility, enabling fast redistribution of free volume elements and, consequently, high gas diffusivity through a PDMS membrane. At 35°C, Stern et al. reported the CO_2 permeability of PDMS to be 4500 barrer [61], while Merkel et al. obtained 3800 barrer [59].

3-[tris-(trimethylsiloxy)silyl] propyl methacrylate, TRIS, has structural features in common with PDMS, and is an important component of contact lenses due, in part, to its high oxygen permeability [118, 136, 137]. In a continuing exploration of the gas transport properties of membrane materials based on cross-linked poly(ethylene oxide), the current chapter reports results from a structure/property investigation involving copolymerization of a hydrophilic, ethylene-oxide-bearing diacrylate cross-linker with an acrylate analog of TRIS. Specifically, poly(ethylene glycol) diacrylate (n=14) (PEGDA) was copolymerized with 3-[tris-(trimethylsiloxy)silyl] propyl acrylate (TRIS-A) in the presence of toluene, which increases the compatibility between the hydrophobic TRIS-A and the hydrophilic PEGDA (*cf.* Tables 3.1 and 3.2). Gas transport properties of the resulting copolymers – pure gas permeability (CO_2, CH_4, H_2, O_2 and N_2) and pure gas

solubility (CO_2 and CH_4) at 35°C – were determined. The results are interpreted in terms of the influence of TRIS-A on polymer chain mobility, as determined by calorimetric and dynamic mechanical analysis, and fractional free volume, as estimated from hydrostatic density measurement. The results are also compared to the gas transport properties of PEGDA copolymers with co-monomers previously studied, *i.e.*, poly(ethylene glycol) methyl ether acrylate (*n*=8) (PEGMEA; *cf*. Chapter 4) [32] and diethylene glycol ethyl ether acrylate (DEGEEA; *cf*. Chapter 6).

7.3. Results and Discussion

7.3.1. Physical Characterization

Figure 7.1 compares the FTIR-ATR spectra of representative PEGDA/TRIS-A copolymers with the pure monomer spectra. The signature peaks corresponding to acrylate double bonds, highlighted in the monomer spectra (Fig. 7.1a), are largely absent in the polymer spectra (Fig. 7.1b). This disappearance indicates virtually complete conversion of the acrylate double bonds during polymerization, which is consistent with previous results for copolymerizations conducted without additional solvent (see previous chapters), as well as polymerizations of PEGDA in the presence of varying amounts of water [18]. Acrylate double bonds typically exhibit very high reactivity [35], and the presence of toluene in the reaction mixtures studied here did not measurably impact conversion of the acrylate groups.

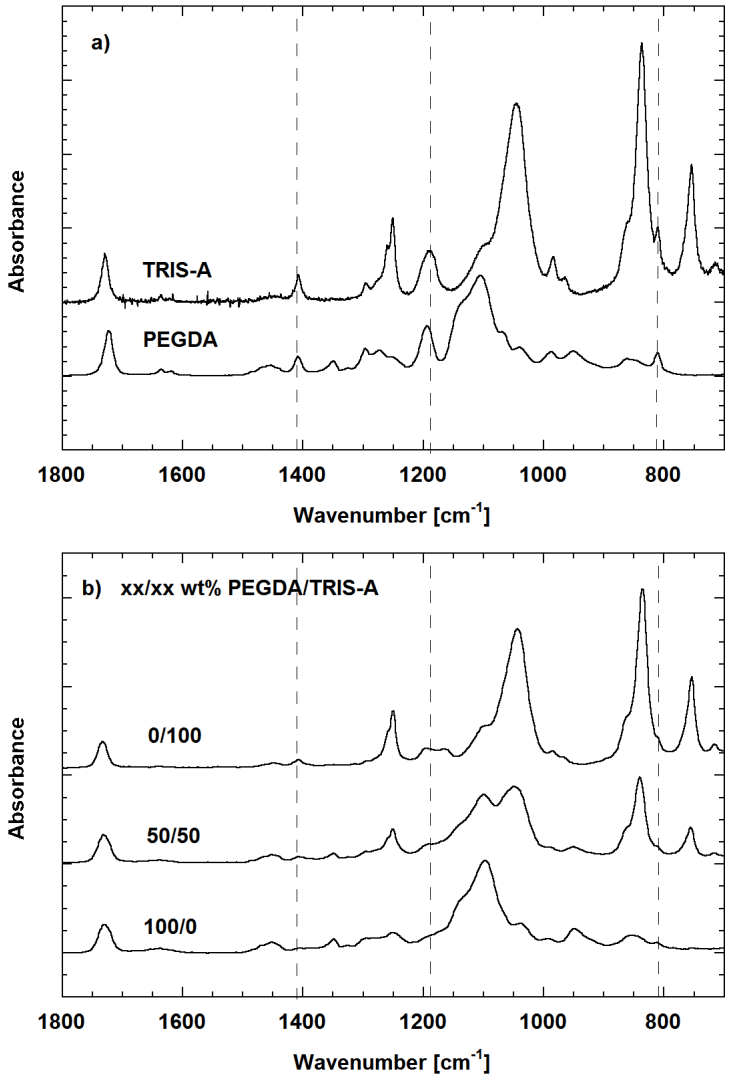

Figure 7.1: FTIR-ATR spectra of a) TRIS-A and PEGDA monomers and b) polymerized PEGDA, 50/50 wt% PEGDA/TRIS-A, and TRIS-A. All polymers were prepared from prepolymerization solutions containing 37 wt% toluene and air-dried prior to analysis. The spectra have been displaced vertically for clarity. The characteristic acrylate peaks (810, 1190 and 1410 cm^{-1}) are marked by vertical lines (see Section 3.5).

The polymerization of PEGDA cross-linker in the presence of diluents (*i.e.*, water, toluene) increases the probability of intramolecular cyclization or loop formation in the polymer network [138, 139]. These loops, or "wasted" cross-links, do not contribute to

the elastic character of the polymer, and the effective cross-link density decreases with increasing diluent concentration in the prepolymerization mixture (see, for example, results for the PEGDA/water system in Figure 4.2). For the PEGDA/TRIS-A system, toluene was included at constant concentration (37 wt%) to maintain a homogeneous prepolymerization mixture at all co-monomer compositions. To independently assess the influence of toluene on the properties of the resulting polymers, 100% PEGDA (*i.e.*, XLPEGDA) networks were photopolymerized in the presence of varying amounts of toluene. Dynamic mechanical results for these XLPEGDA control networks are presented in Figure 7.2, with glass-rubber relaxation properties, density and fractional free volume (*FFV*) values recorded in Table 7.1. In the vicinity of the glass-rubber transition, a distinct, step-wise decrease in storage modulus (E') is observed, accompanied by a peak in tan δ. The dynamic mechanical glass transition temperatures reported in Table 7.1 (T_α) correspond to the maximum in tan δ at a test frequency of 1 Hz. Increasing toluene concentration in the prepolymerization mixture had only a minimal influence on the glassy modulus, but led to a progressive reduction in the measured rubbery modulus (E_R) above T_α, which is consistent with a systematic decrease in the effective cross-link density for these networks [81-83]. The intensity of tan δ increased with decreasing cross-link density, and the measured glass transition shifted to slightly lower temperatures, apparently as a result of a lower degree of cross-link constraint inherent to these networks.

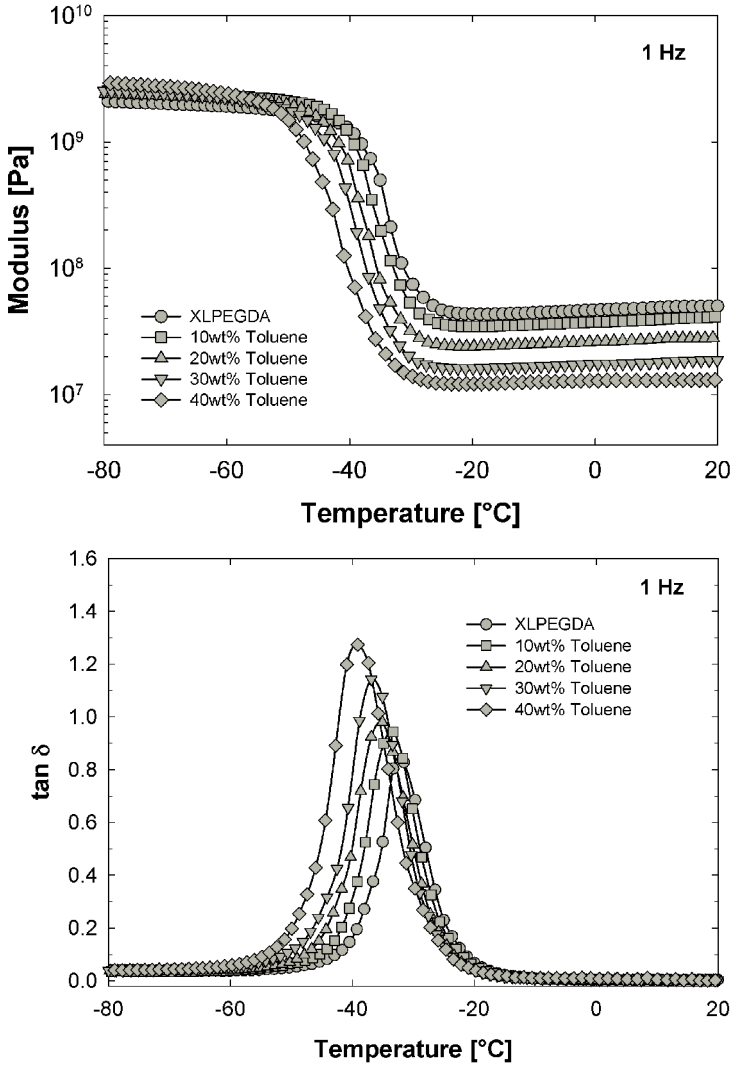

Figure 7.2: a) Dynamic mechanical storage modulus (E') [Pa] and b) tan δ vs. temperature [°C] for XLPEGDA networks, UV-polymerized with varying amounts of toluene in the prepolymerization mixture. Frequency of 1 Hz; heating rate of 1°C/min.

Table 7.1: Characteristics of XLPEGDA networks, UV-polymerized with varying amounts of toluene in the prepolymerization mixture.

Toluene [wt%]	T_α **[°C]** ± 1°C	β_{KWW} ± 0.01	**Density [g/cm^3]** ± 0.003	***FFV*** ± 0.003
0	-32	0.30	1.189	0.120
10	-33	0.29	1.183	0.125
20	-35	0.28	1.180	0.127
30	-37	0.29	1.180	0.127
40	-39	0.29	1.171	0.134

Note: T_α (°C) is the dynamic mechanical peak temperature at 1 Hz; β_{KWW} is the Kohlrausch-Williams-Watts distribution parameter.

Time-temperature superposition was used to obtain master curves of E' vs. ωa_T across the glass-rubber relaxation (*cf.* Section 2.4). The resulting curves could be satisfactorily described according to the Kohlrausch-Williams-Watts (KWW) "stretched exponential" relaxation time distribution function (Equation 2.19) to obtain β_{KWW}. For the XLPEGDA networks synthesized in the presence of varying amounts of toluene, the value of the exponent remained essentially constant ($\beta_{KWW} \sim 0.30$; see Table 7.1), indicating no significant variation in relaxation breadth with decreasing effective cross-link density.

Table 7.1 also reports the measured density of these materials, as well as estimated values of *FFV*. Increasing the amount of toluene present during polymerization resulted in networks with somewhat lower density and correspondingly higher levels of free volume. Here again, the observed trends likely reflect the decrease in effective cross-link density obtained in networks prepared with higher amounts of toluene in the prepolymerization solution.

Polymer chain mobility is a useful indicator for polymer gas transport properties. The gas permeability of cross-linked poly(ethylene oxide) copolymers is a strong function of penetrant diffusivity, which depends not only on penetrant size but also on polymer chain characteristics [90]. Chain mobility is typically characterized by the glass-rubber transition temperature, obtained via either calorimetric (T_g) or dynamic mechanical (T_α) methods [2, 32, 74, 89, 90, 95]. In some XLPEO systems such as PEGDA/PEGPEA or PEGDA/DEGPEA (*cf*. Chapter 6), chain mobility may be a stronger determinant for gas diffusivity than *FFV*.

Figure 7.3 presents the DSC (second scan) heating thermograms for select members of the PEGDA/TRIS-A copolymer series. Within the range of the instrument, only one glass transition event was observed for each copolymer studied, suggesting that the introduction of toluene did indeed produce a homogeneous mixture of the co-monomers in the prepolymerization solution, yielding single phase polymers. The glass transition temperature as measured by the mid-point method did not vary with increasing co-monomer content up to approximately 20/80 PEGDA/TRIS-A (T_g ~ -40°C; see Table 7.2). However, a progressive broadening of the glass transition event was evident at TRIS-A co-monomer concentrations of 40 wt% and greater, suggesting a more heterogeneous motional environment experienced by the relaxing copolymer chains. Increasing co-monomer concentration beyond 80 wt% TRIS-A led to an upward shift in glass transition temperature; T_g for the 0/100 TRIS-A homopolymer was -7°C as determined by DSC.

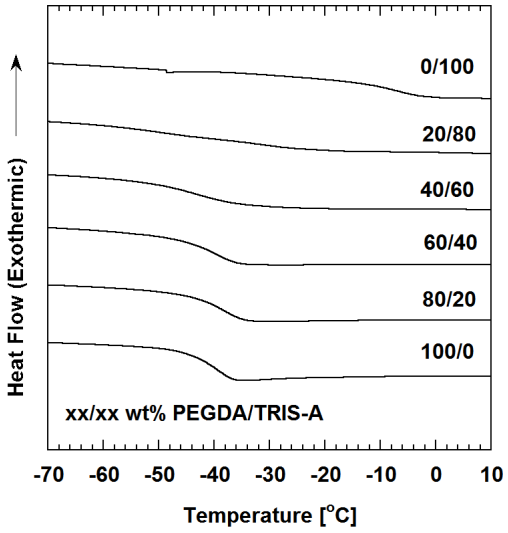

Figure 7.3: Second scan DSC thermograms for cross-linked PEGDA with TRIS-A at different concentrations. The heating rate was 10°C/min. The thermograms have been displaced vertically for clarity.

Table 7.2: Characteristics of PEGDA/TRIS-A copolymers.

PEGDA [wt%]	**PEGDA [vol%]**	T_g **[°C]** ± 1°C	T_α **[°C]** ± 1°C	β_{KWW} ± 0.01	***FFV*** ± 0.003
100	100	-39	-34	0.29	0.128
90	89	-38	-33	0.26	0.129
80	77	-38	-32	0.22	0.132
70	67	-39	-34	0.19	0.134
60	56	-40	-33	0.16	0.138
50	46	-40	-26	0.13	0.141
40	36	-43	-23	0.12	0.142
20	18	-42	---	---	0.150
10	9	-22	---	---	0.156
0	0	-7	---	---	0.158

Note: T_g (°C) is the glass transition temperature determined by DSC; second scan (10°C/min). T_α (°C) is the dynamic mechanical peak temperature at 1 Hz; β_{KWW} is the Kohlrausch-Williams-Watts distribution parameter. All copolymers were cross-linked in 37 wt% toluene.

Dynamic mechanical results for the PEGDA/TRIS-A networks are presented in Figure 7.4, with T_α (1 Hz) values reported in Table 7.2. The storage modulus data for the copolymer networks (Fig. 7.4a) display glass transition characteristics that are largely consistent with the results for the XLPEGDA controls. Notably, however, the measured rubbery modulus for the copolymers showed only a modest downward variation with increasing co-monomer content. In PEGDA copolymer systems polymerized without the addition of diluent, a strong, systematic decrease in rubbery modulus was typically observed consistent with the stoichiometrically-controlled reduction in cross-link density that was obtained upon copolymerization (see, for example, XLPEO copolymer systems studied in refs. [74, 89, 95]). This trend is muted in the PEGDA/TRIS-A copolymer series (re: decreasing E_R with increasing co-monomer content), and may reflect the simultaneous influence of the toluene diluent, which promotes lower cross-link densities owing to potential cyclization, and the inclusion of mono-functional TRIS acrylate, which engenders lower levels of cross-linking as a result of reaction stoichiometry.

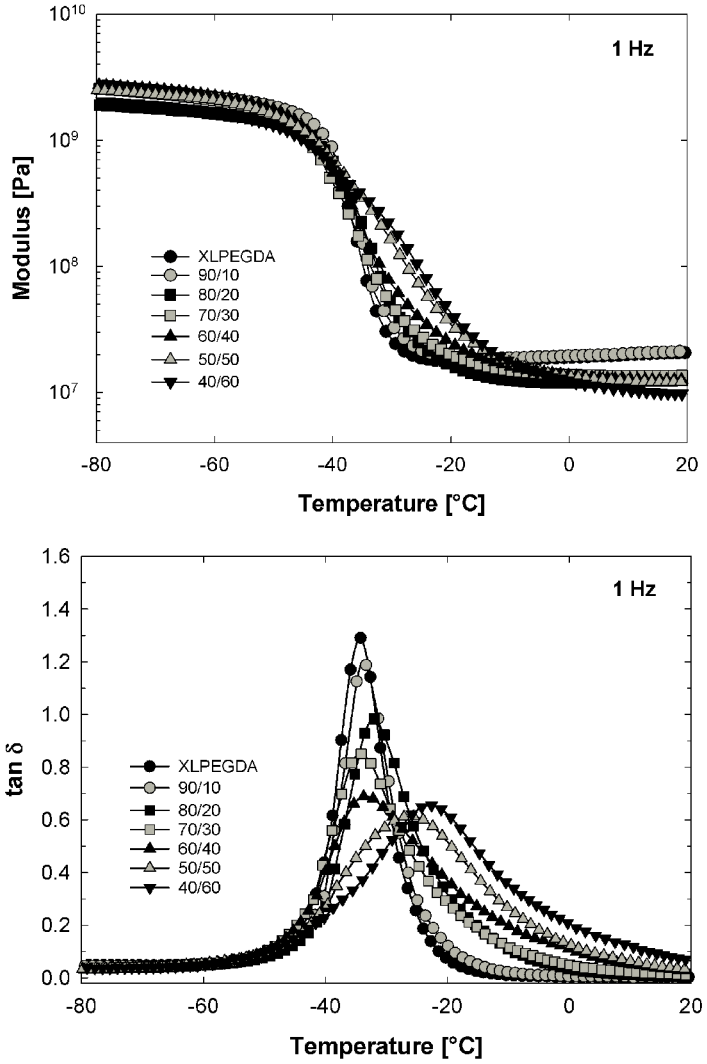

Figure 7.4: a) Dynamic mechanical storage modulus (E') [Pa] and b) tan δ vs. temperature [°C] for PEGDA/TRIS-A copolymer networks. Frequency of 1 Hz; heating rate of 1°C/min.

The tan δ vs. temperature curves for the copolymers (Fig. 7.4b) reveal a single glass transition peak for all compositions, with substantial broadening of the relaxation at higher levels of TRIS-A co-monomer. The glass transition peak temperatures (T_α) presented in Table 7.2 follow the same trend obtained for the calorimetric T_g values, with

T_α shifting to higher temperatures at greater levels of TRIS-A incorporation. The observed upward shift in glass transition temperature was detected at somewhat lower levels of TRIS-A content in the DMA experiments, as compared to the DSC studies. Dynamic mechanical time-temperature master curves (E' vs. ωa_T) for the PEGDA/TRIS-A series are presented in Figure 7.5, and illustrate the strong, progressive relaxation broadening encountered with increasing amounts of TRIS branches in the cross-linked network. The master curves were fit according to the KWW function (see solid curves in Fig. 7.5), and the corresponding exponent values (β_{KWW}) are reported in Table 7.2. The systematic decrease in β_{KWW} with higher co-monomer content reflects a heightened degree of intermolecular cooperativity inherent to the glass-rubber relaxation in these copolymers, as necessitated by the greater level of steric interference introduced by the side groups [105].

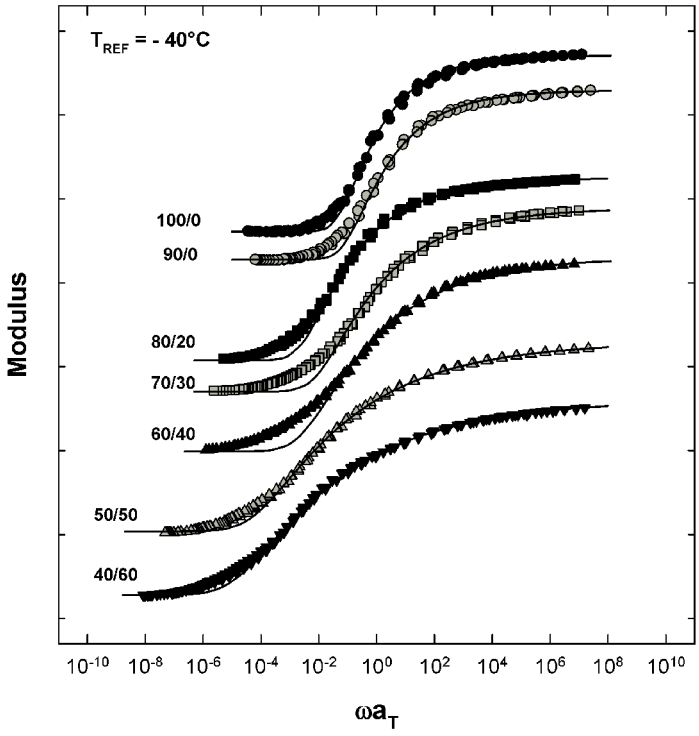

Figure 7.5: Time-temperature master curves (E' vs. ωaT) for PEGDA/TRIS-A copolymer networks. Reference temperature is -40°C. Solid curves are best fits to the Kohlrausch-Williams-Watts equation. Data are offset vertically for clarity.

In addition to their influence on the dynamic relaxation characteristics of the copolymer networks, the insertion of short branches containing bulky functional groups along the network backbone may increase local free volume when the branches are flexible and non-interactive with respect to the surrounding network [2, 32, 74, 89, 95]. The *FFV* of the PEGDA/TRIS-A networks can be estimated from polymer density measurements via Equation 2.14; density and *FFV* values for the copolymer series are reported in Table 7.2. Figure 7.6 presents comparisons of the density and *FFV* trends for the PEGDA/TRIS-A and PEGDA/DEGEEA series of copolymers (*cf.* Section 6.3.1). As discussed before, diluting the pre-polymer solution decreases the effective cross-link density of the

network due to an apparent increase in cyclization during gel formation [18, 75], potentially altering the *FFV* of the resulting copolymer [140]. However, as shown by the comparison of networks polymerized from diluted and undiluted PEGDA/DEGEEA solutions (re: Fig. 7.6), dilution has only a relatively minor effect on the polymer density and *FFV* relative to the influence of copolymerization. This outcome is consistent with previous results obtained for XLPEGDA prepared in the presence of varying amounts of water [18]. Further, despite the introduction of inherently bulkier branch groups in the PEGDA/TRIS-A series (see structures in Tables 3.1 and 3.2), the calculated polymer *FFV*s for the PEGDA/DEGEEA and PEGDA/TRIS-A copolymers are found to be similar at equal PEGDA concentration (weight percent basis, as per Fig. 7.6).

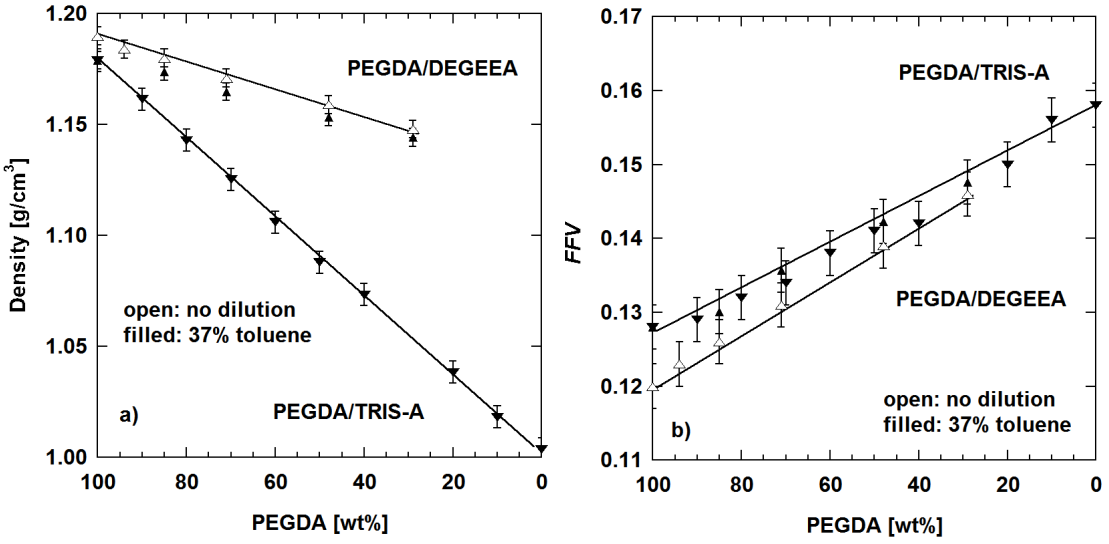

Figure 7.6: Effect of PEGDA content in the prepolymer solution on: a) density and b) *FFV* at room temperature. The results for toluene-diluted PEGDA/TRIS-A series (▼) of copolymers are compared with the undiluted (Δ), and toluene-diluted (▲) PEGDA/DEGEEA series (*cf.* Table 6.1). The lines are drawn to guide the eye.

7.3.2. Gas Transport Properties

The fugacity dependence of gas permeability for a representative PEGDA/TRIS-A copolymer is presented in Figure 7.7. Consistent with results for light gas permeability in other XLPEO polymers in this project, only carbon dioxide permeability depends significantly on upstream fugacity. To compare the CO_2 permeability with that of other penetrants, the data are extrapolated to infinite dilution (*i.e.*, an upstream fugacity of zero) using Equation 2.10; the infinite dilution gas permeability coefficients for PEGDA/ TRIS-A series are tabulated in Table 7.3 and plotted in Figure 7.8a. For convenience, the data can be compared with the undiluted PEGDA/DEGEEA series depicted in Figure 7.8b, which was taken from Figure 6.8. The order of gas permeability in all cases is: $CO_2 > H_2 > CH_4 \geq O_2 > N_2$.

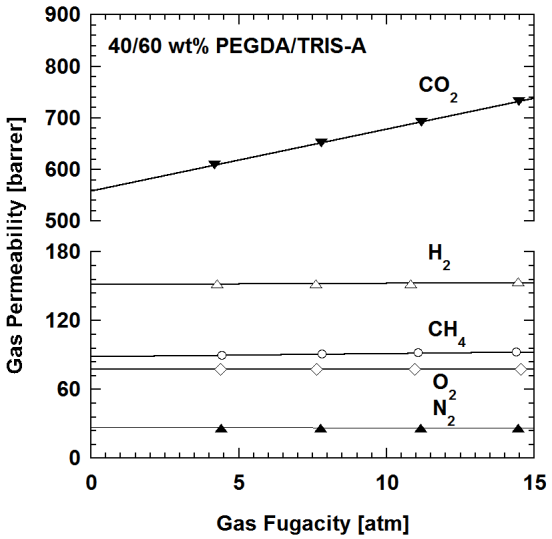

Figure 7.7: Effect of upstream gas fugacity on pure gas permeability coefficients at 35°C in 40/60 wt% PEGDA/TRIS-A copolymer. The gases are ▼: CO_2, Δ: H_2, ○: CH_4, ◊: O_2 and ▲: N_2. The lines are drawn based on Equation 2.10. Average uncertainty is ±6% of value.

Table 7.3: Infinite dilution gas permeability and solubility of PEGDA/TRIS-A copolymers at 35°C, determined experimentally. All uncertainties are estimated using the propagation of error method.

PEGDA content		Permeability ± 6% [barrer]					Solubility ± 0.03 [cm^3(STP)/cm^3 atm]	
wt%	vol%	CO_2	H_2	CH_4	O_2	N_2	CO_2	CH_4
100[a]	100[a]	143	18	7.6	6.7	2.6	1.39	0.079
80	77	233	40	18	16	6.0	1.50	0.12
70	66	275	60	27	24	8.9	---	---
60	56	406	86	47	42	14	1.58	0.21
50	46	490	110	68	58	20	1.61	0.23
40	37	560	150	89	78	27	---	---
20	17	800	250	160	140	51	1.58	0.33
0	0	---	---	---	---	---	1.51	0.38

Note: [a]Data for PEGDA diluted with 37 wt% toluene in prepolymer solution are given here, in place of those given in previous chapters (*cf.* Section 3.3).

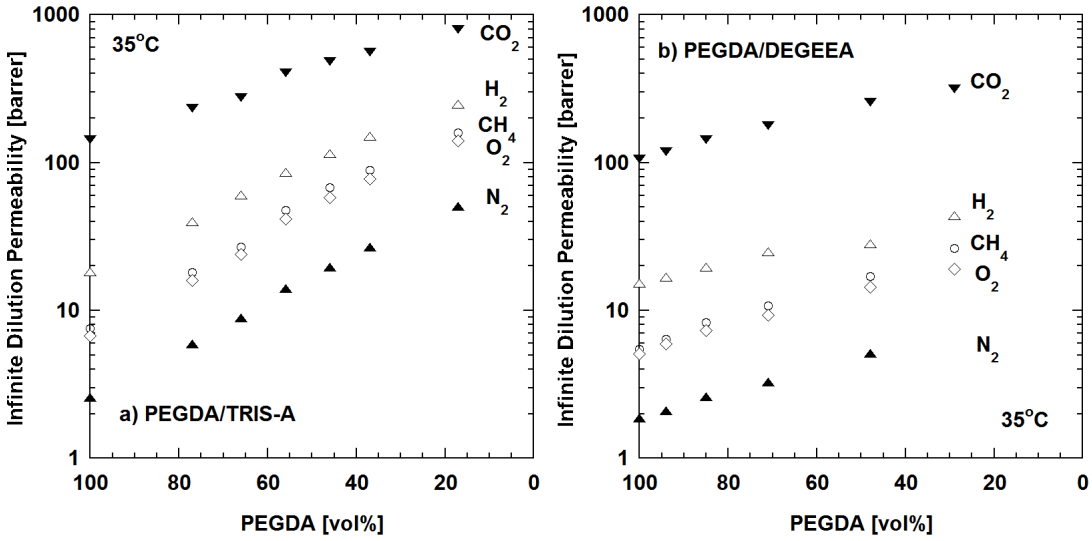

Figure 7.8: Effect of PEGDA content on infinite dilution gas permeability at 35°C. The a) PEGDA/TRIS-A series is compared with the b) PEGDA/DEGEEA series of copolymers, which is from Table 6.3. The average uncertainty is ±6% of value. The gases are ▼: CO_2, Δ: H_2, ○: CH_4, ◊: O_2 and ▲: N_2.

As TRIS-A concentration in the prepolymer solution increases, gas permeability increases. This increase is greater than that seen with incorporation of similar amounts of DEGEEA (volume percent basis). For example, the infinite dilution CO_2 permeability in a copolymer with 48 vol% DEGEEA is 260 ± 15 barrer, compared to 490 ± 30 barrer with 50 wt% (54 vol%) TRIS-A. Gas permeability of the PEGDA/TRIS-A copolymer presented in Figure 7.7 are also in marked contrast with PEGDA/2-HEA and PEGDA/2-EEA copolymers with similar cross-linker concentration (*cf*. Figure 5.6) The presence of more mobile chain elements in the PEGDA/TRIS-A copolymer regardless of dilution (*cf*. Figure 7.6) likely results in higher gas diffusivity, and in turn, permeability. The effect of reduced cross-link density on gas permeability due to the inclusion of diluent during polymerization was insignificant compared to the diffusivity increase achieved with copolymerization of TRIS-A. This outcome is consistent with the minimal influence of dilution observed for the characteristics of the glass transition and *FFV* (see section 7.3.1. and ref. [18]).

To confirm the effect of TRIS-A incorporation on gas diffusivity, independent gas solubility measurements were performed, with diffusivity values subsequently determined according to Equation 2.6. Due to the low solubility of non-polar permanent gases in polar rubbers such as XLPEO [2, 41], these gases were not included in this study. The infinite dilution solubility coefficients of carbon dioxide and methane in the PEGDA/TRIS-A copolymers are presented in Figure 7.9.

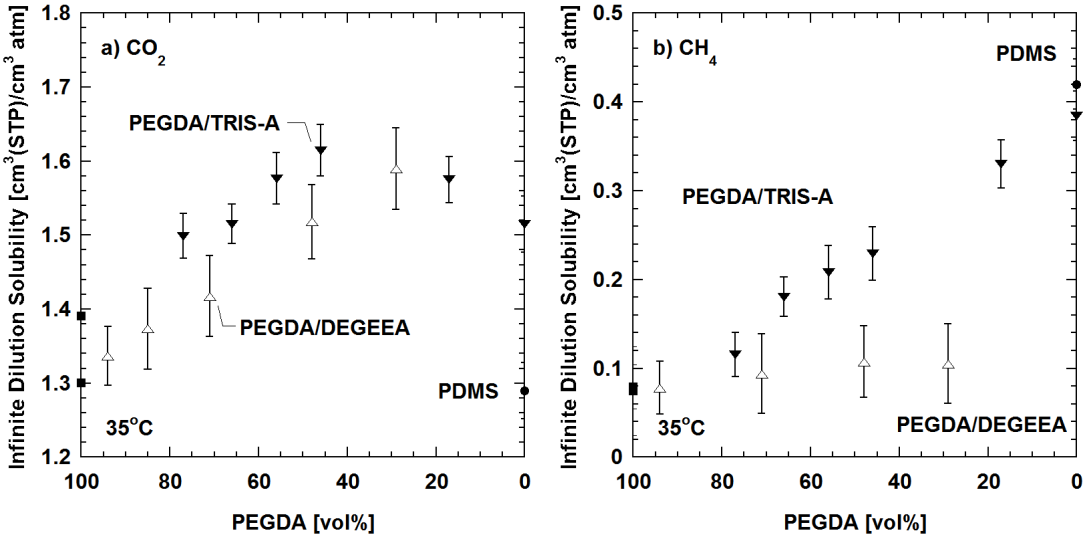

Figure 7.9: Effect of PEGDA (■) content on infinite dilution gas solubility at 35°C. The gases are a) CO_2 and b) CH_4. The PEGDA/TRIS-A series (▼) is compared with the PEGDA/DEGEEA series of copolymers (Δ) (*cf.* Figure 6.10). The corresponding infinite dilution solubility in poly(dimethylsiloxane) (PDMS) (●) is provided for comparison [59].

As shown in Figure 7.9a, carbon dioxide solubility initially increases with increasing TRIS-A concentration (*i.e.*, decreasing PEGDA content). Beyond 54 vol% TRIS-A, the CO_2 solubility decreases somewhat. For comparison, in the PEGDA/DEGEEA series, CO_2 solubility increases systematically as PEGDA content decreases. These trends are rationalized as follows. Carbon dioxide affinity for the polymer matrix should be strongest in samples containing the highest content of polar ethylene oxide moieties (*i.e.*, in 100% XLPEGDA). As the PEGDA concentration decreases due to the presence of monomers containing fewer ethylene oxide moieties (*e.g.*, DEGEEA and, in particular, TRIS-A), the inherent carbon dioxide affinity for the polymer chains should decrease, which would tend to reduce CO_2 solubility. However, since these monomers are also less polar than PEGDA, the incorporation of these groups into the polymer network will

decrease the cohesive energy density of the polymer, which would tend to increase solubility of all gases. The resulting solubility trend with polymer composition presumably reflects the competition between these two factors. CO_2 solubility coefficients in PEGDA/TRIS-A copolymers are slightly larger but still of the same order as in PDMS [59], demonstrating that the observed variations in CO_2 solubility are not a significant determinant for CO_2 transport behavior in these networks.

Methane, a non-polar penetrant, is not subject to the same interactions with ethylene oxide groups as experienced by CO_2. The interaction of gases with the polymer matrix can be quantified with, for instance, the Flory-Huggins interaction parameter. Based on the Flory-Huggins model, maximum value of gas solubility should be observed when the polymer has a solubility parameter equal to that of the gas of interest (*e.g.*, CO_2 or CH_4) [17, 107]. The increasing non-polar character of the PEGDA/TRIS-A polymer matrix with increasing TRIS-A content may change its solubility parameter closer to that of methane. This factor, combined with the decrease in the polymer cohesive energy density that accompanies the introduction of the less polar TRIS-A groups, increases methane solubility with increasing TRIS-A content, as shown in Figure 7.9b. At concentrations approaching 100 wt% TRIS-A in the polymer, the CH_4 solubility coefficient approaches that in PDMS, which also has a high concentration of siloxane moieties. This strong increase in methane solubility was not observed in any XLPEO systems studied previously, *e.g.*, PEGDA/DEGEEA (*cf.* Figures 6.10 and 7.9b).

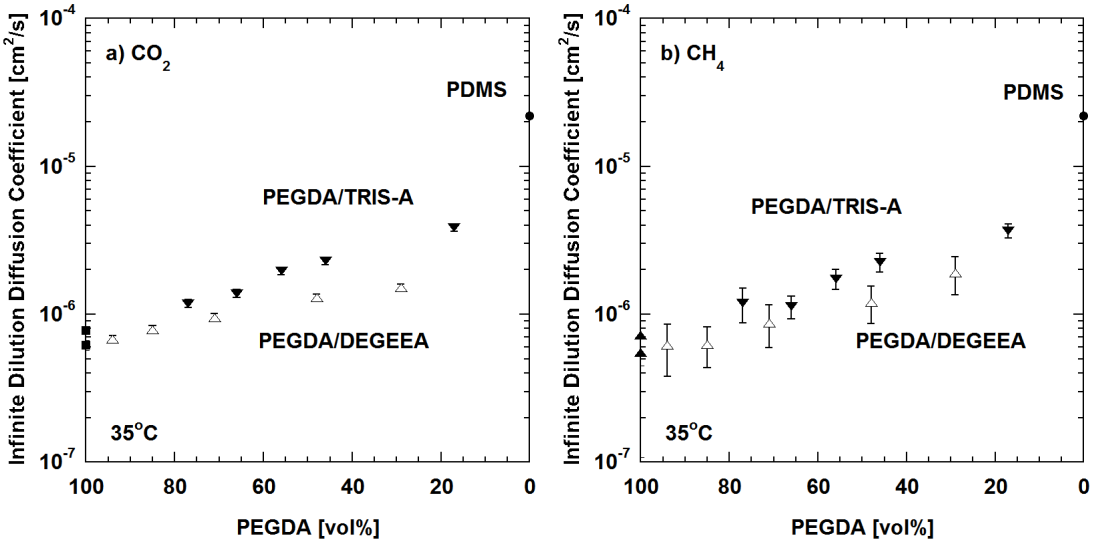

Figure 7.10: Effect of PEGDA (■) content on infinite dilution gas diffusivity at 35°C. The gases are a) CO_2 and b) CH_4. The PEGDA/TRIS-A series (▼) is compared with the PEGDA/DEGEEA series of copolymers (Δ) (*cf.* Figure 6.11). The corresponding infinite dilution diffusivity in poly(dimethylsiloxane) (PDMS) (●) is provided for comparison [59].

Infinite dilution gas diffusivity coefficients for the two copolymer series, as calculated using Equation 2.2, are shown in Figure 7.10. Diffusivity coefficients of CO_2 and CH_4 are higher in the PEGDA/TRIS-A system than in the PEGDA/DEGEEA system at similar co-monomer concentrations (by volume). According to the Cohen-Turnbull relationships (*cf.* Equations 2.12 and 2.13), changes in diffusivity should be closely correlated with fractional free volume. In this regard, Figure 7.11 presents the effect of *FFV* on diffusivity and compares the results for the two copolymer systems with Equation 2.12 with parameters given in Table 2.1. Diffusivity closely follows the *FFV* increase for the two aforementioned copolymers. The projected gas diffusivity coefficients in the 100% cross-linked TRIS-A network, however, are still lower than that

in PDMS as reported by Merkel et al. [59], perhaps because the TRIS-A chains are still inherently less flexible than PDMS.

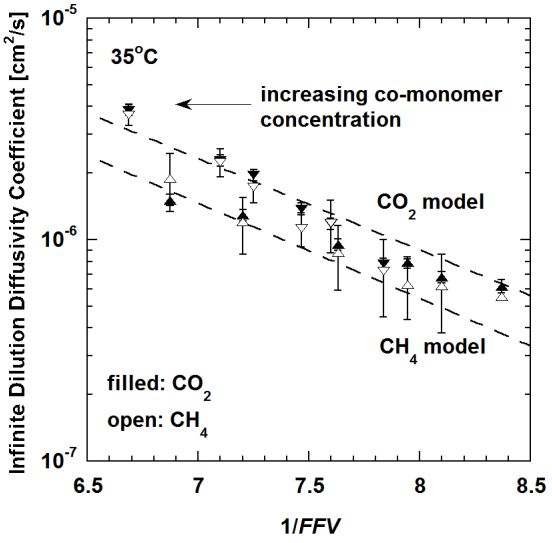

Figure 7.11: Correlation between infinite dilution gas diffusivity at 35°C and polymer free volume. The data shown are for both CO_2 (▼: PEGDA/TRIS-A, ▲: PEGDA/DEGEEA) and CH_4 (corresponding open symbols). The co-monomer content increases from right to left. The model parameters are from Table 2.1.

The correlation of gas permeability with *FFV* (Equation 2.13) in the PEGDA/TRIS-A polymers is somewhat different from that observed in other XLPEO systems (*e.g.*, PEGDA/DEGEEA), where penetrant solubility did not change significantly with co-monomer composition; as a result, in those systems, gas permeability and diffusivity followed very similar trends with *FFV* (see previous chapters). In PEGDA/TRIS-A, the solubility of non-polar penetrants (such as methane and, potentially, all other permanent gases) increases significantly with increasing concentration of non-polar TRIS-A (*cf.* Figure 7.9b). The increased solubility is reflected in the value of S_A in Equation 2.13, which means the adjustable parameter A_P will no longer be independent of TRIS-A

concentration. The observed deviation from the linear Cohen-Turnbull model for permeability, as evident in Figure 7.12, thus reflects the increasing importance of the penetrant solubility contribution to permeability in the case of methane and the permanent gases.

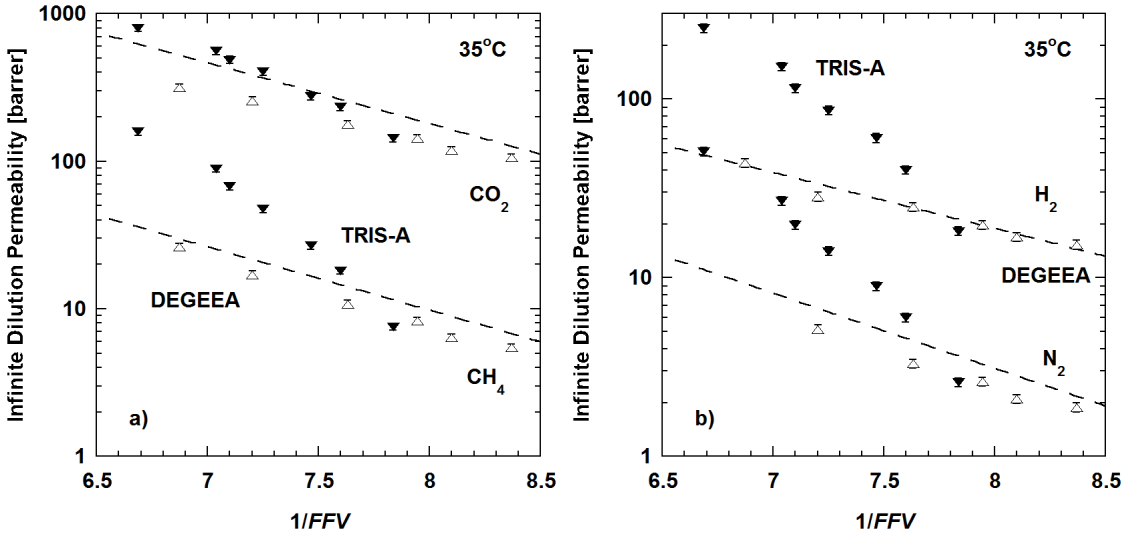

Figure 7.12: Comparison between experimental and predicted infinite dilution permeability based on the free volume model, using model parameters from Table 2.1, for (from top to bottom): a) CO_2 and CH_4 and b) H_2 and N_2. The co-monomer content increases from right to left. The co-monomers of PEGDA are TRIS-A (▼) and DEGEEA (Δ).

The solubility trends for the non-polar penetrants relative to CO_2 in PEGDA/TRIS-A also influence the corresponding ideal gas selectivities. The non-polar penetrants are increasingly favored over CO_2 as TRIS-A concentration increases, as shown in Figures 7.13a and 7.13b for CO_2/CH_4 and CO_2/H_2 ideal selectivity, respectively. This selectivity decrease is greater than that for other copolymer systems containing more polar co-

monomers, such as PEGDA/PEGMEA (Figure 4.6) and PEGDA/DEGEEA (Figure 6.9). As shown in Figure 7.13c, for gases with highly dissimilar molecular size, such as H_2 and N_2 (with kinetic diameter of 2.89 Å and 3.64 Å, respectively; see Table 2.2), there is a slight further weakening of the size-sieving effect in the three copolymer systems shown. This trend is due to the overall *FFV* increase, reflecting the increase in free volume element size that tends to favor diffusion of the larger penetrant, N_2, in the polymer [44]. No change in selectivity is observed for penetrant pairs with more similar kinetic diameters, such as N_2 and O_2 (kinetic diameter 3.46 Å).

The separation performance of the PEGDA/TRIS-A series of copolymers can be characterized by the so-called 'upper bound' plot of permeability and ideal gas selectivity [114, 126]. Figure 7.14 compares the copolymers from this study with various other polymers from the literature as well as PEGDA/PEGMEA (*cf*. Figure 4.11) and PEGDA/DEGEEA. The upper bound lines drawn in Figures 7.14a and 7.14c are based on maximum theoretical pure gas selectivity for a given gas permeability through dense polymeric materials at 25°C [36], whereas the line in Figure 7.14b is based on the curve defined by Robeson at 35°C [126]. With increasing TRIS-A concentration, the performance of the PEGDA/TRIS-A series of copolymers approaches that of PDMS, *i.e.*, moving away from the upper bound curves for the gas pairs given here. PDMS is a weakly size-sieving material with high gas permeability, thanks to its non-polar character and highly flexible siloxane chains [41, 59]. Addition of TRIS-A (which has characteristics similar to PDMS) to PEGDA, therefore, produces a copolymer with gas

transport properties intermediate to those of polar cross-linked PEGDA and non-polar PDMS, which may prove advantageous in tailoring polymeric membrane materials for some gas separation applications.

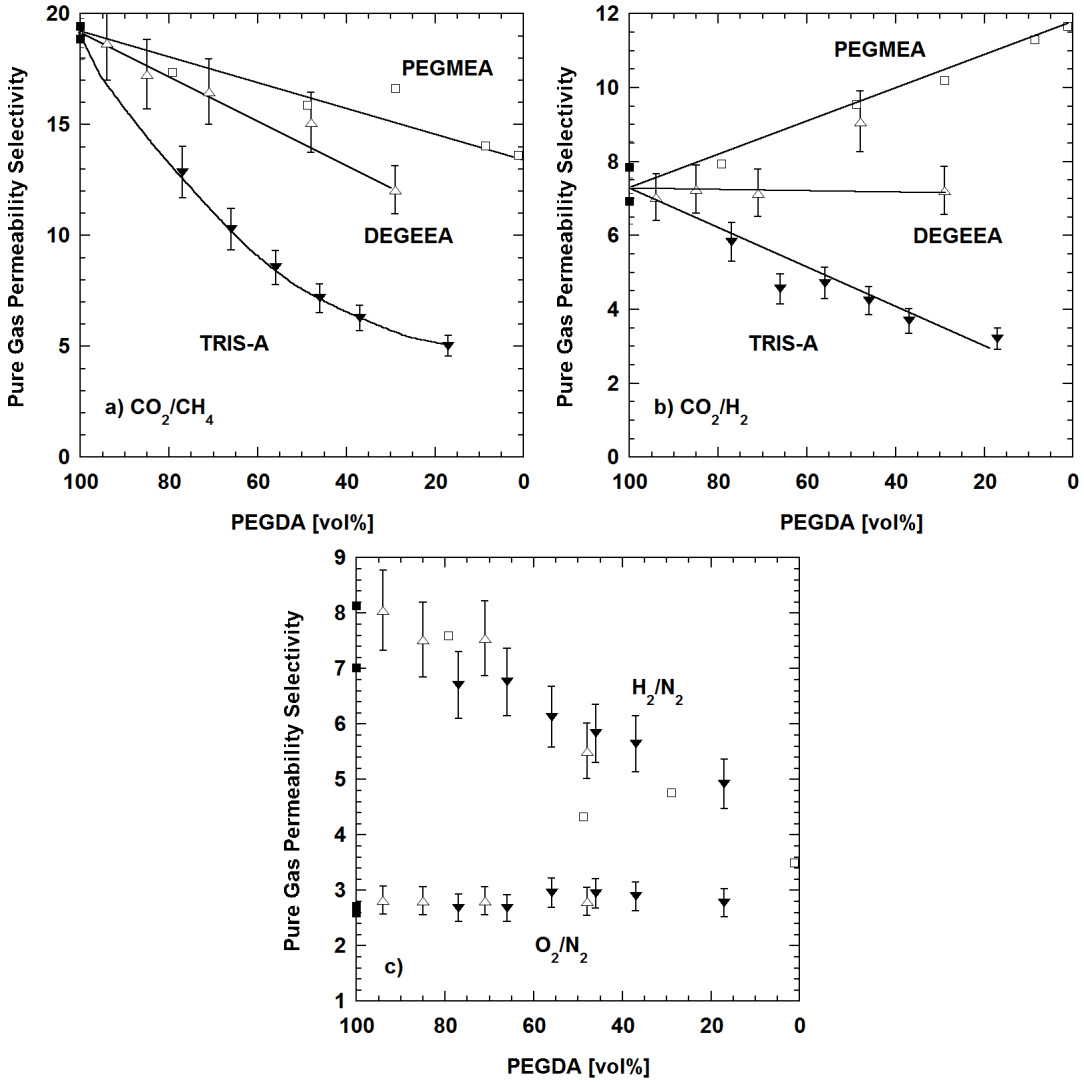

Figure 7.13: Effect of PEGDA content on infinite dilution gas selectivity at 35°C. The solid lines through the data are drawn to guide the eye. The selectivity data shown are for: a) CO_2/CH_4, b) CO_2/H_2, and c) H_2/N_2 and O_2/N_2. The co-monomers of PEGDA (■) are TRIS-A (▼), PEGMEA (□) and DEGEEA (Δ). PEGMEA data are from ref. [32] (*cf.* Figure 4.6).

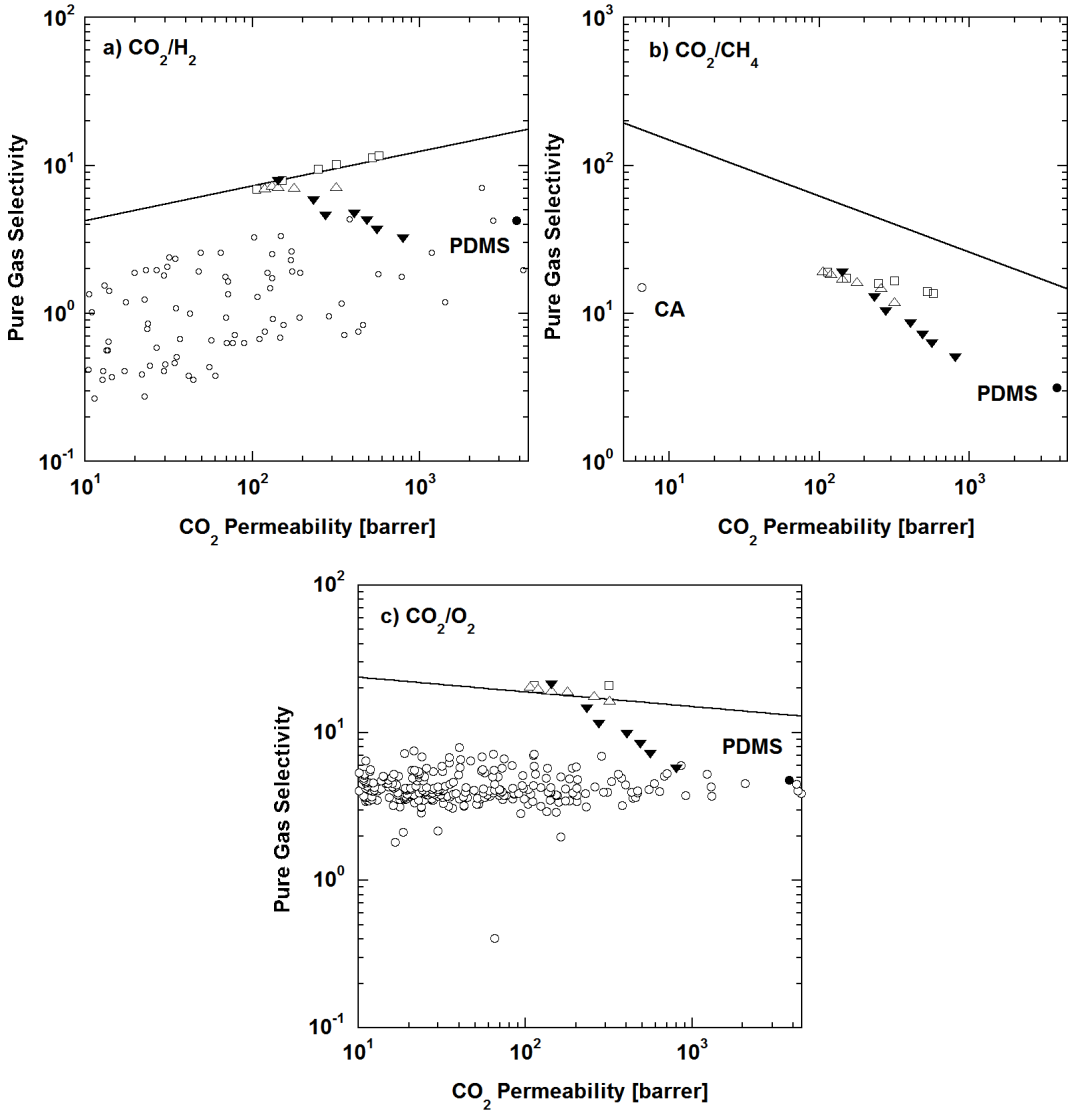

Figure 7.14: Permeability/selectivity map for a) CO_2/H_2, b) CO_2/CH_4 and c) CO_2/O_2, and comparison of copolymers studied (▼: PEGDA/TRIS-A, □: PEGDA/PEGMEA, Δ: PEGDA/DEGEEA); the data are reported at 35°C. All other points in Figure 7.14a and Figure 7.14c are from literature. Poly(dimethylsiloxane) (PDMS) (●) is given as comparison [59]. Cellulose acetate (CA) is also provided for comparison in Figure 7.14b.

7.4. Conclusions

The effects of introducing bulky, strongly non-polar branches into cross-linked poly(ethylene oxide) to increase gas permeability were explored. Poly(ethylene glycol) diacrylate, *n*=14 (PEGDA) was UV-copolymerized with 3-[tris-(trimethylsiloxy) silyl] propyl acrylate (TRIS-A) using toluene as a co-solvent. The effect of toluene dilution on polymer properties was shown to be less important than copolymerization with TRIS-A. The resulting copolymers exhibited increased fractional free volume and a broader, more heterogeneous glass-rubber relaxation response with increasing TRIS-A concentration. Gas diffusivity increased due to insertion of the bulky tris-(trimethylsiloxy)silyl pendant groups, which also contained flexible siloxane linkages. Further, gas solubility for methane (and perhaps other non-polar permanent gases) rose significantly with increasing TRIS-A content, presumably due to decreasing polymer solubility parameter as TRIS-A content increased. The overall result was a strong increase in permeability with increasing TRIS-A concentration for all gases considered, accompanied by decreasing CO_2/light gas selectivity.

Chapter 8: Relation Between Structure and Gas Transport Properties of Poly(ethylene oxide) Networks Based on Cross-linked Bisphenol-A Ethoxylate Diacrylate

8.1. Summary

In this chapter, the properties of PEO networks prepared via photopolymerization of bisphenol-A ethoxylate diacrylate (BPAEDA) were investigated as a function of cross-linker molecular weight and copolymer composition. Gas transport properties of these networks were related to the thermal relaxation characteristics, as measured by dynamic mechanical and dielectric methods, showing the effect of varying the network composition and architecture on transport properties. Network free volume can be enhanced by copolymerizing these cross-linkers with co-monomers that contain flexible free PEO side chains along the network backbone, resulting in permeability increase. The gas transport performance of amorphous rubbery membranes based on BPAEDA (n=15) cross-linker compared favorably to those based on PEGDA (n=14).

This chapter, written by the author, is based on an article [89] published under the same title in *Chemical Engineering Science* for the occasion of Prof. Morton M. Denn's 70th birthday Festschrift. The *Chemical Engineering Science* manuscript was originally written by Prof. Douglass S. Kalika with the author's assistance and contains the author's original work. Additional information, not appearing in the published version, has been incorporated herein.

8.2. Introduction

Hirayama et al. [5], in a survey of XLPEO materials based on methacrylate and dimethacrylate precursors for CO_2/N_2 gas separation, noted the interesting properties of polymers based on bisphenol-A ethoxylate dimethacrylate (*n*=30, denoting the total of 30 EO moieties in the molecule) (DB30), as compared to poly(ethylene glycol) dimethacrylate (*n*=14) (DM14). The main difference between the two cross-linkers was the insertion of a bisphenol-A functional group to interrupt the run of 30 EO moieties between the methacrylate groups in DB30. Both cross-linkers were polymerized with poly(ethylene glycol) methyl ether methacrylate (*n*=9) (MM9) at various compositions (by weight) and compared with each other. DSC analysis of copolymers based on DB30 showed no crystallinity despite the presence of 30 EO chains between the methacrylate groups (*cf*. cross-linked PEGDA23, which contains 23 continuous EO chains, in Figure 4.12). Based on this observation, insertion of the bisphenol-A group to interrupt the PEO chain appeared to effectively suppress crystallinity. In addition, the DB30/MM9 series of copolymers displayed higher gas permeability than did DM14/MM9 copolymers with similar concentration. This was attributed to larger gas diffusion coefficients as a result of the higher fractional free volume (*FFV*) of the DB30/MM9 series. The bulky bisphenol-A functional groups also increased local free volume, in addition to disrupting chain packing and forcing the flexible chains apart.

In this chapter, the properties of copolymers based on bisphenol-A ethoxylate diacrylate (BPAEDA) are examined, with chemical structures given in Table 3.1. BPAEDA contains symmetric -$(CH_2CH_2O)_n$- repeat segments and a central bisphenol-A linkage that frustrates chain packing and limits potential crystallization, much like their methacrylate analogs (*i.e.*, the DB series). Homopolymer and copolymer networks were prepared using three different BPAEDA molecular weights (n = 2, 4 and 15); the nomenclature used in this chapter is such that BPAEDA15 (*i.e.*, BPAEDA with n=15 EO on either side of the central bisphenol-A group, with a molecular total of 30 EO moieties) is a direct acrylate analog to DB30. These networks were also copolymerized with the longer acrylate co-monomers, PEGMEA and PEGA, and with lower molecular weight co-monomers that introduce shorter pendants along the backbone: EGMEA and DEGEEA (*cf.* Table 3.2, also Chapters 5 and 6, respectively). The objective of this chapter is to examine systematically the effect of polymer cross-link density and co-monomer composition in the prepolymer mixture on the static and dynamic properties of the resulting networks, using a BPAEDA cross-linker with previously-characterized co-monomers, and to relate the physical characterization results to the networks' gas separation performance.

Dynamic mechanical analysis and dielectric spectroscopy results are used to elucidate the molecular characteristics of the BPAEDA-based networks. Gas transport properties of these networks are reported from pure gas permeability studies of CO_2, H_2, CH_4, O_2 and N_2 at 35°C, as well as pure gas solubility studies of CO_2 and CH_4 at the same temperature

on the homopolymer networks. The gas transport properties are compared with the networks based on PEGDA as cross-linker (*cf.* Chapters 4 through 6) and with the bisphenol-A ethoxylate dimethacrylate analogs studied by Hirayama et al. [5].

8.3. Results and Discussions

8.3.1. Properties of Polymer Networks

Like the networks obtained by Hirayama et al., the photopolymerized BPAEDA homopolymers are completely amorphous. For BPAEDA4 and BPAEDA15 (n = 4 and 15, respectively), the effective distance between cross-links is large enough to yield rubbery networks (*i.e.*, T_g < 25°C), while for BPAEDA2, a glassy solid was obtained. The dynamic mechanical glass transition temperatures (T_α) for the networks are given in Table 8.1. The polymerization degree of conversion was obtained by examining the FTIR-ATR spectra, especially the disappearance of the acrylate characteristic double bonds (*cf.* Section 3.5: peaks examined here are 810 and 1410 cm^{-1}); the spectra of cross-linked copolymer networks based on BPAEDA2 and BPAEDA4 are presented in Figure 8.1. In the case of the cross-linked BPAEDA2 homopolymer network, comparison with the BPAEDA2 monomer spectrum reveals the presence of residual acrylate groups that are not fully converted during polymerization. The relatively short cross-link bridges associated with the n=2 monomer limit polymer chain mobility; as the reaction proceeds and cross-link density increases, the network eventually vitrifies, limiting the diffusion of unreacted monomer molecules and thus further reaction. The remaining CH_2=CH groups

in the polymer are, consequently, present as dangling chain ends. In contrast, the cross-linked BPAEDA4 homopolymer network remains rubbery throughout the polymerization process, allowing easier diffusion of the unreacted monomers to complete the polymerization, leaving only a small amount of residual acrylate. If both cross-linkers are copolymerized with flexible monomers such as PEGMEA or PEGA, the effective glass transition temperature of the copolymer decreases, and the reaction can proceed under conditions of even higher molecular mobility. Virtually complete acrylate conversion can be obtained for these materials (*re*: copolymer spectra in Figure 8.1). Complete acrylate conversion was obtained for homopolymer and copolymer networks based on BPAEDA15, by virtue of cross-linker chain flexibility and the final network's low glass transition temperature (*spectra not shown*). The result is consistent with polymerization studies on PEGDA cross-linkers (n = 3, 10 and 14) prepared under the same reaction conditions [18, 75] (see also: Figure 4.12).

The cross-linked polymer networks obtained in this manner were tested as-prepared, with no additional steps taken to influence the acrylate conversion [75].

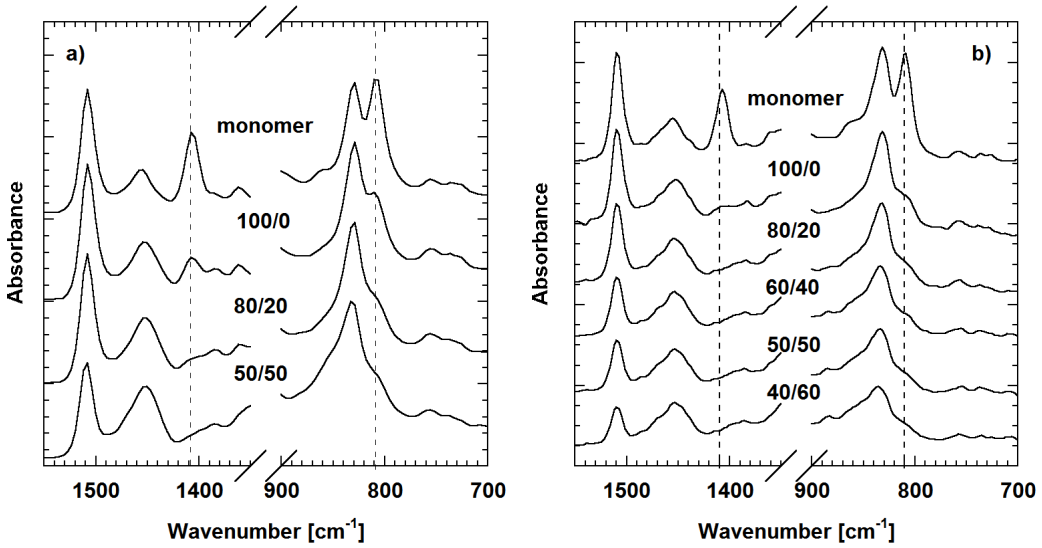

Figure 8.1: FTIR spectra of BPAEDA liquid monomer and solid cross-linked copolymer films: a) BPAEDA2 cross-linker and BPAEDA2/PEGMEA copolymers, b) BPAEDA4 cross-linker and BPAEDA4/PEGA copolymers. All copolymer compositions reported on a (cross-linker/co-monomer) wt% basis. The characteristic acrylate peaks (810 and 1410 cm^{-1}) are marked by vertical lines (see Section 3.5).

Table 8.1: Physical properties of BPAEDA-based copolymers.

Cross-linker	Co-monomer	XL wt%	T_α (1 Hz)[°C][a]	β_{KWW}[b]	FFV[c]
BPAEDA2	---	100	43	0.16	0.119
	PEGMEA	80	41	0.15	0.117
		60	9	0.17	0.122
		50	-11	0.16	0.126
		40	-23	0.17	0.130
	PEGA	80	38	0.15	0.114
		60	16	0.15	0.116
		50	3	0.14	0.117
		40	-6	0.13	0.119

(*continued on next page*)

Table 8.1 (*continued*): Physical properties of BPAEDA-based copolymers.

Cross-linker	Co-monomer	XL wt%	T_α (1 Hz)[°C][a]	β_{KWW}[b]	*FFV*[c]
BPAEDA4	----	100	11	0.21	0.118
	PEGMEA	80	-8	0.21	0.122
		60	-24	0.21	0.126
		50	-30	0.19	0.127
	PEGA	80	-2	0.21	0.119
		60	-15	0.20	0.118
		50	-21	0.19	0.119
BPAEDA15	----	100	-34	0.28	0.125
	PEGMEA	90	-36	0.28	0.126
		80	-39	0.29	0.128
		70	-41	0.28	0.130
		60	-44	---	0.132
	DEGEEA	90	-36	0.29	0.127
		80	-38	0.29	0.131
		70	-38	0.28	0.135
		60	-38	0.29	0.138
	EGMEA	90	-34	0.30	0.128
		80	-33	0.29	0.130
		70	-31	0.28	0.133
		60	-30	0.29	0.135

[a]T_α (°C) is the dynamic mechanical peak temperature at 1 Hz; [b]β_{KWW} is the Kohlrausch-Williams-Watts distribution parameter (see Equation 2.19); [c]*FFV* is the estimated fractional free volume based on bulk density measurements at ambient temperature (see Equation 2.16). All polymer compositions are reported on a wt% basis.

8.3.2. Dynamic Mechanical Analysis

The dynamic mechanical results of the cross-linked BPAEDA homopolymer networks are presented in Figure 8.2 as storage modulus (E') vs. temperature at 1 Hz. Glass-rubber relaxation is indicated by a drop of ~2 orders of magnitude in storage modulus, with an accompanying maximum in loss tangent, tan δ. The dynamic mechanical glass transition temperature, T_α, was determined from the peak of the tan δ curve. As is the case with PEGDA-based XLPEO networks [75], T_α shifts to higher values with decreasing distance between cross-links, reflecting the decreased chain mobility. For the XLBPAEDA15 network, which contains cross-link bridges encompassing 30 EO units plus the central bisphenol-A linkage, T_α is essentially the same as that obtained previously for XLPEGDA (n=14) networks with 14 EO units between cross-link junctions (T_α = -35°C).

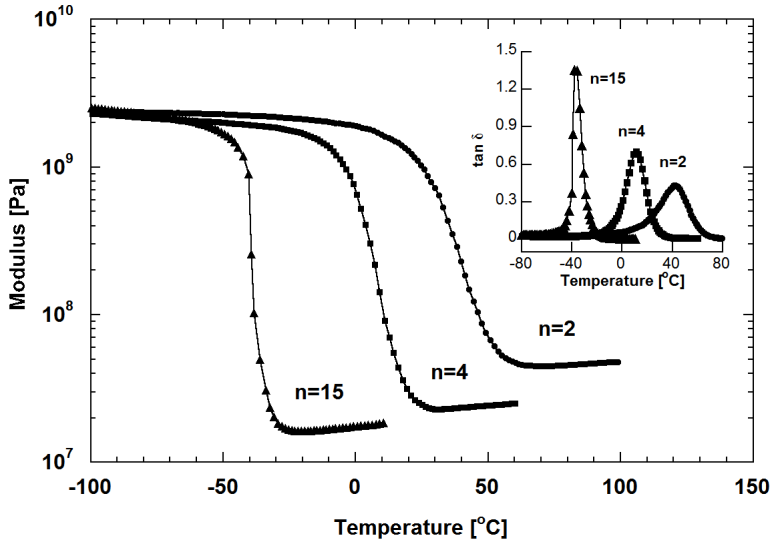

Figure 8.2: Storage modulus (E') [Pa] versus temperature [°C] for cross-linked BPAEDA networks. Frequency of 1 Hz; heating rate of 1°C/min. *Inset*: tan δ versus temperature.

The storage modulus value in the glassy region is relatively independent of cross-linked molecular weight and chain length. In the rubbery region, the rubbery modulus increases systematically with effective cross-link density, consistent with the predictions of classical elasticity theory [83]. Relaxation breadth also increases with cross-link density (*i.e.*, at lower BPAEDA molecular weight) as the constraints imposed by the covalent cross-link junctions produce an increasingly heterogeneous relaxation response. XLBPAEDA2 exhibits especially broad relaxation in the tan δ plot (Figure 8.2 *inset*) that includes a weak low-temperature shoulder; the latter reflects contributions from the dangling residual chain ends in the sample.

Copolymerization of BPAEDA cross-linkers with the monoacrylates controls the network cross-link density and *FFV* via insertion of side pendants with varying chemical characters; some aspects of this have been explored in the preceding chapters. Relatively long PEGMEA and PEGA co-monomers can be introduced to the lower molecular weight BPAEDA cross-linkers (n=2, n=4) to increase both the overall network flexibility and the ethylene oxide content. Dynamic mechanical properties of a representative network, BPAEDA4/PEGA, are presented in Figure 8.3. With increasing PEGA concentration, the copolymer's glass transition temperature decreases progressively, accompanied by a reduction in rubbery modulus associated with a decrease in cross-link density (from stoichiometric considerations) (*cf*. Figure 4.2). Not surprisingly, consistent with earlier studies (*cf*. Table 4.1), the -OCH_3 terminated PEGMEA is more effective in reducing T_α than is -OH terminated PEGA (also *cf*. Table 8.1).

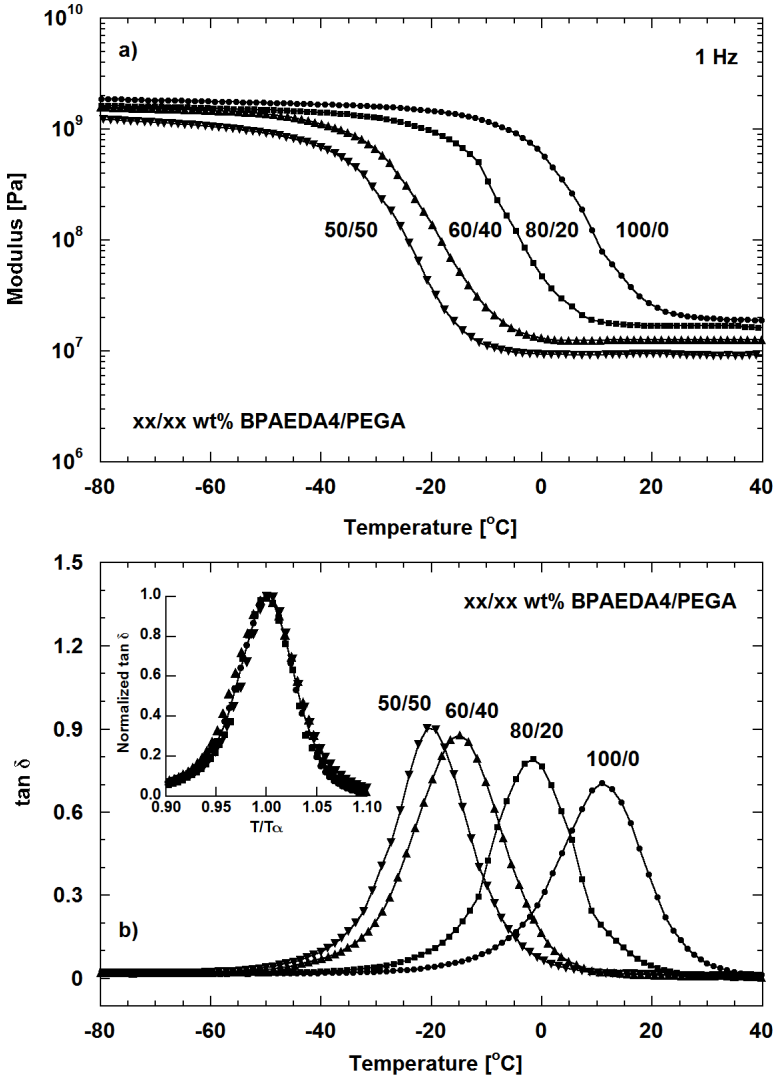

Figure 8.3: Dynamic mechanical properties: a) *E′*; b) tan δ versus temperature [°C] for BPAEDA4/PEGA copolymer networks. Frequency of 1 Hz, heating rate of 1°C/min. *Inset*: normalized tan δ as a function of temperature at 1 Hz.

The T_α and *FFV* of the copolymers based on BPAEDA15 are also given in Table 8.1. BPAEDA15-based copolymers with PEGMEA, EGMEA or DEGEEA, display similar characteristics as their respective corresponding copolymers with PEGDA (n=14) as cross-linker [2, 32, 90] (*cf.* Chapters 4, 5 and 6, respectively). Insertion of the relatively long PEGMEA chains results in significant reduction of T_α and increase in *FFV*. The inclusion of ≥ 40 wt% PEGMEA into a BPAEDA15 network also results in crystallization, as evidenced by cold-crystallization and melting events during the course of the dynamic mechanical heating sweeps. This threshold PEGMEA concentration is lower than required to induce crystallization in PEGDA/PEGMEA (> 70 wt%) [32]. The crystallization at lower concentration may be attributed to the additional leeway for PEGMEA chains to crystallize in BPAEDA15/PEGMEA networks, due to the higher inherent network *FFV* and/or the lower cross-link density that comes from the longer chain length between cross-link junctions. In this sense, although the bisphenol-A functional group is effective in suppressing the crystallization tendency of the interrupted PEO segments, it may also promote the crystalline rearrangement of other remaining PEO segments with sufficient chain length to crystallize in the absence of extensive cross-links, *e.g.*, those dangling branches found in PEGDA/PEGMEA networks [32].

The shorter co-monomers with non-polar ends, DEGEEA and EGMEA, are effective in increasing *FFV* to a similar extent as PEGMEA. This is attributed to the relative contribution of the endgroups to *FFV* enhancement compared to the volume occupied by the short polymer chains [2, 90]. DEGEEA is flexible enough to decrease the copolymer

T_α progressively with increasing co-monomer concentration, whereas EGMEA insertion causes stiffening of the polymer backbone and, subsequently, a slight progressive increase in T_α.

Time-temperature superposition can be utilized to construct master curves of storage modulus versus frequency [84] so as to further characterize the chain mobility; representative results for the BPAEDA4/PEGA series of networks are presented in Figure 8.4. The fit, described as the Kohlrausch-Williams-Watts (KWW) stretched exponential function (Equation 2.19) [85], gives the exponent β_{KWW}, which describes the relative breadth of the relaxation. Values of β_{KWW} range from 0 to 1, where lower values reflect relaxation broadening as a result of both inhomogeneities arising from chemical or physical cross-links and possible chain interactions [77, 79]. These values, as applied to the copolymers, are given in Table 8.1 and in Figure 8.4 for BPAEDA4/PEGA specifically.

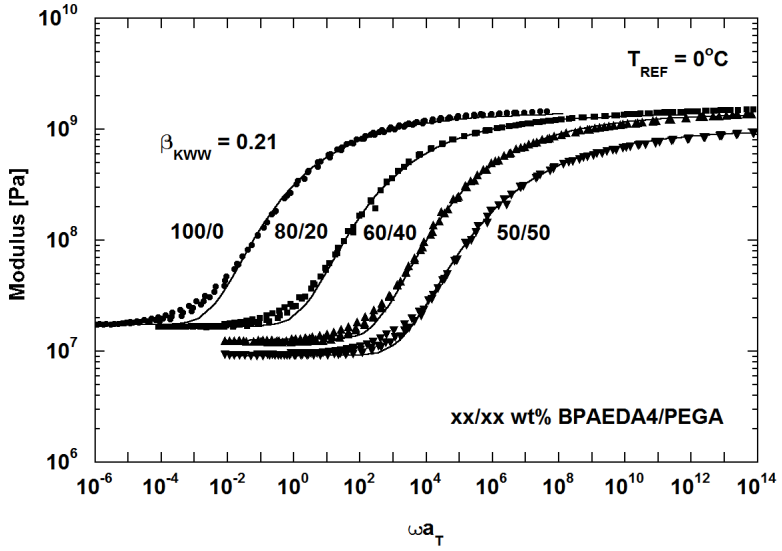

Figure 8.4: Time-temperature master curves (E' vs. ωa_T) for BPAEDA4/PEGA copolymers, with T_{REF} = 0°C. Solid curves are KWW fit (Equation 2.19).

The KWW exponents of the homopolymers decrease from 0.28 for BPAEDA15 to 0.16 for BPAEDA2, reflecting a progressively more constrained relaxation environment for segmental motion associated with glass transition for the networks with higher cross-link density. This observation is also captured by the shape change of the loss tangent curves shown in Figure 8.3b. Notably, the β_{KWW} value for the relatively unconstrained XLBPAEDA15 homopolymer is nearly the same as that measured for XLPEGDA14 (β_{KWW} = 0.30) [74, 75]. For the BPAEDA copolymers in this chapter, regardless of the co-monomer, there is little variation in the KWW exponent with co-monomer content. This is in contrast to the narrowing of the glass transition (*i.e.*, increasing β_{KWW} value) with increasing co-monomer concentration in PEGDA/PEGA and PEGDA/PEGMEA networks [74], due to both decreasing cross-link density and an equivalent concentration of flexible EO moieties in the co-monomer backbone to the one in PEGDA. With

BPAEDA-based copolymers, this narrowing effect may be offset by the disparate character of the bisphenol-A bearing cross-linker which tends to cause a modest increase in heterogeneity. The net result would thus be relaxations of similar breadth across the various copolymer series, confirmed by the shape of the normalized loss curves (Figure 8.3b *inset*).

8.3.3. Dielectric Relaxation Spectroscopy

Broadband dielectric spectroscopy complements the dynamic mechanical analysis above by providing a wider range of experimental test frequencies and is often more effective in probing local sub-glass motions. Sub-glass transitions in polymers typically reflect highly localized, non-cooperative relaxation processes such as side-group rotations or limited in-chain motions [74] - as such, observing sub-glass transition behavior is often useful in further describing molecular motion. The dielectric characteristics of the BPAEDA-based copolymer networks are compared to the properties of PEGDA-based networks with PEGMEA or PEGA [86, 87], or with 2-HEA, EGMEA or DEGEEA [95]. Salient results from the dielectric relaxation spectroscopy studies with BPAEDA are summarized in this sub-chapter; additional details are furnished in ref. [89].

Plots of the dielectric constant (ε') and loss (ε'') vs. temperature reveal not only the primary glass-rubber (α) relaxation, which corresponds to the dynamic mechanical α-transition, but also two overlapping sub-glass (β_1 and β_2) processes. Figure 8.5 provides a detailed view of this loss response for the BPAEDA homopolymers in the sub-glass

region (-78°C). The positions of both sub-glass relaxations are close to those observed for the XLPEGDA14 network [87], as well as for crystalline PEO [141], and are nearly independent of cross-linker molecular weight. The β_1 sub-glass relaxation corresponds with localized ethylene oxide chain motions, while the β_2 sub-glass relaxation is identified as a 'fast', non-cooperative segmental process in the vicinity of the cross-link junctions, and is thus sensitive to the degree of cross-linking in the network [86, 87, 95]. The resulting curves can be analyzed using a dual Havriliak-Negami (HN) expression [142], as described in ref. [87].

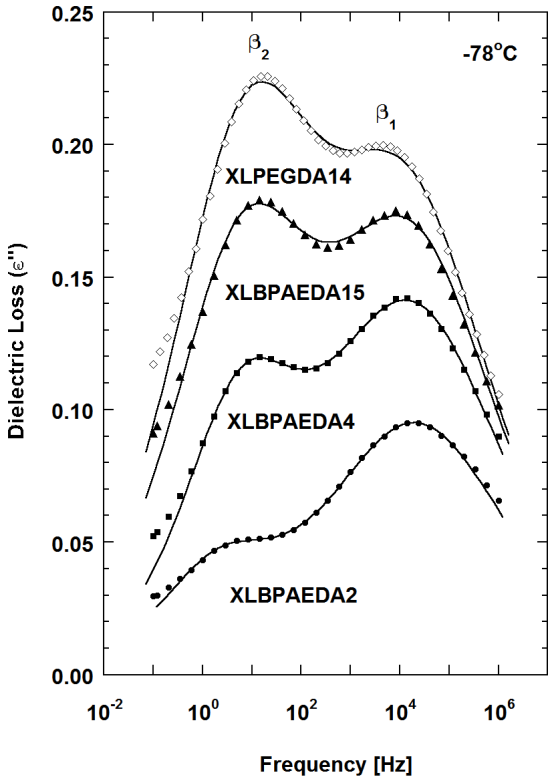

Figure 8.5: Dielectric loss (ε'') versus frequency [Hz] for XLBPAEDA homopolymer networks at -78°C. XLPEGDA14 data reported from ref. [87]. Solid curves are dual HN fits.

Using the HN expression, although the β_1 relaxation of all homopolymers coincides regardless of molecular weight, the β_2 relaxation of the XLBPAEDA2 is offset to a slightly higher temperature than the others. The dielectric sub-glass relaxation times measured for the XLBPAEDA and XLPEGDA are similar, regardless of the precursor molecular weight, reflecting the highly localized nature of the underlying motions responsible for these relaxation responses. As shown in Figure 8.5, the relative intensity of the sub-glass relaxation processes increases with increasing cross-linker molecular weight in the XLBPAEDA networks. This trend may be due to variations in the networks' chemical constituents (specifically, number and type of constituent dipoles), as well as to changing dipole mobility owing to varying cross-link density [143]. The changes in β_1 relaxation intensity can be explained solely on the basis of changes in dipolar composition, accounting for contributions from both ether oxygen and ester dipoles [89]. Meanwhile, β_2 relaxation intensity is again dependent on cross-link density, being strongly suppressed in highly cross-linked XLBPAEDA2, and matching that of XLPEGDA14 in XLBPAEDA15 [89].

The dielectric sub-glass relaxation properties of the BPAEDA-based copolymer networks match closely with the corresponding PEGDA-based copolymer networks. The relaxation activation energy and position associated with individual sub-glass relaxations are largely independent of copolymer composition, whereas the relative intensities of the β_1 and β_2 processes reflect changes in both dipolar content and network constraint [86, 87, 95]. For further details, the reader is again referred to the source paper, ref. [89].

Table 8.2: Pure gas permeability and ideal gas selectivity of BPAEDA-based copolymers at 35°C and infinite dilution

Cross-linker	Co-monomer	XL content		Permeability [barrer]					Ideal Selectivity			
		wt%	vol%	CO_2	H_2	CH_4	O_2	N_2	CO_2/H_2	CO_2/CH_4	CO_2/N_2	O_2/N_2
BPAEDA4	---	100	100	12	5.3	0.6	0.9	0.2	2.2	19	55	4.3
	PEGMEA	85	86	23	8.3	1.1	1.6	0.4	2.8	20	61	4.2
		70	69	54	12	3.1	3.2	1.2	4.5	17	45	2.7
		50	49	132	20	8.4	7.5	3.0	6.8	16	44	2.5
		28	27	288	30	17	14	5.6	9.7	17	52	2.6
	PEGA[a]	88	88	14	5.4	0.7	1.0	---	2.5	18	---	---
		73	73	25	6.8	1.4	1.9	---	3.6	17	---	---
		55	55	33	7.6	2.0	2.1	---	4.4	16	---	---
		31	31	68	12	3.8	3.5	---	5.5	18	---	---
BPAEDA15	---	100	100	152	20	8.3	7.3	2.8	7.6	18	54	2.6
	PEGMEA	80	77	198	24	11	9.3	3.5	8.2	18	57	2.6
		70	67	221	26	13	11	4.2	8.4	17	53	2.6
		60	58	261	28	15	12	4.7	9.2	17	56	2.6
		50	48	300	31	19	15	5.9	9.5	16	51	2.5
	DEGEEA	80	77	197	26	13	11	4.0	7.5	16	49	2.6
		70	67	205	28	14	12	4.8	7.4	15	43	2.5
		60	57	252	33	17	14	5.8	7.6	15	43	2.5
		50	47	270	37	19	15	5.9	7.3	14	46	2.6
PEGDA14[b]	---	100	100	110	15	5.8	5.1	2.2	7.3	19	50	2.3

[a]BPAEDA4/PEGA data is reported here in addition to original dataset in ref. [89]; [b]Data reproduced based on Chapter 5 [2].

Table 8.3: Pure gas solubility and diffusivity coefficients of homopolymer networks at 35°C and infinite dilution

Cross-linker	Solubility [cm^3(STP)/cm^3 atm]		Diffusivity [cm^2/s]	
	CO_2	CH_4	CO_2	CH_4
BPAEDA4	0.940 ± 0.030	0.053 ± 0.027	$(9.62\pm0.61) \times 10^{-8}$	$(9.0\pm4.6) \times 10^{-8}$
BPAEDA15	1.29 ± 0.03	0.081 ± 0.027	$(8.98\pm0.54) \times 10^{-7}$	$(7.8\pm2.6) \times 10^{-7}$
PEGDA14[a]	1.30 ± 0.06	0.075 ± 0.028	$(6.18\pm0.45) \times 10^{-7}$	$(5.5\pm2.0) \times 10^{-7}$

[a]Data reproduced based on Chapter 5 [2].

8.3.4. Gas Transport Properties

The permeability values for the copolymer networks based on BPAEDA4 and BPAEDA15 cross-linkers are presented in Table 8.2. The average uncertainty is ±6%. Due to incomplete polymerization of BPAEDA2, which is glassy at room temperature, transport studies of XLBPAEDA2 and its copolymers have been omitted from this study. Ideal pure gas selectivities are calculated from these values using Equation 2.8. Carbon dioxide and methane solubility experiments were performed only on BPAEDA4 and BPAEDA15 homopolymer networks; infinite dilution solubility coefficients (and diffusivity, calculated using the solution-diffusion model expressed by Equation 2.6) for these networks are presented in Table 8.3.

The XLBPAEDA15 homopolymer network shows a CO_2 permeability of 152 ± 8 barrer, which is slightly (~ 40%) higher than that obtained with the XLPEGDA14 network. On a stoichiometric basis, the two networks have similar ethylene oxide content (80 wt% EO

in BPAEDA15, versus 82 wt% EO in PEGDA14 [18]) and display comparable CO_2 and CH_4 solubilities, suggesting that the difference in *FFV* (and diffusivity, *cf.* Table 8.3) for these materials is the decisive factor in determining their relative permeability values. The estimated *FFV* for XLBPAEDA15 is 0.125, compared to 0.120 for XLPEGDA14. This difference may be caused by the presence of the bulky bisphenol-A linkage at the midpoint of the BPAEDA cross-linker, and to a lesser extent, lower overall cross-link density owing to longer chain distance between cross-link junctions. The degree of change in gas permeability between XLPEGDA14 and XLBPAEDA15 as a result of changing *FFV* is in line with the result shown by XLPEGDA copolymers containing alkoxy-terminated short chains, *e.g.* 79/21 wt% PEGDA/EGMEA (*cf.* Tables 5.1 and 5.3)

The cross-linked BPAEDA4 homopolymer network exhibits lower gas diffusivity and permeability values than do the two aforementioned cross-linked homopolymer networks. Although the difference in *FFV* is smaller (*FFV* of XLBPAEDA4 is 0.118), XLBPAEDA4 also has higher effective cross-link density and lower chain mobility, as indicated by the higher glass transition temperatures. Table 8.3 shows that both CO_2 and CH_4 diffusivity values in XLBPAEDA4 are nearly an order of magnitude lower than those in XLBPAEDA15. Solubility of both gases also appears to decrease as a result of closer chain packing and increased energy penalty for chain motion. Consequently, the lower gas diffusivity and solubility values contribute to the diminished gas permeability through the XLBPAEDA4 network. This finding agrees with those of Hirayama et al. [5] on DB10/MM9 with 90/10 wt% composition as compared to DB30/MM9 of similar

composition, where DB10 is the methacrylate analog of BPAEDA4. Interestingly, the *FFV* value of the XLBPAEDA2 network is also similar, despite the presumably lower gas diffusion coefficients due to the glassy nature of the polymer – perhaps due to the presence of bisphenol-A functional groups. As in the PEGDA/2-HEA network (*cf.* Figure 5.12) and PEGDA copolymerized with phenoxy-terminated co-monomers (*cf.* Section 6.3.2), changes in chain mobility due to additional constraints in this case are as influential as *FFV* in determining gas diffusion behavior through the polymer.

Ideal gas selectivity is interpreted in terms of diffusivity and solubility selectivity (*cf.* Equation 2.8), based on the relative size and condensability of the penetrants (*cf.* Table 2.2). While the rubbery XLPEO networks typically exhibit no significant size-sieving character (diffusivity selectivity is close to unity, *cf.* Figure 5.14), exceptions may occur when the polymer chain mobility is restricted and/or *FFV* is reduced as in, *e.g.*, the PEGDA/2-HEA network (Chapter 5). In this case, lacking direct diffusivity selectivity measurements, the ideal gas permeability selectivity trends of non-interacting permanent gases (such as O_2/N_2) are particularly instructive in identifying size-sieving character because these separations are strictly determined by the penetrants' relative size. XLBPAEDA4, being rubbery at 35°C, nevertheless has reduced chain mobility (as a result of higher cross-link density) and lower *FFV* than does XLBPAEDA15. The reduced chain mobility increases the network's size-sieving character, as shown by increased O_2/N_2 selectivity of the network (4.3, *vs.* a value of 2.6 exhibited by many other copolymers listed in Table 8.2); stronger size-sieving, in turn, favors faster permeation of

the smaller penetrant. CO_2/H_2 selectivity of XLBPAEDA4 suffers from both loss of CO_2 affinity as a result of decreased EO moiety concentration, which lowers CO_2 permeability relative to the non-polar penetrants, and a greater size-sieving effect, which favors faster H_2 permeation. In contrast, CO_2/CH_4 and CO_2/N_2 selectivities actually remain similar to those of the other copolymers, as the same two effects compete: in these cases, however, the size-sieving effect favors the smaller CO_2 molecules over the larger CH_4 and N_2 penetrants.

Unlike the case of XLBPAEDA4, ideal gas selectivity values for XLBPAEDA15 closely match those of XLPEGDA14. This trend is not surprising, considering that the gas solubility coefficients of the two polymers are similar, and that XLBPAEDA15 does *not* exhibit significantly different size-sieving character. In the absence of strong size-sieving effects in XLPEO copolymers, ideal gas selectivity tends to be determined by the relative gas solubilities, *i.e.*, solubility selectivity [2] (specifically, *cf*. Figure 5.14).

As shown in previous chapters, the copolymerization of BPAEDA cross-linker with EO-bearing co-monomers may yield changes in gas transport properties of the resulting copolymer networks. As with the corresponding PEGDA-based copolymer, the insertion of flexible (n=8) PEGMEA branches along the network backbone may enhance *FFV* and chain mobility, which leads to higher gas permeability. The same effect is evident for both BPAEDA4 and BPAEDA15 copolymer series, as shown in Table 8.2. In the case of BPAEDA15, the EO content of the PEGMEA co-monomer (81 wt% EO) is virtually

identical with that of the cross-linker, and thus copolymerization does not appreciably alter the overall EO fraction in the resulting network. Accordingly, no significant changes in CO_2 solubility are expected in the BPAEDA15/PEGMEA copolymer as a function of composition due to changing penetrant affinity. Comparable to the case of the PEGDA/PEGMEA network shown in Chapter 4, permeability increase of all gases through BPAEDA15/PEGMEA copolymer networks as a result of PEGMEA insertion is attributed mainly to changes in *FFV* and increased chain mobility, which in turn positively influences diffusivity.

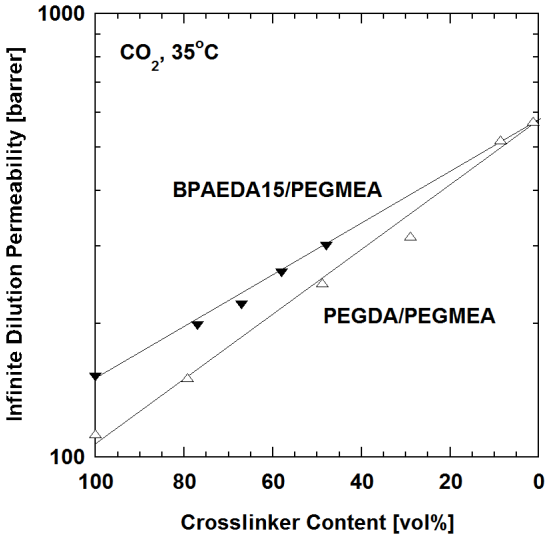

Figure 8.6: CO_2 infinite dilution permeability of ▼: BPAEDA15/PEGMEA copolymer networks as a function of copolymer composition. Values of Δ: PEGDA/PEGMEA are plotted for comparison (reproduced from Figure 4.5a). The line is based on the random homogeneous copolymer addition model, given by Equation 4.1.

The extent of permeability increase as a result of PEGMEA addition to BPAEDA15 is illustrated in Figure 8.6, taking CO_2 as an example. Like the PEGDA/PEGMEA series,

the BPAEDA15/PEGMEA copolymer is well described by the semi-logarithmic addition model for homogeneous copolymers, Equation 4.1 [106], which provides a convenient basis for estimating copolymer permeability. A similar trend is also observed for BPAEDA4/PEGMEA networks (*cf*. Table 8.2). As PEGMEA concentration increases, CO_2 permeability approaches that in the pure PEGMEA network, regardless of the cross-linker identity. The permeability trends agree nicely with the analogous study of methacrylates by Hirayama et al. [5], as described in the opening of this chapter (*cf*. Section 8.2). The cross-linked DB30 series in that study has higher *FFV* than does the BPAEDA15 series, owing to the presence of methyl pendant groups at the cross-link junctions, but it also suffers from an inherently lower overall EO content. Copolymerizing DB30 with the methacrylate analog of PEGMEA, MM9, leads to the decrease in T_g and a progressive increase in *FFV*, again consistent with the results presented here. The homopolymer DB30 network has a CO_2 permeability of 93 barrer at 25°C, which increases to 179 barrer for 50/50 wt% DB30/MM9 copolymer (see experimental details in ref. [5]).

Slightly weaker size-sieving effects with respect to H_2 in the rubbery XLPEO network can be observed as the PEGMEA co-monomer is incorporated into BPAEDA15. CO_2/H_2 selectivity increases with an increase in PEGMEA content, as a reduction in size discrimination tends to favor the permeation of the larger molecules (CO_2) over smaller (H_2). This observation is consistent with that previously observed in the PEGDA/PEGMEA network by Lin et al. [44]: the plasticization associated with CO_2

sorption (which increases *FFV*) can actually improve the CO_2/H_2 separation characteristics by increasing permeability without significant loss of selectivity. A similar outcome is observed in the BPAEDA4/PEGMEA series, which reflects both reduced size-sieving effects and increased CO_2 affinity for the polymer as the concentration of PEGMEA increases. The weaker size-sieving effect appears to affect mainly gas pairs with significantly different size (such as CO_2/H_2). With increased PEGMEA content, the CO_2/CH_4 selectivity (with CO_2 as the smaller penetrant in this case) decreases only slightly as a result of size-sieving, and the effect is almost negligible for gas pairs that are closer in size, *e.g.*, O_2/N_2. Thus, practically speaking, the benefits of improved material permeability realized by this synthetic strategy would likely outweigh losses in selectivity due to weakening size-discrimination ability of the polymer.

The addition model (Equation 4.1) accurately predicts the transport properties of BPAEDA4 and BPAEDA15 with other co-monomers studied previously. BPAEDA4/PEGA copolymers, for instance, display gas transport properties intermediate between those of BPAEDA4 and PEGA homopolymers. While PEGA slightly increases the gas permeability of BPAEDA4, this increase is due mostly to the increased EO content and overall higher chain mobility that comes with incorporating chains containing longer (n=7) uninterrupted EO moieties. In this respect, PEGMEA and other monoacrylate co-monomers with non-interacting terminal groups (such as methoxy or ethoxy) should bring about greater increases in permeability. An example of the ethoxy-terminated co-monomer is DEGEEA; the transport properties of the

BPAEDA15/DEGEEA copolymer series, which are also well-described by the addition model, are shown in Table 8.2. The shorter DEGEEA chains have lower EO content (47 wt%) than do either PEGMEA or PEGA [90], leading to decreased CO_2 affinity for the polymer. Thus, DEGEEA incorporation involves a trade-off in terms of composition and network architecture, as the ethoxy terminal groups are very effective in increasing network *FFV*, facilitating diffusion for all gases. While the gas permeability values of the BPAEDA15/ DEGEEA copolymer series are comparable to those obtained for BPAEDA15/PEGMEA, the selectivity values are slightly lower, especially for gas pairs in which CO_2 is the smaller penetrant, *e.g.*, CO_2/CH_4 or CO_2/N_2, reflecting this reduced CO_2 affinity. This behavior is similar to the PEGDA/DEGEEA copolymers, when compared to the PEGDA/PEGMEA copolymers (*cf*. Chapter 6).

8.4. Conclusions

This chapter examined the dynamic relaxation and gas transport properties of homopolymer and copolymer networks based on bisphenol-A ethoxylate diacrylate as a cross-linker, compared with the poly(ethylene glycol) diacrylate-based networks studied in other chapters. Three BPAEDA cross-linkers with different molecular weights were considered. The dynamic mechanical and dielectric relaxation measurements of the homopolymer networks reflected both inherent variations in chemical composition and the effective cross-link density encompassed by the monomers, influenced by the length of flexible ethylene oxide moieties (and by the bisphenol-A functional group at the midpoint) between cross-link junctions. The results were explained in terms of chain

mobility of the copolymer networks. In particular, the bisphenol-A group, when inserted to interrupt continuous EO moieties, could effectively disrupt PEO chain packing that would otherwise lead to crystallization. For the highest molecular weight BPAEDA considered here (n=15), the glass-rubber and sub-glass relaxation characteristics of the homopolymer were nearly identical to the properties of the cross-linked PEGDA networks. Copolymer networks of BPAEDA with co-monomers studied elsewhere in this project possessed properties that were predictable from prior studies of PEGDA copolymerized with the corresponding co-monomers. In particular, the methoxy-terminated PEGMEA was studied as a model co-monomer and was effective in increasing chain mobility (via significant reduction in glass transition temperature) and fractional free volume. Gas transport results for the networks were evaluated within the context of changing penetrant solubility and diffusivity as a result of changing fractional free volume, chain mobility and relative penetrant affinity. The permeability values of cross-linked BPAEDA films compared favorably with those reported for cross-linked PEGDA, with the XLBPAEDA15 network displaying gas permeability at infinite dilution that was 40% higher than the XLPEGDA14 values. The gas transport properties of the BPAEDA-based networks, intermediate between those of their constituents' homopolymer networks, were successfully predicted using the random copolymer addition model.

Chapter 9: Conclusions and Recommendations

9.1. Conclusions

The transport properties of cross-linked poly(ethylene oxide) (XLPEO) have been further explored to increase the polymer's CO_2 permeability and CO_2/light gas selectivity for applications involving CO_2 separation from mixtures with light gases. The light gases studied in this project were H_2, CH_4, N_2 and O_2. XLPEO was prepared by copolymerizing a diacrylate cross-linker containing ethylene oxide (EO) moieties with a monoacrylate co-monomer. The principal cross-linker used in this study was poly(ethylene glycol) diacrylate (PEGDA) with an average of 14 EO repeat units. Chemical structure modification of the cross-linked network significantly influenced polymer transport properties, and a wide array of modification strategies was explored to elucidate further this structure-property relationship.

9.1.1. Effect of Polymer Cross-link Density and Cross-linker Modification

Many modification strategies pursued in this project yielded changes in polymer cross-link density. For instance, introducing an additional diluent (such as water or toluene) to the prepolymer solution prior to cross-linking led to the formation of loops and 'wasted' cross-links during gel formation, increasing cyclization and reducing the effective cross-link density (see sections 4.2.1 and 7.3.1). Based on studies with PEGDA/H_2O and

PEGDA/toluene systems, prepolymer dilution did not significantly affect the density, fractional free volume (*FFV*), glass transition temperature, or transport properties of the resulting polymer. For example, diluting PEGDA with 80 wt% water in the prepolymer only increased CO_2 permeability in the resulting polymer from 110 to 145 barrer [18].

Cross-link density was also influenced by varying the concentration of the acrylate groups through modification of cross-linker chain length. Reducing the ethylene oxide content, for instance, decreased the distance between cross-links and thus increased cross-link density. Sufficiently high cross-link density led to severe restriction in chain mobility: for example, cross-linked PEGDA with n=3 exhibited a broad glass transition that occurred at much higher temperature than for cross-linked PEGDA with n=14 (-37°C at the transition midpoint). Following the gas permeability trends [120], gas diffusivity should be much smaller through the former than the latter, as a result of decreasing chain mobility. In addition, replacing every other cross-link junction with a bulky functional group (such as bisphenol-A) in line with the ethylene oxide moieties also decreased cross-link density. Bisphenol-A groups were effective in replacing cross-link junctions to frustrate chain packing and reduce (or eliminate) crystallinity. Cross-linked bisphenol-A ethoxylate diacrylate (XLBPAEDA) with n=15 exhibited properties similar to those of XLPEGDA14 without evidence of crystallinity, despite the lower cross-link density (see section 8.3.1). For example, at 35°C and infinite dilution, XLBPAEDA15 had a *FFV* of 0.125, a CO_2 permeability of 152 barrer and an ideal CO_2/ H_2 selectivity of 7.6, compared to 0.120, 110 barrer and 7.3, respectively, for

XLPEGDA14. The increase in *FFV* (and gas diffusivity) may be attributed to incorporation of bulky bisphenol-A moieties and, to a lesser extent, the cross-link density reduction.

Copolymerizing the cross-linker with various amounts of a monoacrylate co-monomer led to variations of the cross-link junction concentration in the resulting polymer, thus modifying its cross-link density. However, as Figures 4.2 and 4.5 show, the different chemical properties of the co-monomers' dangling end-groups tended to cause relatively more significant changes in polymer properties. Thus, cross-link density reduction due to copolymerization by itself should not be used to account for changes in various polymer properties studied here (see next section).

9.1.2. Effect of Co-monomer Chemical Properties

Adding a monoacrylate co-monomer containing ethylene oxide groups (as described by Table 3.2) into the prepolymer solution introduced dangling chains onto the polymer backbone (see Figure 1.1). Relatively minor changes in the chemical structure of these chains induced significant changes in the resulting copolymer's physical properties.

The effects of co-monomer chain length were compared in Chapters 5 and 6. The length of these co-monomers was defined by the number of continuous, highly flexible ethylene oxide moieties. Thus, polymer chains containing larger numbers of ethylene oxide repeat units tended to be more mobile, resulting in lower overall polymer glass transition

temperature and higher gas diffusivity in the polymer. For example, as shown in Figure 6.4, pure polymerized di(ethylene glycol) ethyl ether acrylate (DEGEEA), which has one more ethylene oxide repeat unit than 2-ethoxyethyl acrylate (2-EEA), exhibited a glass transition temperature of -50°C, compared to -45°C for 2-EEA. DEGEEA-based copolymers also showed slightly higher gas diffusivity than 2-EEA-based copolymers at similar composition (see Figure 6.11). In addition, higher ethylene oxide content increased CO_2 affinity for the polymer, and thus, CO_2/light gas selectivity.

The effects of dangling chain terminal groups were discussed in Chapters 5 through 7. Due to the polar character of the ethylene oxide chains, incorporating non-polar groups at the end of the dangling chains increased *FFV*, because these groups open local free volume. Short alkoxy groups, such as methoxy or ethoxy, were effective in increasing *FFV*. Such alkoxy-terminated chain ends were less polar than the ethylene oxide moieties without being excessively bulky, and thus insertion of sufficiently long branches allowed a significant increase in the polymer chain mobility (*e.g.*, copolymers based on poly(ethylene glycol) methyl ether acrylate, n=8 (PEGMEA) or DEGEEA). Ethoxy-terminated chain ends were more effective in increasing *FFV* than their methoxy-terminated counterparts, leading to higher gas diffusivity at similar concentrations. For example, with approximately 35 wt% PEGDA, PEGDA/2-EEA copolymer exhibited a CO_2 permeability of 250 barrer at 35°C and infinite dilution, compared with its methoxy counterpart, PEGDA/EGMEA, at 160 barrer (see Table 5.3).

An increase in polymer *FFV* was also observed upon addition of phenoxy-terminated branches. However, whether due to shape-induced steric hindrance or additional chain interactions, these branches were less mobile, which adversely affected gas permeability. For example, although polymerized diethylene glycol phenyl ether acrylate (DEGPEA) has a *FFV* of 0.135, its glass transition temperature is -12°C. Its CO_2 permeability at 35°C and infinite dilution was 35 barrer, which was much less than that of XLPEGDA. Incorporation of tris-(trimethylsiloxy) silyl groups, which are very bulky and non-polar, reduced the density of cross-linked PEGDA, increased *FFV* and also gas diffusivity (see section 7.3.2). However, the diffusivity increase is countered by changes in chemical character of the network, which increased polymer affinity for the non-polar penetrants, and subsequently, reduced CO_2/light gas selectivity. Thus, transport properties of the PEGDA copolymer with TRIS-A, which contained the aforementioned functional group, were intermediate between those of XLPEGDA and poly(dimethylsiloxane) (PDMS).

In contrast, adding side-chains terminated by polar groups (*e.g.*, hydroxy) led to significant chain interaction with the polar network, severely restricting chain mobility and reducing *FFV*. These factors reduced gas diffusivity.

Gas transport properties of all polymers studied here varied systematically, and were well-described by Equation 4.1. These rubbery polymers generally had weak size-sieving ability, which was significantly affected *only* if polymer chain mobility was restricted due to chain interaction; therefore, gas selectivity was influenced primarily by

changing CO_2-polymer affinity relative to the other light gases. Gas permeability was generally a strong function of gas diffusivity; however, in cases where functional groups significantly modified polymer-penetrant affinity (*e.g.*, in PEGDA/TRIS-A systems), the effect of gas solubility on permeability becomes increasingly more significant.

9.1.3. Reevaluation of the *D* vs. *FFV* Relationship Paradigm

This project highlighted the need to reevaluate the modified free volume model to predict gas diffusivity (Equation 4.5) as advocated previously [10, 88]. Gas diffusivity was previously correlated using the Fujita-modified Cohen-Turnbull model with fractional free volume [65, 66], which in turn was assumed to undergo linear expansion as a function of temperature [108] (Equations 2.12 and 4.4, respectively). Figure 9.1 summarizes the correlations, as applied to CO_2 diffusivity, in the polymers studied: with *FFV*, and with the difference between glass transition temperature and measurement temperature (T - T_g), following the plot by van Amerongen [41]. The broad modified free volume correlation proposed in previous XLPEO studies (*cf.* Equation 4.5) [43, 88] did not quantitatively predict gas diffusivity within many individual XLPEO systems studied here since the model did not always properly capture the relation of free volume and chain flexibility. For example, the model assumed that polymers containing more flexible chains would have higher free volume, which was not the case for all XLPEO systems (see Figure 6.5). Chain mobility seemed to be at least as important, if not more so, than free volume in determining gas diffusivity in the rubbery polymers of interest in this study.

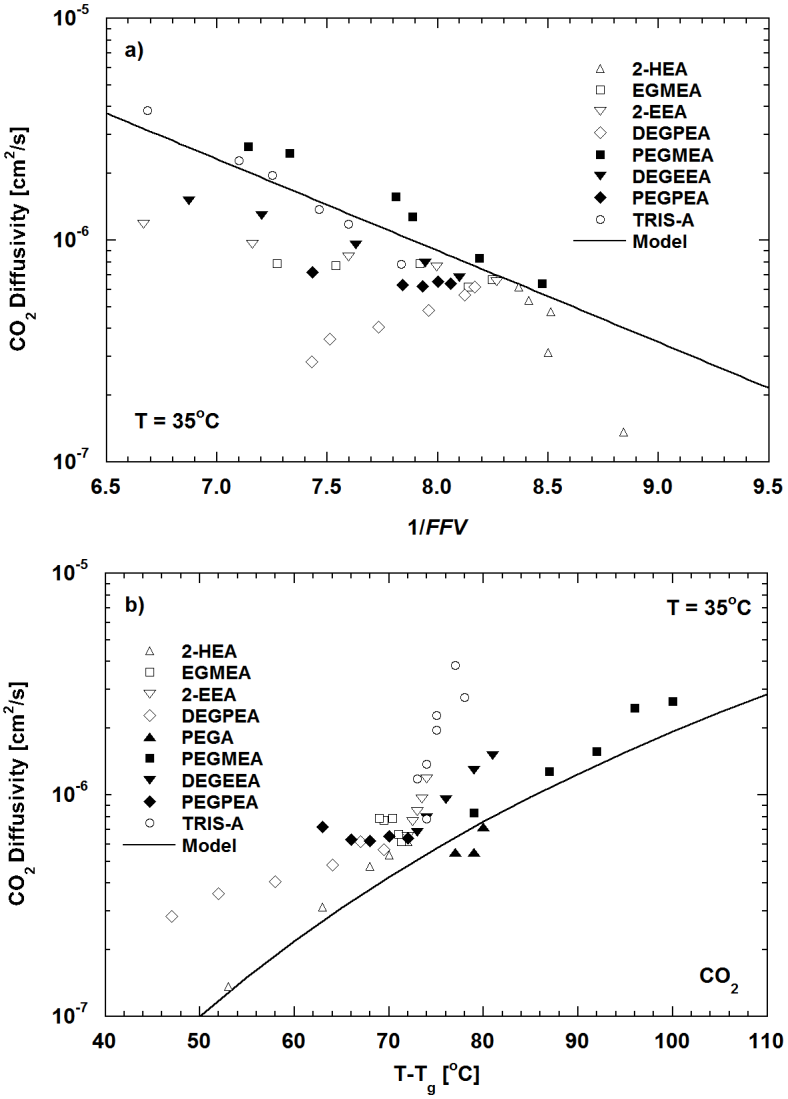

Figure 9.1: CO_2 diffusivity coefficients as a function of: a) *FFV* and b) T - T_g of the polymer. The data are from Chapters 4 through 7. The cross-linker is PEGDA; the co-monomers are defined in the legends (refer to Table 3.2). The model line in Figure 9.1a is drawn based on the Fujita-modified Cohen-Turnbull model (Equation 2.12) with parameters in Table 2.1. The model line in Figure 9.1b is drawn based on the *FFV*-T_g correlation that appears in Equation 4.4.

In addition, the Fujita-modified Cohen-Turnbull model depended on an operational definition of fractional free volume, which in some cases can be inadequate for assessing

the actual distribution of free volume elements [124] and was dependent on the accuracy of the chosen group contribution method [133]. Predicting gas diffusivity in XLPEO required a full appreciation of the specific polymer's chain properties, from both free volume and chain mobility standpoints.

9.2. Recommendations for Future Work

9.2.1. Co-monomer Modification Strategies

A successful strategy for influencing gas diffusion behavior in a polymer was insertion of dangling side-chains with different chemical properties. While this study explored a variety of co-monomers to modify XLPEO transport properties, the list is by no means exhaustive. Incorporation of pendant chains terminated by other non-polar, non-interacting side groups may be more effective than the methoxy or ethoxy terminal moieties in improving transport properties, as long as chemical character of the polymer remains similar to that of CO_2. In addition to using commercially available acrylate-based co-monomers, direct chemical modifications can be performed on PEGA. Many chemical reactions can be achieved by exploiting the sterically accessible primary alcohol terminal functional groups (see Table 3.2). End-groups of interest, such as *tert*-butyl, trimethylsilyl, trifluoromethyl, or cyclohexyl, can be attached by utilizing functional groups, *e.g.*, acid chlorides [144] or isocyanates [145-147] that can react with this alcohol group. Two recommended substances of interest are trimethylacetyl chloride [148] and N-trimethylsilyl isocyanate [149]. In addition, the compatibility of TRIS-A

with cross-linkers that have high polar content may be improved by incorporating additional polar groups into the co-monomer structure [150-152]. An example monomer with such feature is SiGMA ((3-methacryloxy-2-hydroxypropoxy)-propyl-bis(trimethylsiloxy)methylsilane), catalog number SIM6481.15 from Gelest, Inc. [153].

9.2.2. Additional Gas Transport Experiments

This study was focused on evaluating pure gas transport properties at 35°C, a strategy adapted to obtain the structure-property relationship from a wide variety of XLPEO membranes. Pure gas measurements could be extended to include the temperature dependence of gas transport properties in several copolymer systems, especially PEGDA/DEGEEA, PEGDA/DEGPEA and PEGDA/2-HEA (*cf.* Section 4.2.3). While size discrimination ability (*i.e.*, diffusivity selectivity) changed only slightly with copolymer composition in many systems considered (*e.g.*, noticeable only in the case of CO_2/H_2 selectivity in PEGDA/PEGMEA), the changes were particularly pronounced in PEGDA/2-HEA. These changes might be due to the changing relative activation energy of penetrant diffusion as a function of penetrant kinetic size, brought about by changes in the polymer chemical properties as a result of copolymerization. XLPEGDA showed a higher activation energy of penetrant diffusion (E_D) than does natural rubber, due to the presence of polar groups within the polymer chains, as well as a slight dependence of E_D on penetrant size, implying weak size-sieving ability [43]. It would be interesting to compare these relationships with those of PEGDA/2-HEA, which should display greater such interdependence. For future sorption studies, based on the findings of Ribeiro Jr.

and Freeman on CO_2/C_2H_6 sorption in PEGDA/PEGMEA [154], the effect of polymer dilation with penetrant concentration and the variation of penetrant partial molar volumes with temperature may also be considered.

The modified free volume model, as performed by Lin and Freeman [43], might be expanded using the systems in Figure 9.1 through mixed-gas permeability and solubility studies at different temperatures. After all, the adjustable parameters shown in Table 2.1 were obtained from an extensive multi-temperature mixed-gas transport analysis of XLPEGDA and some PEGDA/PEGMEA copolymers. The result may yield additional insights into the effect of chain flexibility on transport in rubbery polymers. In addition, mixed-gas transport analysis with the inclusion of water would be of significant interest for practical applications. Water, a ubiquitous penetrant in many separation applications (*e.g.*, natural gas sweetening), is highly polar, and the effect of water-XLPEO interactions on polymer CO_2 separation performance has not yet been studied.

9.2.3. Free Volume Distribution

A major limitation of the modified free volume method is its dependence on fractional free volume (see Section 9.1.3), which is not always representative of the actual distribution of free volume elements within the polymer. For instance, two stereoisomers of polynorbornene with identical *FFV* and different free volume element distribution had very different gas transport properties [124]: both positron annihilation lifetime spectroscopy (PALS) and molecular modeling were used to explain the gas transport

properties based on structural differences. A similar study using these techniques, particularly on PEGDA/2-HEA, PEGDA/DEGPEA, PEGDA/TRIS-A and BPAEDA systems, may yield additional insights into the free volume characteristics in these polymers and their effects on gas transport properties, as observed in this study.

9.2.4. Mechanical Properties

In practical applications, XLPEO membranes are most likely to be utilized in the form of thin layer composite membranes (see Section 1.2). To the author's knowledge, there has been no thorough, systematic attempt to characterize relevant mechanical properties of membrane materials in this form, or even in free-standing film form. The rubbery modulus values obtained through dynamic mechanical analysis are likely to be of limited value for practical applications. One study, which looked at tensile strength and maximum elongation of XLBPAEDA [155], is likewise inadequate. Qualitatively, the author observed significant variations in membrane mechanical properties in terms of flexural strength and shear modulus, which affected the ease of material handling. For instance, XLBPAEDA had higher flexural strength and shear modulus than did XLPEGDA; PEGDA/DEGEEA polymers remained mechanically robust even at high DEGEEA concentration, in contrast to PEGDA/PEGMEA; and the mechanical integrity of PEGDA/TRIS-A decreased rapidly with decreasing PEGDA content. Without an appropriate, rigorous quantitative characterization and discussion of mechanical properties in addition to gas separation properties, a full appreciation of the merits of some materials in this study might not be fully realized.

9.2.5. Effect of Nanostructured Fillers

Incorporation of impermeable nanostructure fillers into membranes resulted, in some cases, in gas transport property improvements. In those cases, the fillers acted as nanospacers that disrupt chain packing and increase gas permeability [156], but not to the point where interconnected pores would induce the Knudsen diffusion mechanism for penetrants, which may lead to decreased selectivity for particular separation applications [157, 158]. The increase in gas permeability did not follow the Maxwell model, which dictates that adding impermeable fillers will systematically reduce penetrant diffusivity and solubility [159]. Permeability increase has been observed in, among others, poly(4-methyl-2-pentyne) with fumed silica fillers [156], poly(1-trimethylsilyl-1-propyne) with MgO and TiO_2 fillers [157, 160], and 1,2-polybutadiene with MgO and TiO_2 fillers [161, 162]. Matteucci et al. observed that these permeability enhancements were achieved through discrete void space formation, with the exact mechanism depending on the nature of the nanofillers and the matrix [157, 160-162]. Although the incorporation of fillers to improve transport properties in chemically cross-linked PEO and related materials has been explored using fumed silica, the effect seemed limited instead to better mechanical strength [47, 120, 163, 164]. Studies on the interaction and distribution of fillers in different XLPEO systems are vital to understand and improve the gas transport properties of specific polymer/filler systems [165, 166].

References

1. Baker, R.W., *Membrane Technology and Applications*, 2nd ed., Wiley, New York, **2004**.

2. Kusuma, V.A., Freeman, B.D., Borns, M.A., Kalika, D.S., Influence of Chemical Structure of Short Chain Pendant Groups on Gas Transport Properties of Cross-linked Poly(ethylene oxide) Copolymers, *Journal of Membrane Science***, 2009**, *327*, 195-207.

3. Kusuma, V.A., Lin, H., Freeman, B.D., Jose-Yacaman, M., Kalakkunnath, S., Kalika, D.S., Structure/Property Characteristics of Polar Rubbery Polymeric Membranes for Carbon Dioxide Removal from Mixtures with Light Gases, in *Advanced Membrane Technology and Applications* (Eds.: Li, N.N., Fane, A.G., Ho, W.S.W., Matsuura, T.), Wiley, New York, **2008**, pp. 929-953.

4. Kohl, A.L., Nielsen, R.B., *Gas Purification*, 5th ed., Gulf Publishing, Houston, TX, **1997**.

5. Hirayama, Y., Kase, Y., Tanihara, N., Sumiyama, Y., Kusuki, Y., Haraya, K., Permeation Properties to CO_2 and N_2 of Poly(ethylene oxide)-Containing and Crosslinked Polymer Films, *Journal of Membrane Science***, 1999**, *160*, 87-99.

6. Baker, R.W., Lokhandwala, K., Natural Gas Processing with Membranes: An Overview, *Industrial & Engineering Chemistry Research***, 2008**, *47*, 2109-2121.

7. Bhide, B.D., Stern, S.A., Membrane Process for the Removal of Acid Gases from Natural Gas. I. Process Configurations and Optimization of Operating Conditions, *Journal of Membrane Science***, 1993**, *81*, 209-237.

8. Crabtree, G.W., Dresselhaus, M.S., The Hydrogen Fuel Alternative, *MRS Bulletin***, 2008**, *33*, 421-428.

9. Service, R.F., Hydrogen Power: Bringing Fuel Cells Down to Earth, *Science***, 1999**, *285*, 682, 684-685.

10 Lin, H., Solubility Selective Membrane Materials for Carbon Dioxide Removal from Mixtures with Light Gases, PhD thesis, The University of Texas at Austin (2005).

11. Shao, L., Low, B.T., Chung, T.S., Greenberg, A.R., Polymeric Membranes for the Hydrogen Economy: Contemporary Approaches and Prospects for the Future, *Journal of Membrane Science***, 2009**, *327*, 18-31.

12. Milliken, J., 2007 Annual Progress Report for DOE Hydrogen Program: I. Introduction, http://www.hydrogen.energy.gov/annual_progress07.html, U.S. Department of Energy, **2007**.

13. Paul, D.R., Clarke, R., Modeling of Modified Atmosphere Packaging Based on Designs with a Membrane and Perforations, *Journal of Membrane Science***, 2002**, *208*,

269-283.

14. Kirkland, B.S., Paul, D.R., Gas Transport in Poly(*n*-alkyl acrylate)/Poly(*m*-alkyl acrylate) Blends, *Polymer***, 2008**, *49*, 507-524.

15. Murphy, T.M., Offord, G.T., Paul, D.R. in *Membrane Operations: Innovative Separations and Transformations* (Eds. Drioli, E. & Giorno, L.), Wiley-VCH Verlag, Weinheim, 2009. (ISBN: 3527320385).

16. Lin, H., Freeman, B.D., Gas Solubility, Diffusivity and Permeability in Poly(ethylene oxide), *Journal of Membrane Science***, 2004**, *239*, 105-117.

17. Lin, H., Freeman, B.D., Materials Selection Guidelines for Membranes that Remove CO_2 from Gas Mixtures, *Journal of Molecular Structure***, 2005**, *739*, 57-74.

18. Lin, H., Kai, T., Freeman, B.D., Kalakkunnath, S., Kalika, D.S., The Effect of Crosslinking on Gas Permeability in Crosslinked Poly(ethylene glycol diacrylate), *Macromolecules***, 2005**, *38*, 8381-8393.

19. Ghosal, K., Chern, R.T., Freeman, B.D., Daly, W.H., Negulescu, I.I., Effect of Basic Substituents on Gas Sorption and Permeation in Polysulfone, *Macromolecules***, 1996**, *29*, 4360-4369.

20. Koros, W.J., Simplified Analysis of Gas/Polymer Selective Solubility Behavior, *Journal of Polymer Science: Polymer Physics Edition***, 1985**, *23*, 1611-1628.

21. Graham, N.B., Poly(ethylene oxide) and Related Hydrogels, in *Hydrogels in Medicine and Pharmacy* (Ed.: Peppas, N.A.), CRC Press, Boca Raton, FL, **1987**, pp. 95-113.

22. Weinkauf, D.H., Paul, D.R., Gas Transport Properties of Thermotropic Liquid-Crystalline Copolyesters. I. The Effects of Orientation and Annealing, *Journal of Polymer Science: Part B: Polymer Physics***, 1992**, *30*, 817-835.

23. Michaels, A.S., Bixler, H.J., Flow of Gases through Polyethylene, *Journal of Polymer Science***, 1961**, *50*, 413-439.

24. Li, J., Nagai, K., Nakagawa, T., Wang, S., Preparation of Polyethyleneglycol (PEG) and Cellulose Acetate (CA) Blend Membranes and Their Gas Permeabilities, *Journal of Applied Polymer Science***, 1995**, *58*, 1455-1463.

25. Yoshino, M., Ito, K., Kita, H., Okamoto, K., Effects of Hard-Segment Polymers on CO_2/N_2 Gas Separation Properties of Poly(Ethylene Oxide)-Segmented Copolymers, *Journal of Polymer Science: Part B: Polymer Physics***, 2000**, *38*, 1707-1715.

26. Okamoto, K., Fujii, M., Okamyo, S., Suzuki, H., Tanaka, K., Kita, H., Gas Permeation Properties of Poly(ether imide) Segmented Copolymers, *Macromolecules***, 1995**, *28*, 6950-6956.

27. Bondar, V.I., Freeman, B.D., Pinnau, I., Gas Sorption and Characterization of

Poly(ether-*b*-amide) Segmented Block Copolymers, *Journal of Polymer Science: Part B: Polymer Physics*, **1999**, *37*, 2463-2475.

28. Bondar, V.I., Freeman, B.D., Pinnau, I., Gas Transport Properties of Poly(ether-*b*-amide) Segmented Block Copolymers, *Journal of Polymer Science: Part B: Polymer Physics*, **2000**, *38*, 2051-2062.

29. Chen, J.C., Feng, X., Penlidis, A., Gas Permeation Through Poly(ether-*b*-amide) (Pebax 2533) Block Copolymer Membranes, *Separation Science and Technology*, **2004**, *39*, 149-164.

30. Car, A., Stropnik, C., Yave, W., Peinemann, K.V., PEG Modified Poly(amide-*b*-ethylene oxide) Membranes for CO_2 Separation, *Journal of Membrane Science*, **2008**, *307*, 88-95.

31. Hirayama, Y., Tanihara, N., Kusuki, Y., Kase, Y., Haraya, K., Okamoto, K., Permeation Properties to Hydrocarbons, Perfluorocarbons and Chlorofluorocarbons of Cross-linked Membranes of Polymethacrylates with Poly(ethylene oxide) and Perfluorononyl Moieties, *Journal of Membrane Science*, **1999**, *163*, 373-381.

32. Lin, H., Van Wagner, E., Swinnea, J.S., Freeman, B.D., Pas, S.J., Hill, A.J., Kalakkunnath, S., Kalika, D.S., Transport and Structural Characteristics of Crosslinked Poly(ethylene oxide) Rubbers, *Journal of Membrane Science*, **2006**, *276*, 145-161.

33. Dickey, M.D., Burns, R.L., Kim, E.K., Johnson, S.C., Stacey, N.A., Willson, C.G., Study of the Kinetics of Step and Flash Imprint Lithography Photopolymerization, *AIChE Journal*, **2005**, *51*, 2547-2555.

34. Priola, A., Gozzelino, G., Ferrero, F., Malucelli, G., Properties of Polymeric Films Obtained from U.V. Cured Poly(ethylene glycol) Diacrylate, *Polymer*, **1993**, *34*, 3653-3657.

35. Decker, C., Kinetic Study and New Application of UV Radiation Curing, *Macromolecular Rapid Communications*, **2002**, *23*, 1067-1093.

36. Freeman, B.D., Basis of Permeability/Selectivity Tradeoff Relations in Polymeric Gas Separation Membranes, *Macromolecules*, **1999**, *32*, 375-380.

37. Koros, W.J., Coleman, M.R., Walker, D.R.B., Controlled Permeability Polymer Membranes, *Annual Review in Materials Science*, **1992**, *22*, 375-380.

38. Staudt-Bickel, C., Koros, W.J., Improvement of CO_2/CH_4 Separation Characteristics of Polyimides by Chemical Crosslinking, *Journal of Membrane Science*, **1999**, *155*, 145-154.

39. White, L.S., Blinka, T.A., Kloczewski, H.A., Wang, I.F., Properties of a Polyimide Gas Separation Membrane in Natural Gas Streams, *Journal of Membrane Science*, **1995**, *103*, 73-82.

40. Koros, W.J., Hellums, M.W., Gas Separation Membrane Material Selection Criteria: Differences for Weakly and Strongly Interacting Feed Components, *Fluid Phase Equilibria***, 1989**, *53*, 339-354.

41. van Amerongen, G.J., Diffusion in Elastomers, *Rubber Chemistry and Technology***, 1964**, *37*, 1065-1152.

42. Baker, R.W., Vapor and Gas Separation by Membranes, in *Advanced Membrane Technology and Applications* (Eds.: Li, N.N., Fane, A.G., Ho, W.S.W., Matsuura, T.), Wiley, New York, **2008**, pp. 559-580.

43. Lin, H., Freeman, B.D., Gas Permeation and Diffusion in Crosslinked Poly(ethylene glycol diacrylate), *Macromolecules***, 2006**, *39*, 3568-3580.

44. Lin, H., Van Wagner, E., Freeman, B.D., Toy, L.G., Gupta, R.P., Plasticization-Enhanced H_2 Purification Using Polymeric Membranes, *Science***, 2006**, *311*, 639-642.

45. Lin, H., Van Wagner, E., Raharjo, R., Freeman, B.D., Roman, I., High Performance Polymer Membranes for Natural Gas Sweetening, *Advanced Materials***, 2006**, *18*, 39-44.

46. Kelman, S., Lin, H., Sanders, E.S., Freeman, B.D., CO_2/C_2H_6 Separation using Solubility Selective Membranes, *Journal of Membrane Science***, 2007**, *305*, 57-68.

47. Patel, N.P., Aberg, C.M., Sanchez, A.M., Capracotta, M.D., Martin, J.D., Spontak, R.J., Morphological, Mechanical and Gas-Transport Characteristics of Crosslinked Poly(propylene glycol): Homopolymers, Nanocomposites and Blends, *Polymer***, 2004**, *45*, 5941-5950.

48. Patel, N.P., Hunt, M.A., Lin-Gibson, S., Bencherif, S., Spontak, R.J., Tunable CO_2 Transport through Mixed Polyether Membranes, *Journal of Membrane Science***, 2005**, *251*, 51-57.

49. Ju, H., McCloskey, B.D., Sagle, A.C., Wu, Y.H., Kusuma, V.A., Freeman, B.D., Crosslinked Poly(ethylene oxide) Fouling Resistant Coating Materials for Oil/Water Separation, *Journal of Membrane Science***, 2008**, *307*, 260-267.

50. CO_2 Removal from Syngas, Membrane Technology and Research, Inc.: http://www.mtrinc.com/co2_removal_from_syngas.html

51. Graham, T., On the Absorption and Dialytic Separation of Gases by Colloid Septa Part I: Action of a Septum of Caoutchouc, *Philosophical Magazine***, 1886**, *32*, 401-420.

52. Wijmans, J.G., Baker, R.W., The Solution-Diffusion Model: A Review, *Journal of Membrane Science***, 1995**, *107*, 1-21.

53. Bird, R.B., Stewart, W.E., Lightfoot, E.N., *Transport Phenomena*, 2nd ed., Wiley, New York, **2002**.

54. Ghosal, K., Freeman, B.D., Gas Separation Using Polymer Membranes: An Overview, *Polymers for Advanced Technologies***, 1994**, *5*, 673-697.

55. Petropoulos, J.H., Mechanisms and Theories for Sorption and Diffusion of Gases in Polymers, in *Polymeric Gas Separation Membranes* (Eds.: Paul, D., Yampolskii, Yu.), CRC Press, Inc., Boca Raton, FL, **1994**, pp. 17-81.

56. Lin, H., Freeman, B.D., Gas and Vapor Solubility in Crosslinked Poly(ethylene glycol Diacrylate), *Macromolecules***, 2005**, *38*, 8394-8407.

57. Dymond, J.H., Marsh, K.N., Wilhoit, R.C., Wong, K.C., *Virial Coefficients of Pure Gases*, 8th ed., Springer, Darmstadt, Germany, **2002**.

58. Stern, S.A., Mullhaupt, J.T., Gareis, P.J., The Effect of Pressure on the Permeation of Gases and Vapors through Polyethylene: Usefulness of the Corresponding States Principle, *AIChE Journal***, 1969**, *15*, 64-73.

59. Merkel, T.C., Bondar, V.I., Nagai, K., Freeman, B.D., Pinnau, I., Gas Sorption, Diffusion, and Permeation in Poly(dimethylsiloxane), *Journal of Polymer Science: Part B: Polymer Physics***, 2000**, *38*, 415-434.

60. Koros, W.J., Chan, A.H., Paul, D.R., Sorption and Transport of Various Gases in Polycarbonate, *Journal of Membrane Science***, 1977**, *2*, 165-190.

61. Stern, S.A., Shah, V.M., Hardy, B.J., Structure-Permeability Relationships in Silicone Polymers, *Journal of Polymer Science B: Polymer Physics***, 1987**, *25*, 1263-1298.

62. Freeman, B.D., Pinnau, I., Polymeric Materials for Gas Separations, in *Polymer Membranes for Gas and Vapor Separation* (Eds.: Freeman, B.D., Pinnau, I.), ACS, Washington D.C, **1999**, pp. 1-27.

63. Stern, S.A., Fang, S., Jobbins, R.M., Permeation of Gases at High Pressures, *Journal of Macromolecular Science - Physics***, 1971**, *B5*, 41-70.

64. Flory, P.J., *Principles of Polymer Chemistry*, Cornell University Press, Ithaca, NY, **1953**.

65. Cohen, M.H., Turnbull, D., Molecular Transport in Liquids and Glasses, *The Journal of Chemical Physics***, 1959**, *31*, 1164-1169.

66. Fujita, H., Diffusion in Polymer-Diluent Systems, *Fortschritte der Hochpolymeren-Forschung***, 1961**, *3*, 1-47.

67. Breck, D.W., *Zeolite Molecular Sieves*, Krieger Publishing Company, Melbourne, FL, **1974**.

68. Reid, R.C., Prausnitz, J.M., Poling, B.E., *The Properties of Gases and Liquids*, McGraw-Hill, New York, **1987**.

69. Lee, W.M., Selection of Barrier Materials from Molecular Structure, *Polymer Engineering and Science***, 1980**, *20*, 65-69.

70. Kumins, C.A., Kwei, T.K., Free Volume and Other Theories, in *Diffusion in Polymers* (Eds.: Crank, J., Park, G.), Academic Press, New York, **1968**, pp. 107-140.

71. van Krevelen, D.W., *Properties of Polymers: Their Correlation with Chemical Structure: Their Numerical Estimation and Prediction from Additive Group Contributions*, 3rd ed., Elsevier, Amsterdam, **1990**.

72. Bondi, A., van der Waals Volumes and Radii, *The Journal of Physical Chemistry***, 1964**, *68*, 441-451.

73. Weinkauf, D.H., Paul, D.R., Gas Transport Properties of Thermotropic Liquid-Crystalline Copolyesters. II. The Effects of Copolymer Composition, *Journal of Polymer Science: Part B: Polymer Physics***, 1992**, *30*, 837-849.

74. Kalakkunnath, S., Kalika, D.S., Lin, H., Freeman, B.D., Segmental Relaxation Characteristics of Crosslinked Poly(ethylene oxide) Copolymer Networks, *Macromolecules***, 2005**, *38*, 9679-9687.

75. Kalakkunnath, S., Kalika, D.S., Lin, H., Freeman, B.D., Viscoelastic Characteristics of U.V. Polymerized Poly(ethylene glycol diacrylate) Networks with Varying Extents of Crosslinking, *Journal of Polymer Science: Part B: Polymer Physics***, 2006**, *44*, 2058-2070.

76. Kannurpatti, A.R., Anseth, J.W., Bowman, C.N., A Study of the Evolution of Mechanical Properties and Structural Heterogeneity of Polymer Networks Formed by Photopolymerizations of Multifunctional (Meth)Acrylates, *Polymer***, 1998**, *39*, 2507-2513.

77. Schroeder, M.J., Roland, C.M., Segmental Relaxation in End-Linked Poly(dimethylsiloxane) Networks, *Macromolecules***, 2002**, *35*, 2676-2681.

78. Alves, N.M., Gomez Ribelles, J.L., Gomez Tejedor, J.A., Mano, J.F., Viscoelastic Behavior of Poly(methyl methacrylate) Networks with Different Cross-Linking Degrees, *Macromolecules***, 2004**, *37*, 3735-3744.

79. Roland, C.M., Constraints on Local Segmental Motion in Poly(vinylethylene) Networks, *Macromolecules***, 1994**, *27*, 4242-4247.

80. Kannurpatti, A.R., Bowman, C.N., Structural Evolution of Dimethacrylate Networks Studied by Dielectric Spectroscopy, *Macromolecules***, 1998**, *31*, 3311-3316.

81. Hill, L.W., Calculation of Crosslink Density in Short Chain Networks, *Progress in Organic Coatings***, 1997**, *31*, 235-243.

82. Mark, J.E., Experimental Determinations of Crosslink Densities, *Rubber Chemistry and Technology***, 1982**, *55*, 762-768.

83. Treloar, L.R.G., *The Physics of Rubber Elasticity*, 3rd ed., Oxford University Press, New York, **1975**.

84. Ferry, J.D., *Viscoelastic Properties of Polymers*, 3rd ed., Wiley, New York, **1980**.

85. Williams, G., Watts, D.C., Dev, S.B., North, A.M., Further Considerations of Non Symmetrical Dielectric Relaxation Behaviour arising from a Simple Empirical Decay Function, *Transactions of the Faraday Society*, **1971**, *67*, 1323-1235.

86. Kalakkunnath, S., Kalika, D.S., Lin, H., Raharjo, R., Freeman, B.D., Molecular Dynamics of Poly(ethylene glycol) and Poly(propylene glycol) Copolymer Networks by Broadband Dielectric Spectroscopy, *Macromolecules*, **2007**, *40*, 2773-2781.

87. Kalakkunnath, S., Kalika, D.S., Lin, H., Raharjo, R., Freeman, B.D., Molecular Relaxation in Cross-linked Poly(ethylene glycol) and Poly(propylene glycol) Diacrylate Networks by Dielectric Spectroscopy, *Polymer*, **2007**, *48*, 579-589.

88. Lin, H., Freeman, B.D., Kalakkunnath, S., Kalika, D.S., Effect of Copolymer Composition, Temperature, and Carbon Dioxide Fugacity on Pure- and Mixed-Gas Permeability in Poly(ethylene glycol)-Based Materials: Free Volume Interpretation, *Journal of Membrane Science*, **2007**, *291*, 131-139.

89. Richards, J.J., Danquah, M.K., Kalakkunnath, S., Kalika, D.S., Kusuma, V.A., Matteucci, S.T., Freeman, B.D., Relation Between Structure and Gas Transport Properties of Polyethylene Oxide Networks Based on Crosslinked Bisphenol A Ethoxylate Diacrylate, *Chemical Engineering Science*, doi:10.1016/j.ces.2008.11.026.

90. Kusuma, V.A., Matteucci, S., Freeman, B.D., Danquah, M.K., Kalika, D.S., Influence of Phenoxy-Terminated Short Chain Pendant Groups on Gas Transport Properties of Crosslinked Poly(ethylene oxide) Copolymers, *Journal of Membrane Science*, submitted.

91. Kusuma, V.A., Freeman, B.D., Smith, S.L., Heilman, A.L., Kalika, D.S., Influence of a TRIS-based Co-monomer on Structure and Gas Transport Properties of Cross-linked Poly(ethylene oxide), *Journal of Membrane Science*, in preparation.

92. Gottlieb, H.E., Kotlyar, V., Nudelman, A., NMR Chemical Shifts of Common Laboratory Solvents as Trace Impurities, *Journal of Organic Chemistry*, **1997**, *62*, 7512-7515.

93. Cruise, G.M., Scharp, D.S., Hubbell, J.A., Characterization of Permeability and Network Structure of Interfacially Photopolymerized Poly(ethylene glycol) Diacrylate Hydrogels, *Biomaterials*, **1998**, *19*, 1287-1294.

94. Peppas, N.A., Moynihan, H.J., Lucht, L.M., The Structure of Highly Crosslinked Poly(2-hydroxyethyl methacrylate) Hydrogels, *Journal of Biomedical Materials Research*, **1985**, *19*, 397-411.

95. Borns, M.A., Kalakkunnath, S., Kalika, D.S., Kusuma, V.A., Freeman, B.D., Dynamic Relaxation Characteristics of Crosslinked Poly(ethylene oxide) Copolymer Networks: Influence of Short Chain Pendant Groups, *Polymer*, **2007**, *48*, 7316-7328.

96. Decker, C., Moussa, K., Photopolymerization of Multifunctional Monomers in Condensed Phase, *Journal of Applied Polymer Science*, **1987**, *34*, 1603-1618.

97. Colthup, N.B., Daly, L.H., Wiberley, S.E., *Introduction to Infrared and Raman Spectroscopy*, Academic Press, New York, **1975**.

98. Lin, H., Freeman, B.D., Permeation and Diffusion, in *Springer-Handbook of Materials Measurement Methods* (Eds.: Czichos, H., Smith, L.E., Saito, T.), Springer, Berlin, **2006**, pp. 371-387.

99. Mogri, Z., Paul, D.R., Membrane Formation Techniques for Gas Permeation Measurements for Side-Chain Crystalline Polymers, *Journal of Membrane Science*, **2000**, *175*, 253-265.

100. Jordan, S.M., Koros, W.J., Fleming, G.K., The Effects of CO_2 Exposure on Pure and Mixed Gas Permeation Behavior: Comparison of Glassy Polycarbonate and Silicone Rubber, *Journal of Membrane Science*, **1987**, *30*, 191-212.

101. Burnett, E.S., Compressibility Determinations Without Volume Measurements, *Journal of Applied Mechanics*, **1936**, *3*, 136-140.

102. Bevington, P.R., Robinson, D.K., *Data Reduction and Error Analysis for the Physical Sciences*, 2nd ed., McGraw-Hill, Inc, New York, **1992**.

103. Kannurpatti, A.R., Anderson, K.J., Anseth, J.W., Bowman, C.N., Use of Living Radical Polymerizations to Study the Structural Evolution and Properties of Highly Crosslinked Polymer Networks, *Journal of Polymer Science: Part B: Polymer Physics*, **1997**, *35*, 2297-2307.

104. Angell, C.A., Relaxation in Liquids, Polymers and Plastic Crystals - Strong/Fragile Patterns and Problems, *Journal of Non-Crystalline Solids*, **1991**, *131-133*, 13-31.

105. Ngai, K.L., Roland, C.M., Chemical Structure and Intermolecular Cooperativity: Dielectric Relaxation Results, *Macromolecules*, **1993**, *26*, 6824-6830.

106. Paul, D.R., Gas Transport in Homogeneous Multicomponent Polymers, *Journal of Membrane Science*, **1984**, *18*, 75-86.

107. Sperling, L.H., *Introduction to Physical Polymer Science*, 3rd ed., Wiley, New York, **2001**.

108. Yampolskii, Yu.P., Kamiya, Y., Alentiev, A.Yu., Transport Parameters and Solubility Coefficients of Polymers at Their Glass Transition Temperatures, *Journal of Applied Polymer Science*, **2000**, *76*, 1691-1705.

109. Simha, R., Boyer, R.F., On a General Relation Involving the Glass Temperature and Coefficients of Expansion of Polymers, *The Journal of Chemical Physics*, **1962**, *37*, 1003-1007.

110. Williams, M.L., Landel, R.F., Ferry, J.D., The Temperature Dependence of

Relaxation Mechanisms in Amorphous Polymers and Other Glass-Forming Liquids, *Journal of American Chemical Society*, **1955**, *77*, 3701-3707.

111. Zoller, P., Walsh, D., *Standard Pressure-Volume-Temperature Data for Polymers*, Technomic Publishing Co. Inc., Lancaster, PA, **1995**.

112. Ismail, A.F., Lorna, W., Penetrant-Induced Plasticization Phenomenon in Glassy Polymers for Gas Separation Membrane, *Separation and Purification Technology*, **2002**, *27*, 173-194.

113. Chow, T.S., Molecular Interpretation of the Glass Transition Temperature of Polymer-Diluent Systems, *Macromolecules*, **1980**, *13*, 362-364.

114. Robeson, L.M., Correlation of Separation Factor versus Permeability for Polymeric Membranes, *Journal of Membrane Science*, **1991**, *62*, 165-185.

115. Barrer, R.M., Permeability in Relation to Viscosity and Structure of Rubber, *Transactions of the Faraday Society*, **1942**, *38*, 322-329.

116. van Amerongen, G.J., Permeability of Different Rubbers to Gases and Its Relation to Diffusivity and Solubility, *Journal of Applied Physics*, **1946**, *17*, 972-985.

117. Li, N.N., Funk, E.W., Chang, Y.A., Kulkarn, S.S., Swamikannu, A.X., White, L.S., Membrane Separation Processes in the Petrochemical Industry: Phase II, Final Report for U.S. Dept. of Energy, ID/12422-2, Allied-Signal, Des Plaines, IL, **1987**.

118. Nicolson, P.C., Vogt, J., Soft Contact Lens Polymers: An Evolution, *Biomaterials*, **2001**, *22*, 3273-3283.

119. Simon, F.T., Rutherford, J.M., Crystallization and Melting Behavior of Polyethylene Oxide Copolymers, *Journal of Applied Physics*, **1964**, *35*, 82-86.

120. Patel, N.P., Miller, A.C., Spontak, R.J., Highly CO_2-Permeable and -Selective Membranes Derived from Crosslinked Poly(ethylene glycol) and Its Nanocomposites, *Advanced Functional Materials*, **2004**, *14*, 699-707.

121. Raharjo, R.D., Lin, H., Sanders, D.F., Freeman, B.D., Kalakkunnath, S., Kalika, D.S., Relation Between Network Structure and Gas Transport in Crosslinked Poly(propylene glycol diacrylate), *Journal of Membrane Science*, **2006**, *283*, 253-265.

122. Morisato, A., Ghosal, K., Freeman, B.D., Chern, R.T., Alvarez, J.C., de la Campa, J.G., Lozano, A.E., de Abajo, J., Gas Separation Properties of Aromatic Polyamides Containing Hexafluoroisopropylidene Groups, *Journal of Membrane Science*, **1995**, *104*, 231-241.

123. Barrer, R.M., Skirrow, G., Transport and Equilibrium Phenomena in Gas-Elastomer Systems. I. Kinetic Phenomena, *Journal of Polymer Science*, **1948**, *3*, 549-563.

124. Wilks, B.R., Chung, W.J., Ludovice, P.J., Rezac, M.R., Meakin, P., Hill, A.J., Impact of Average Free-Volume Element Size on Transport in Stereoisomers of

Polynorbornene. I. Properties at 35°C., *Journal of Polymer Science: Part B: Polymer Physics*, **2003**, *41*, 2185-2199.

125. Meares, P., The Diffusion of Gases Through Polyvinyl Acetate, *Journal of American Chemical Society*, **1954**, *76*, 3415-3422.

126. Robeson, L.M., The Upper Bound Revisited, *Journal of Membrane Science*, **2008**, *320*, 390-400.

127. Ribeiro Jr, C.P., Freeman, B.D., Sorption and Dilation of Carbon Dioxide, Ethane, and Their Mixtures in a Cross-linked Poly(ethylene oxide) Copolymer, *Journal of Membrane Science*, submitted.

128. McHattie, J.S., Koros, W.J., Paul, D.R., Gas Transport Properties of Polysulphones: 1. Role of Symmetry of Methyl Group Placement on Bisphenol Rings, *Polymer*, **1991**, *32*, 840-850.

129. McHattie, J.S., Koros, W.J., Paul, D.R., Gas Transport Properties of Polysulphones: 2. Effect of Bisphenol Connector Groups, *Polymer*, **1991**, *32*, 2618-2625.

130. Michaels, A.S., Vieth, W.R., Barrie, J.A., Diffusion of Gases in Polyethylene Terephthalate, *Journal of Applied Physics*, **1963**, *34*, 13-20.

131. Narten, A.H., X-ray Diffraction Pattern and Models of Liquid Benzene, *Journal of Chemical Physics*, **1977**, *67*, 2102-8.

132. Mitchell, G.R., Windle, A.H., Structure of Polystyrene Glasses, *Polymer*, **1984**, *25*, 906-920.

133. Park, J.Y., Paul, D.R., Correlation and Prediction of Gas Permeability in Glassy Polymer Membrane Materials via a Modified Free Volume Based Group Contribution Method, *Journal of Membrane Science*, **1997**, *125*, 23-39.

134. Barrer, R.M., Barrie, J.A., Raman, N.K., Solution and Diffusion in Silicone Rubber I - A Comparison with Natural Rubber, *Rubber Chemistry and Technology*, **1963**, *36*, 642-650.

135. Raharjo, R.D., Freeman, B.D., Paul, D.R., Sarti, G.C., Sanders, E.S., Pure and Mixed Gas CH_4 and *n*-C_4H_{10} Permeability and Diffusivity in Poly(dimethylsiloxane), *Journal of Membrane Science*, **2007**, *306*, 75-92.

136. Gaylord, N.G., Oxygen-Permeable Contact Lens Composition, Methods and Article of Manufacture, US Patent 3,808,178, **1974**.

137. Lai, Y.C., The Role of Bulky Polysiloxanylalkyl Methacrylates in Polyurethane-Polysiloxane Hydrogels, *Journal of Applied Polymer Science*, **1996**, *60*, 1193-1199.

138. Okay, O., Kurz, M., Lutz, K., Funke, W., Cyclization and Reduced Pendant Vinyl Group Reactivity During the Free-Radical Cross-linking Polymerization of 1,4-Divinylbenzene, *Macromolecules*, **1995**, *28*, 2728-2737.

139. Kizilay, M.Y., Okay, O., Effect of Initial Monomer Concentration on Spatial Inhomogeneity in Poly(acrylamide) Gels, *Macromolecules*, **2003**, *36*, 6856-6862.

140. Zhang, R., Mallon, P.E., Chen, H., Huang, C.M., Zhang, J., Li, Y., Wu, Y., Sandreczki, T.C. et al., Characterization of Photodegradation of a Polyurethane Coating by Positron Annihilation Spectroscopy: Correlation with Cross-link Density, *Progress in Organic Coatings*, **2001**, *42*, 244-252.

141. Jin, X., Zhang, S., Runt, J., Observation of a Fast Dielectric Relaxation in Semi-Crystalline Poly(ethylene oxide), *Polymer*, **2002**, *43*, 6247-6254.

142. Havriliak, S., Negami, S., Complex Plane Analysis of α-Dispersions in Some Polymer Systems, *Journal of Polymer Science, Polymer Symposia*, **1966**, *14*, 99-103.

143. Froehlich, H., *Theory of Dielectrics*, Oxford University Press, London, **1958**.

144. McMurry, J., *Organic Chemistry*, 5th ed., Brooks/Cole, Thomson Learning, Pacific Grove, CA, **2000**.

145. Ulrich, H., *The Chemistry and Technology of Isocyanates*, Wiley, New York, **1996**.

146. Raspoet, G., Nguyen, M.T., McGarraghy, M., Hegarty, A.F., The Alcoholysis Reaction of Isocyanates Giving Urethanes: Evidence for a Multimolecular Mechanism, *Journal of Organic Chemistry*, **1998**, *63*, 6878-6885.

147. Davis, T.L., Farnum, J.M., Relative Velocities of Reaction of Alcohols with Phenyl Isocyanates, *Journal of American Chemical Society*, **1934**, *56*, 883-885.

148. Cai, D., Larsen, R.D., Reider, P.J., Efficient Synthesis of 6-mono-bromo-1,1'-bi-2-naphthol, *Tetrahedron Letters*, **2002**, *43*, 4055-4057.

149. Kim, H., Lim, C., Hong, S., Gas Permeation Properties of Organic-Inorganic Hybrid Membranes Prepared from Hydroxyl-Terminated Polyether and 3-isocyanatopropyltriethoxysilane, *Journal of Sol-Gel Science and Technology*, **2005**, *36*, 213-221.

150. Tanaka, K., Takahashi, K., Kanada, M., Kanome, S., Nakajima, T., Copolymer for Soft Contact Lens, Its Preparation and Soft Contact Lens Made Thereof, U.S. Patent 4,139,513, **1979**.

151. Tighe, B.J., Silicone Hydrogels: Structure, Properties and Behaviour, in *Silicone Hydrogels: Continuous-Wear Contact Lenses* (Ed.: Sweeney, D.), 2nd ed., Butterworth-Heinemann, Edinburgh, **2004**, pp. 1-27.

152. Künzler, J.F., Silicone Hydrogels for Contact Lens Application, *Trends in Polymer Science*, **1996**, *4*, 52-59.

153. Hong, Y., Chen, C., Manesis, N., Wettable Silicone Hydrogel Contact Lenses and Related Compositions and Methods, World Patent WO 2007/146312 A2, **2007**.

154. Ribeiro Jr, C.P., Freeman, B.D., Sorption, Dilation, and Partial Molar Volumes of Carbon Dioxide and Ethane in Cross-linked Poly(ethylene oxide), *Macromolecules*, **2008**, *41*, 9458-9468.

155. Kang, Y., Cheong, K., Noh, K.A., Lee, C., Seun, D.Y., A Study of Cross-linked PEO Gel Polymer Electrolytes Using Bisphenol A Ethoxylate Diacrylate: Ionic Conductivity and Mechanical Properties, *Journal of Power Sources*, **2003**, *119-121*, 432-437.

156. Merkel, T.C., Freeman, B.D., Spontak, R.J., He, Z., Pinnau, I., Meakin, P., Hill, A.J., Ultrapermeable, Reverse-Selective Nanocomposite Membranes, *Science*, **2002**, *296*, 519-522.

157. Matteucci, S., Kusuma, V.A., Sanders, D., Swinnea, S., Freeman, B.D., Gas Transport in TiO_2 Nanoparticle-Filled Poly(1-trimethylsilyl-1-propyne), *Journal of Membrane Science*, **2008**, *307*, 196-217.

158. Gruener, S., Huber, P., Knudsen Diffusion in Silicon Nanochannels, *Physical Review Letters*, **2008**, *100*, 064502 (1-4).

159. Barrer, R.M., Diffusion and Permeation in Heterogeneous Media, in *Diffusion in Polymers* (Eds.: Crank, J., Park, G.S.), Academic Press, New York, **1968**, pp. 165-217.

160. Matteucci, S., Kusuma, V.A., Kelman, S.D., Freeman, B.D., Gas Transport Properties of MgO Filled Poly(1-trimethylsilyl-1-propyne) Nanocomposites, *Polymer*, **2008**, *49*, 1659-1675.

161. Matteucci, S., Kusuma, V.A., Swinnea, S., Freeman, B.D., Gas Permeability, Solubility and Diffusivity in 1,2-Polybutadiene Containing Brookite Nanoparticles, *Polymer*, **2008**, *49*, 757-773.

162. Matteucci, S., Raharjo, R.D., Kusuma, V.A., Swinnea, S., Freeman, B.D., Gas Permeability, Solubility, and Diffusion Coefficients in 1,2-Polybutadiene Containing Magnesium Oxide, *Macromolecules*, **2008**, *41*, 2144-2156.

163. Patel, N.P., Miller, A.C., Spontak, R.J., Highly CO_2-Permeable and Selective Polymer Nanocomposite Membranes, *Advanced Materials*, **2003**, *15*, 729-733.

164. Patel, N.P., Zielinski, J.M., Samseth, J., Spontak, R.J., Effects of Pressure and Nanoparticle Functionality on CO_2-Selective Nanocomposites Derived from Crosslinked Poly(ethylene glycol), *Macromolecular Chemistry and Physics*, **2004**, *205*, 2409-2419.

165. Takahashi, S., Paul, D.R., Gas Permeation in Poly(ether imide) Nanocomposite Membranes Based on Surface-Treated Silica. Part 1: Without Chemical Coupling to Matrix, *Polymer*, **2006**, *47*, 7519-7534.

166. Takahashi, S., Paul, D.R., Gas Permeation in Poly(ether imide) Nanocomposite Membranes Based on Surface-Treated Silica. Part 2: With Chemical Coupling to Matrix, *Polymer*, **2006**, *47*, 7535-7547.

Vita

Victor Armanda Kusuma was born in Houston, Texas on 16th of May 1982, the only son of Oktomy Kusuma and Theresia Etty. He grew up in the onshore oil-producing area in Duri, Riau, Indonesia (famed for the Caltex Duri Steam Flood project) and attended elementary and middle school there. He won the Singapore Ministry of Education ASEAN scholarship, upon which he attended upper secondary school in St. Joseph's Institution in Singapore, obtaining his GCE "O" Levels in December 1998. After four months in Victoria Junior College in Singapore, he entered Georgia Institute of Technology in Atlanta, Georgia, from where he graduated with a B.S. in Chemical Engineering with Highest Honors in May 2002. He worked with ChevronTexaco Corporation (now Chevron Corp.) in Houston, Texas for three months as a research intern before entering the Chemical Engineering department in The University of Texas at Austin in August 2002 for graduate work with Professor Miguel Jose-Yacaman. He received a M.S. in Chemical Engineering in December 2004. In July 2005, he joined the research group of Professor Benny Freeman in the same department.

Permanent address:

9800 Mountain Quail Rd.

Austin, Texas, USA, 78758.

This dissertation was typed by the author.